Characterisation of the adsorption and regeneration behaviour of a commercial activated alumina adsorbent when separating 1-hexanol and 1-decanol from n-decane

by

Muzafar Tagelsir Hamza Khalifa

Thesis presented in partial fulfilment
of the requirements for the Degree

of

MASTER OF ENGINEERING
(CHEMICAL ENGINEERING)

in the Faculty of Engineering
at Stellenbosch University

Supervisor
Prof André Burger

March 2023

DECLARATION

By submitting this thesis electronically, I declare that the entirety of the work contained therein is my own original work, that I am the sole author thereof (save to the extent explicitly otherwise stated), that reproduction and publication thereof by Stellenbosch University will not infringe any third-party rights, and that I have not previously in its entirety or in part submitted it for obtaining any qualification.

Date: *March 2023*

Abstract

Paraffins produced in industry are usually associated with impurities such as oxygenates, and adsorption is commonly used to remove these oxygenates (e.g. alcohols). However, the recyclability of such adsorbents has rarely been studied.

In this study, the reusability of activated alumina adsorbent used to adsorb 1-alcohols from a paraffin solvent was investigated. The objectives of this study included: (I) the measurement and investigation of single and binary-component adsorption data; (II) the modelling of equilibrium adsorption isotherms and adsorption kinetics; and (III) the measurement and investigation of the efficiency of adsorbent throughout consecutive adsorption/thermal regeneration cycles. One type of commercialized activated alumina adsorbent was used in this study. 1-hexanol and 1-decanol were used as adsorbates, while n-decane was used as the solvent. The effect of initial adsorbate concentration and alcohol carbon chain length on the adsorption and desorption were also briefly investigated.

A bench-scale batch adsorption set-up was used for adsorption experiments. Schott bottles containing 1-alcohols + n-alkane solutions (at various initial concentrations of adsorbates) and adsorbents (10g of fresh adsorbent at first experiment) were immersed in a water bath, where the water temperature was maintained at 65 °C. The regeneration experiments were carried out at 205 °C, 185 °C and 165 °C using thermal regeneration columns. Heated purging carrier gas (nitrogen) was used to sweep through the adsorbent for the full duration of regeneration.

For both single-component and binary systems, the total equilibrium adsorbent loading was found to increase when increasing the adsorbates' initial concentration. For single-component solutions, the total adsorption capacity increased systematically as the initial concentration of adsorbates increased up to 2.5 mass%, but at even higher initial concentrations the capacity remained relatively constant. For the binary system, the equilibrium adsorbent loading began to plateau at initial concentrations higher than 2.0 mass%. The effect of carbon chain length exhibited different behaviour for single-component and binary systems. The adsorbent proved a slightly higher affinity to adsorb more of the 1-decanol in the single-component system, whereas in the binary system it was inclined to adsorb more of the 1-hexanol. At similar 1-alcohol initial concentrations in single and binary systems, it was found that the adsorption of a specific 1-alcohol from the binary systems was remarkably poorer than the adsorption of the same 1-alcohol from the corresponding single-component systems.

Equilibrium studies showed that the Freundlich and Sips isotherms are suitable for the single 1-hexanol and single 1-decanol adsorption systems, respectively. However, for the binary system,

poor correlation was exhibited between the date and the Extended Langmuir, Extended Freundlich and Extended Sips models. Both single-component and binary systems can be described by Elovich kinetics and the Intra-Particle Diffusional Model.

As expected, higher efficiencies were achieved for the respective single-component systems than for the binary system. As far as regeneration behaviour is concerned, the activated alumina adsorbent exhibited an adverse response to the highest regeneration temperature (205 °C). For both single-component and binary systems, the adsorbent offered a better efficiency at the regeneration temperature of 185 °C than at 205 °C and 165 °C. BET analysis showed a notable reduction in the total surface area of the regenerated adsorbent at 165 °C, indicating incomplete regeneration at such low temperature, was also confirmed by a systematic drop in adsorption efficiency down to 40% at the final regeneration cycle.

Opsomming

Paraffiene wat in die industrie geproduseer word, word gewoonlik geassosieer met onsuiwerhede soos suurstofgebonde komponente (e.g. alkohole). Hierdie komponente word in die algemeen deur middel van adsorpsie verwyder. Gepubliseerde inligting oor die gebruik en regenerasie van die betrokke adsorbente in sulke toepassings is egter skaars.

Hierdie studie het die regenerasie en hergebruik van 'n geaktiveerde alumina adsorbent waarmee 1-alkohole uit 'n paraffienoplosmiddel geadsorbeer is, ondersoek. Die doelwitte van die studie was: (I) die meting en bestudering van enkel- en binêre komponent adsorpsie data; (II) die modellering van ewewigsadsorpsie-isoterme en adsorpsie-kinetika; en (III) die meting van en ondersoek na die doeltreffendheid van die adsorbent deur opeenvolgende adsorpsie/termiese regenerasie-siklusse. Een tipe gekommersialiseerde geaktiveerde alumina adsorbent is vir hierdie studie gebruik. 1-heksanol en 1-dekanol is as adsorbate getoets, terwyl n-dekaan as die oplosmiddel gebruik is. Die effek van die aanvanklike adsorbaatkonsentrasie asook alkohole se koolstofkettinglengte op adsorpsie en desorpsie is ondersoek.

'n Laboratorium-skaal enkellading-adsorpsie opstelling is gebruik vir adsorpsie eksperimente. Schott-bottels bevattende 1-alkohole + n-alkaanoplossings (met verskillende aanvanklike konsentrasies van adsorbate) en adsorbente (10g vars adsorbent by die eerste eksperiment) is in 'n waterbad geplaas, waar die watertemperatuur konstant by 65 °C gehou is. Die regenerasie eksperimente is uitgevoer by 205 °C, 185 °C en 165 °C in termiese regenerasie kolomme. Verhitte spoelgas (stikstof) is gebruik om desorberende komponent mee te sleur vir die volle duur van regenerasie.

By beide enkelkomponent en binêre stelsels is gevind dat die totale ewewigsadsorpsiebelading toeneem wanneer die aanvanklike konsentrasie van adsorbate toeneem. In enkelkomponent oplossings het die totale adsorpsiekapasiteit stelselmatig toegeneem namate die aanvanklike konsentrasie van adsorbate toegeneem het tot 2.5 massa%, maar by nog hoër aanvanklike konsentrasies het die kapasiteit relatief konstant gebly. In die binêre stelsel het die ewewigsadsorpsiebelading afgeplat by aanvanklike konsentrasies hoër as 2.0 massa%. Die effek van die koolstofkettinglengte was verskillend in enkelkomponent en binêre stelsels. Die adsorbent het in die enkel-komponent stelsel effens hoër affiniteit getoon vir 1-dekanol adsorpsie, terwyl dit in die binêre stelsel geneig was om meer van die 1-heksanol te adsorbeer. By soortgelyke aanvanklike 1-alkohol konsentrasies in enkel- en binêre stelsels is bevind dat die adsorpsie van 'n spesifieke 1-alkohol uit die binêre stelsels opmerklik swakker was as die adsorpsie van dieselfde 1-alkohol uit die ooreenstemmende enkelkomponent stelsels.

Ewewigsstudies het getoon dat die Freundlich- en Sips-isoterme geskik is vir onderskeidelik enkel 1-heksanol en enkel 1-dekanoöl adsorpsie stelsels. Vir die binêre stelsel het die Extended Langmuir, Extended Freundlich en Extended Sips modelle egter 'n swak korrelasie met die data getoon. Beide enkel-komponent en binêre stelsels kan beskryf word deur Elovich-kinetika en die Intrapartikeldiffusie Model.

Soos verwag, is hoër doeltreffendheid behaal in die onderskeie enkelkomponent stelsels as in die binêre stelsel. Wat herwinninggedrag betref, het die geaktiveerde alumina adsorbent 'n nadelige reaksie getoon by die hoogste herwinningstemperatuur (205 °C). Vir beide enkelkomponent en binêre stelsels was die adsorbent meer doeltreffend by 'n herwinningstemperatuur van 185 °C as by 205 °C en 165 °C. BET-analise het 'n merkbare afname in die totale oppervlakte van die na-regenerasie adsorbent by 165 °C getoon, wat dui op onvolledige regenerasie by so 'n lae temperatuur. Hierdie waarneming is ook bevestig deur 'n sistematiese afname in adsorpsie doeltreffendheid tot by 40% in die finale herwinningsiklus.

ACKNOWLEDGEMENTS

This dissertation would not have been accomplished in its present form without the invaluable help and support from others. I would like to take this opportunity to express my immeasurable appreciation and gratitude to the following persons and organizations.

Firstly, I want to thank my supervisor, Prof. André Burger, for his continuous support, guidance and help over the years during my stay at Stellenbosch University. This dissertation would not have been completed without his constant feedback and advice.

Special thanks and gratitude go to my ex-supervisor, Dr. L J du Preez, for being super supportive and for his guidance over my first year at Stellenbosch University. I wish him all the best in his new career.

My deepest appreciation and dearest love go to my cherished, talented and beloved wife, Dr. Mai Ahmed, for her endless love and always being there for me during this meaningful journey. Without her company, love and help, I would not have overcome the problems I went through all the way.

Thanks are due to my lab mate, Anke Louw, for the support, discussions and help in the lab.

I am grateful to the technical team for their very precious help.

I sincerely acknowledge the Department of Process Engineering for awarding me the scholarship that has enabled me to get my MEng Degree at Stellenbosch University.

Finally, I would like to give a big thanks to whoever made my journey at Stellenbosch University easier and worth having. I will always be grateful to those who made me feel welcome in South Africa, the country, and for providing me with the chance of pursuing my MEng Degree.

Table of Contents

Nomenclature

Abbreviations & Acronyms

AA	Activated alumina
AC	Activated carbon
BET	Brunauer-Emmett-Teller theory
BJH	Barrett-Joyner-Halenda model
DFT	Density Functional theory model
EFM	The Extended Freundlich isotherm model
ELM	The Extended Langmuir isotherm model
EM	The Elovich Model
ESM	The Extended Sips isotherm model
EXD	Energy dispersive X-ray
FM	Freundlich isotherm model
GC	Gas chromatography
HYBRID	Hybrid fractional error function
IPDM	Intra-particle diffusion model
IUPAC	International union of pure and applied chemistry
LM	Langmuir isotherm model
LPGA	Low-pressure gas adsorption
MC	Molecular sieve
MPSD	Marquardt's percentage standard deviation
PFO	Pseudo-First-Order Model
PSO	Pseudo-Second Order Model
SEM	Scanning electron microscope
SM	Sips isotherm model

Symbols

Δ_y	Uncertainty parameter, mass%
C_0	Adsorbate initial concentration, $mg.mL^{-1}$ / mass%
C_e	Adsorbate concentration at the equilibrium, $mg.mL^{-1}$ / mass%
C_t	Adsorbate concentration at time *t*, $mg.mL^{-1}$ / mass%
h	Initial adsorption rate obtained from Pseudo-Second Order Model, $mg.g^{-1}.min^{-1}$
K_1	Pseudo-First-Order rate constant, min^{-1}
K_2	Pseudo-Second-Order rate constant, min^{-1}
K_f	Freundlich's capacity coefficient, $(mg.g^{-1})(mg.mL^{-1})^{1/n}$
K_{IP}	Intra-particle diffusion constant rate, $mg(g.m^{-0.5})^{-1}$
K_L	Langmuir affinity coefficient, $m^3.g^{-1}$
K_s	Sips constant, $mL.g^{-1}$
m	Mass of the components in the solution, g
m	Mass of the adsorbent, g
n	Exponential constant (Freundlich and Sips isotherm models), dimensionless
n	Number of data point, dimensionless
n	Number of repeats, dimensionless
n_s	Sips model's exponent, dimensionless
p	Number of regression parameters in specific model, dimensionless
q_0	Equilibrium adsorbent loading for the first adsorption cycle, $mg.g^{-1}$
q_e	Equilibrium adsorbent loading, $mg.g^{-1}$
$q_{e,cal}$	Adsorbent loading calculated from the kinetic models (Pseudo-First-Order and Pseudo-Second Order), $mg.g^{-1}$
$q_{e,exp}$	Adsorbent loading obtained from the experiments, $mg.g^{-1}$
q_m	Maximum adsorbent loading (Sips isother model), $mg.g^{-1}$
q_{max}	Maximum adsorbent loading (Langmuir isother model), $mg.g^{-1}$
q_n	Equilibrium adsorbent loading for the adsorption cycle number (n), $mg.g^{-1}$

q_t	Adsorbent loading at any time t, $mg.g^{-1}$
R^2	Correlated coefficient, %
RE	Regeneration efficiency, %
R_i	Ratio of the equilibrium loading of an adsorbate (*i*) in a multicomponent adsorption system, dimensionless
s	Standard deviation, application specific
S_n	Standard error, application specific
V	Volume of the solution, mL
x	Correlative model parameter (the Extended Freundlich isotherm model), dimensionless
z	Correlative model parameter (the Extended Freundlich isotherm model), dimensionless
α	Initial adsorption rate constant, $mg.g^{-1}.min^{-1}$
α	Significant level (uncertainties calculation), dimensionless
ß	Surface coverage (Elovich model), $mg.g^{-1}$
ϴ	Constant and represents fractional loading of adsorbed molecules, %
ϴ	Constant related to the boundary layer thickness, $mg.g^{-1}$
ρ	Density, kg/m^3

Subscripts & Superscripts

1	Component 1 in binary adsorption system
2	Component 2 in binary adsorption system
bin	Binary system
i	Component i in binary adsorption system
j	Component j in binary adsorption system
sin	Single adsorption system

Chapter 1 : Introduction

1.1 Background

The paraffins, a technical name for alkanes, are saturated hydrocarbons with a general formula C_nH_{2n+2}, which at normal conditions are found in gaseous, liquid or viscous liquids and solid wax phases when $n<5$, $5<n<15$ and $n>15$, respectively (Selley and Sonnenberg, 2015; Viswanathan, 2017b). There are two types of paraffins based on the series structure: straight-chain molecules and branched-chain molecules. The paraffins are utilized in various industries such as energy, food, medicine and agriculture (Leckel, 2009; Palou *et al.*, 2014; Aamir *et al.*, 2019; Urlaub *et al.*, 2019).

In petrochemical industries, paraffins can be derived by different processes such as condensation of natural gas, crude oil distillate or by Fischer-Tropsch reaction (Yu and Khosla, 2012; Méndez and Ancheyta, 2020). However, amounts of undesired species like oxygenates, including alcohols, are generated and occur in produced paraffins streams (Méndez and Ancheyta, 2020; Wang *et al.*, 2020). Removal of these oxygenates from paraffins streams is necessary since they could be a source of severe problems for the downstream units, such as deactivation of the catalysts (Leckel, 2005; Kulprathipanja, 2010). Various separation technologies, such as the absorption process, are used to remove the oxygenates from paraffins (Frey *et al.*, 1997). However, the adsorption process can be a more attractive alternative in removing oxygenates due to its ability to separate bulk and small amounts, its high efficiency, low cost and friendly operation since it consumes lower energy than the other separation technologies (Priegnitz *et al.*, 2006; Khas and Delhi, 2013; Abdelwahab Emam, 2018; Thomas, 2019).

Adsorption is defined as a surface phenomenon where dissolved molecules (adsorbates) from a fluid stream are settled down on the surface or pores of a solid substance (adsorbents) (Chiou, 2003). The ability of various types of adsorbents to adsorb 1-alcohols from different solutions has been reported before, such as with zeolite (Milestone and Bibby, 1983; Alturki, 2017), polymer-based adsorbents (Styrene, Copolymer and Sl, 2006; Zhang, Wang and Wang, 2019), clay adsorbent (Mekki and Bagane, 2012), silica (Nayakasinghe, Sivapragasam and Burghaus, 2017), molecular sieves (Remy *et al.*, 2011), and activated carbon (Madero-castro and Peng, 2022). However, although Milestone and Bibby (1983), for example, emphasized that the affinity of zeolite to adsorb 1-alcohols increased as the alumina content increased in the adsorbent, detailed studies on the adsorption and regeneration behaviour of activated alumina during separation of 1-alcohols from paraffin solvents have not been published well.

The adsorption process efficiency is influenced by many variables. Regardless, excellent reusability of adsorbents through multiple adsorption/regeneration cycles is crucial for obvious economic and

environmental reasons (Kumari, Behera and Meikap, 2019; Liu *et al.*, 2020). Regeneration is a frequent-recovery process of saturated and exhausted adsorbents via different technically and economically feasible methods (McQuillan, Stevens and Mumford, 2018; Momina, Shahadat and Isamil, 2018). It needs to be effective, non-destructive and financially viable over time to ensure a viable separation process.

To the author's knowledge, only Bosman (2019) and Groenewald (2019) have investigated multiple and single-component adsorption of alcohols from paraffins, respectively. They used 1-hexanol, 1-octanol, 1-decanol as alcohols, n-decane as solvent and different types of activated alumina adsorbent in their studies. However, only Groenewald studied the reusability of the applied adsorbents. This was done only for 1-hexanol as adsorbate at an initial concentration of 1.5 mass%, so the impact of initial concentration of 1-alcohols and their carbon chain length on the adsorbents' performance was not investigated. The number of adsorption/regeneration cycles carried out by Groenewald was limited to nine cycles, and regeneration tests were performed at two temperatures. Furthermore, the adsorption temperature considered by Bosman and Groenewald varied between 25 °C and 45 °C.

Against this background, the potential need was identified to further characterise the adsorption and regeneration behaviour of activated alumina when separating 1-alcohols from paraffins:

- at adsorption temperatures higher than 45;
- at more regeneration temperatures, and with the same or more adsorption/regeneration cycles than applied by Groenewald (2019);
- at different initial concentrations of 1-alcohols in solution;
- for 1-alcohols with different molecular masses, and for both single-component and binary solutions in a paraffin.

1.2 Problem Statement

Not many studies have been conducted on characterising the adsorption and regeneration behaviour of activated alumina adsorbents utilized to adsorb 1-alcohols from paraffins. In practice, paraffin streams are usually associated with multiple components, while studies regarding the regeneration of the activated alumina adsorbents have pertained only to single-component adsorption systems. Hence, studies are required to estimate the reusability of adsorbents applied to adsorb multiple 1-alcohols from the paraffins.

1.3 Research Aims and Objectives

The aim of this research was to investigate the reusability of industrially used activated alumina utilized to adsorb single and binary 1-alcohol components from a paraffin solvent through multiple adsorption/regeneration cycles. This was achieved by fulfilling the following objectives:

I. Single-component and binary-component adsorption data of 1-alcohols, using one type of activated alumina adsorbent, were measured and investigated.
   a. The effect of initial concentration of 1-alcohol on the adsorption of 1-alcohols was studied;
   b. The effect of alcohol carbon chain length on the adsorption of 1-alcohols was studied;
   c. Single-component and binary-component adsorption of 1-alcohols were compared; and,
   d. The interaction possibility in the binary-component adsorption of 1-alcohols was studied.

II. The data extracted from (I) using existing equilibrium and kinetic models to predict the reversibility of the adsorption process was modelled.
   a. Single-component and binary-component adsorption data, using various equilibrium isotherms and models, were modelled; and,
   b. Single-component and binary-component adsorption data, using various kinetic models, were modelled.

III. Single-component and binary-component adsorption data of 1-alcohols over consecutive adsorption/regeneration cycles were measured and investigated.
   a. The change in equilibrium adsorbent loading in the single-component and binary-component systems throughout the adsorption/regeneration cycles was compared and investigated.
   b. The regeneration efficiency of the adsorbent used throughout the different cycles was compared and investigated.

1.4 Research Approach

A bench-scale batch experimental setup was used to measure the adsorption data.

The data extracted from the experiments was compared at different initial concentrations and alcohol chain lengths to determine the effect of changes in these variables in the adsorption results. The equilibrium isotherm was investigated by modelling the data obtained with various equilibrium isotherm models to understand the equilibrium behaviour of the different systems. The measured experimental data was fitted to different kinetic models to gain insight into the mass transfer of the

adsorbed 1-alcohols onto the utilized adsorbent. Both equilibrium and kinetic models were investigated for the first adsorption cycle where the fresh adsorbent was used. A drop in total adsorption uptake and regeneration efficiency was calculated for each adsorption/regeneration cycle to better comprehend the changes in the adsorbent's performance throughout the multiple cycles.

Single and binary adsorption experiments were carried out to understand how the performance of the adsorbent can be varied and is affected when it is used to adsorb single and binary 1-alcohols during multiple adsorption/regeneration cycles.

1.5 Research Scope and Limitation

This research work was based on previous studies conducted by Groenewald (2019) and Bosman (2019). Hence, the same materials used by them were utilized in this study. These materials included 1-hexanol and 1-decanol as adsorbates, n-decane as a solvent, and a commercially utilized activated alumina as adsorbent. However, values of variables such as adsorption temperature, initial concentration of adsorbates, regeneration temperatures and number of cycles, and the impact of adsorbates' properties on the regenerated adsorbents' performance was varied from Bosman's and Groenewald's values to build on the data extracted from their studies. For instance, Groenewald studied the regeneration impact on the adsorbents used to adsorb only single 1-hexanol at initial concentration 1.5 mass%. Therefore, the regeneration impact on adsorbents utilized to adsorb 1-hexanol and single 1-decanol on various adsorption systems (single-component and binary-component adsorption systems) was conducted and investigated at an initial concentrations of 0.5 mass%, 1.5 mass%, and 3.0 mass%. More details on the variation in the variables considered in Groenewald, Bosman and this study are provided in Section 2.2.4.

The availability of abovementioned materials in the market and their feasible cost added another valid reason for using them in this study. An activated alumina adsorbent was used as it showed high affinity to adsorb 1-alcohols, as outlined by Groenewald (2019) and Bosman (2019). Finally, as these materials are relevant to the petrochemical industries, using them makes the study more relevant to the practical field.

Adsorption equilibrium and kinetic data can be measured by using either batch or dynamic experimental techniques (Khalil *et al.*, 2020). In this study, a batch bench-scale adsorption set-up was used due to its simplicity over the dynamic technique (Xu, Cai and Pan, 2013). Furthermore, the adsorption mechanism and behaviour of the adsorbates on the pores and surfaces of adsorbents are better understood using batch experiments (Sanciolo *et al.*, 2014; Iftekhar *et al.*, 2018). In the real practical field, the adsorption process can be classified based on the operational condition in contrast to continuous or batch processes (Cavalcante, 2000). Since this study was carried out using

batch experimental methods, its output will be more valuable for practical batch adsorption processes. As the adsorption of oxygenates from the paraffin solvents is sometimes processed at up to 65 °C in industry (Priegnitz *et al.*, 2006), the adsorption temperature of 65 °C was conducted for the adsorption experiments in this study. In addition, since the adsorption of 1-alcohols from n-decane solvent was previously investigated at 25 °C, 30 °C, 35 °C and 45 °C by Groenewald (2019) and Bosman (2019), adsorption experiments at 65 °C therefore contributed in widening the database of the corresponding adsorption systems.

A batch, bench-scale thermal regeneration set-up was used for the regeneration experiments. Groenewald (2019) carried out regeneration experiments at only two temperatures: 205 °C and 185 °C. In this study, the regeneration cycles were conducted at the same temperatures carried out by Groenewald, but for a greater number of cycles (10 cycles for each system). In addition, one set of regeneration experiments was conducted at a lower regeneration temperature, 165 °C (for 15 cycles), to figure out the possibility of getting similar or better performance from the adsorbent compared to those regenerated at 205 °C and 185 °C, but with less power consumption and at a lower operational cost.

1.6 Thesis Chapters Overview

Chapter 2 includes extensive literature review and related theories to adsorption and regeneration. The effects of various variables on adsorption processes, interaction in binary-component systems, equilibrium and kinetic models, and adsorbents regeneration were also reviewed.

Chapter 3 outlines the materials and methods applied in this study, experimental design, analytical methods, repeatability of data, uncertainty analysis, and the data processes followed to fulfil the objectives of this study.

Chapter 4 presents the adsorbent characterisation and physical properties such as surface area, pore volume and pore structure of the adsorbent utilized in this study.

Chapter 5 discusses objective (I), and thus consists of the experimental results of the study including investigation and comparison of the alcohol adsorption abilities in the first cycle, comparison of single and binary-component adsorption behaviour, effects of the alcohol's carbon chain length and the alcohol's initial concentration in the adsorption capacity, and potential interaction between the different alcohols in binary-component systems.

Chapter 6 pertains to objective (II), which provides insights into equilibrium of the systems investigated by fitting different equilibrium isotherm models to the extracted equilibrium data.

Chapter 7 also pertains to objective (II), which provides insights into the mass transfer behaviour of the adsorbed molecules in the systems investigated by fitting experimentally measured data onto various kinetic models.

Chapter 8 addresses objective (III), so it discusses the variation in the adsorbent's performance over the succeeding cycles by calculating the drop in total adsorption capacity and regeneration efficiency.

Lastly, Chapter 9 concludes this study, encapsulating the findings and providing recommendations for future work.

Chapter 2 : Literature Review

2.1 Adsorption Phenomenon

Adsorption is an exothermic process that is defined as a surface phenomenon where dissolved molecules from a fluid stream are settled on the surfaces or pores of a solid substance. The adsorbed soluble molecules are referred to as the adsorbates, while the solid substance is referred to as the adsorbent (Chiou, 2003).

Adsorption capacity is described by the adsorbed amount of the adsorbates on the adsorbent surface per unit mass of adsorbent and is quantified by Equation 2.1 (Y. Li *et al.*, 2020):

$$q_t = \frac{(C_0 - C_t)\mathrm{V}}{\mathrm{m}} \qquad [2.1]$$

where q_t is the adsorption capacity at time t, C_0 and C_t are the adsorbate's initial concentration and adsorbate concentration at time t, respectively, V is the volume of the solution and m is the weight of the adsorbent.

2.1.1 Adsorption Mass Transfer

Diffusion of adsorbates from a bulk solution onto the adsorbent surface or pores comprises the following four distinct steps (Kaushal, 2017):

I. Adsorbate diffusion from the bulk solution to the solution film surrounding the external surface of the adsorbent.

II. Film diffusion: the diffusion of adsorbate from the solution film to the adsorbent's surface.

III. Pore diffusion: intraparticle diffusion of adsorbate within the interstices of the adsorbent.

IV. Diffusion of adsorbate on internal surface sites of the adsorbent to settle on the active sites.

The resistance to mass transfer in the fourth step is negligible since the adsorbate diffusion on the adsorbent's internal surface happens very fast. On the other hand, three scenarios are expected in steps 2 and 3: external diffusion is greater than internal diffusion, or external diffusion is lower than internal diffusion, where the limiting steps are the pore and film diffusion, respectively, while the last scenario is external transport which is equal to internal transport, where the rate of molecules which transfer onto the adsorbent's surface is insignificant, and as a result, formation of a liquid film around the adsorbent occurs and subsequently creates a concentrated gradient (Karthikeyan, Sivakumar and Sivakumar, 2010).

2.1.2 Types of Adsorption

The interaction between the soluble species and the adsorbent can take place either physically by London–van der Waals forces, or chemically by chemical bonding forces.

2.1.2.1 Physical Adsorption

Physical adsorption, or physisorption, takes place when the weak intermolecular attractive forces between the dissolved species and the adsorbent are greater than those between the adsorbates' species themselves (Erkey, 2011). These forces are known as van der Waals (Hu *et al.*, 2011). The selectivity between adsorbates and adsorption sites is governed by the polarity and the size of the adsorbate molecules (Le-Minh *et al.*, 2018).

Van der Waals forces are interactions between molecules without affecting their molecular structure (Zhang and Cresswell, 2016), in other words, without changing the electronic orbital patterns (Hu *et al.*, 2011). They can be repulsive or attracting, depending on the distance between the interacting non-bonded atoms and molecules (Zhang and Cresswell, 2016). The van der Waals force is made up of three different atomic or molecular interactions: Keesom interaction, Debye interaction and London dispersion forces (Saunders, 1951). Kessom and Debye interactions arise from a dipole-dipole and dipole-induced dipole interaction, respectively. On the other hand, London dispersion forces are created by the instantaneous dipole-induced dipoles arising from electronic polarization of interacting atoms (Saunders, 1951). Kessom and Debye interaction forces make a lesser contribution to the interaction in colloidal systems because of the existence of permanent dipoles, unlike London dispersion forces. Therefore, London dispersion forces are the only attractive van der Waals contribution among the nonpolar molecules (Cannio *et al.*, 2012).

Physisorption is generally a multilayer adsorption (Xia *et al.*, 2019). However, formation of a second layer is impossible in the adsorption of gaseous molecules at a temperature at or above boiling point at a constant pressure. The reason for this is that the second layer binding energy of adsorbates and the latent heat of sublimation or vaporization of the adsorbate are equal as a result of the interaction between the gaseous molecules with the liquid or solid adsorbate (Hu *et al.*, 2011).

Since physical adsorption is an exothermic process, it mostly occurs at lower temperatures and decreases by increasing the temperature. Moreover, physical adsorption is desired during the adsorption process as it can be easily reversed due to the low activation energy required resulting from the weak interaction forces explained in this section (Chang, 2016; Cheraghi, Ameri and Moheb, 2016).

2.1.2.2 Chemical Adsorption

Chemical adsorption, sometimes referred to as chemisorption, results from the formation of chemical bonds (strong interaction) between the adsorbents and adsorbates (Mukherjee, Kumar and Zaworotko, 2019). In other words, the electrons transfer between the adsorbate and the adsorbent (Erkey, 2011). Chemisorption is a monolayer adsorption due to the limited active site spaces in the adsorbents surfaces and pores (Xia *et al.*, 2019).

There are two types of chemisorption: activated chemisorption and, less likely, non-activated chemisorption (Cheraghi, Ameri and Moheb, 2016). In the activated chemisorption, the chemisorption rate varies with the temperature due to finite activation energy (8.4~83.7 kJ/mol). On the other hand, the activation energy in the non-activated chemisorption is almost zero, hence the chemical adsorption rate takes place rapidly (Dong *et al.*, 2017).

Although the chemical adsorption is an exothermic process, the extent of chemisorption is directly proportional to the temperature due to high kinetic energy barrier. The chemisorption extends up to a certain limit and thereafter starts to descend. In contrast, an inverse relationship is shown between physisorption and temperature, where the physical adsorption decreases as the temperature increases (Anusha, 2013). In addition, and unlike the physical adsorption, chemical adsorption is an irreversible process since high activation energy is needed to desorb the adsorbates from the active sites (Chang, 2016; Cheraghi, Ameri and Moheb, 2016).

2.2 Types of Adsorbents

Various types of adsorbents are used in the oil & gas and petrochemical industries. Using an optimum adsorbent for the corresponding application is a key factor for an effective adsorption process (Thomas, 2019).

2.2.1 Activated Carbon (AC)

Activated carbon (AC) is used in different adsorption applications and its removal efficiency can be above 90% (Pal, 2017). AC is typically produced from natural resources such as wood and coconuts shells, or from synthesis materials such as petroleum coke and lignocellulosic biomass (Le-Minh *et al.*, 2018). AC is manufactured by thermal decomposition of carbonaceous materials and then activated by superheated steam at 800~1100$^{\circ C}$ (Pal, 2017) producing micropores materials with specific surface area up to 3000 m^2/g (Viswanathan, 2017a). Activated carbon is usually made of 88% Carbon, 6-7% Oxygen, 3-4% inorganic ash, 1% Sulphur, 0.5% Hydrogen and 0.5% Nitrogen. Although raw carbon is nonpolar-hydrophobic in nature, it can also be used to adsorb polar

components by modifying their surface chemical functional groups using different methods (Le-Minh *et al.*, 2018).

Activated carbon is a well-known adsorbent in oil & gas and petrochemical industries. For instance, it is widely used in mercury removal from natural gas (Thomas, 2019) and recovering VOCs from gases (Le-Minh *et al.*, 2018). However, regeneration and recovery of the AC adsorbent is difficult and expensive, in particular when it comes to recovering a powdered AC from aqueous streams. Thus, recent research is focused more on developing composite adsorbents to be incorporated in activated carbon to enhance its efficiency (Pal, 2017).

2.2.2 Zeolites

Zeolites are mineral crystalline compounds that are composed of three dimensional frameworks of SiO_4 and AlO_4 tetrahedra linked through oxygen bridges (Yadav *et al.*, 2018). They are well known for their open structures that are composed of H_2O and exchangeable cations, hence they exhibit high selectivity for cations (Bish, 2013). Changing these exchangeable cations through ion-exchange enhances zeolites adsorptive abilities (Pal, 2017). Zeolites are also unique with their orderly distributed micropores in molecular dimensions (Li, Li and Yu, 2017). Zeolites are found naturally and synthetically and can be classified based on their largest pore windows into small-pore (8-ring), medium-pore (10-ring), large-pore (12-ring) and extra-large-pore zeolites (>12-ring) (Li, Li and Yu, 2017).

In terms of applications, aluminium-rich zeolites are commonly used for dehydration processes, while silica-rich zeolites show hydrophobic characteristics, and are therefore used for the adsorption of nonpolar substances such as hydrocarbons (Pal, 2017). Zeolites are also widely used to reduce CO_2, NO_x, NH_3, and non-methane VOCs concentration in the atmosphere (Li, Li and Yu, 2017). Although zeolites have broad applications, they still have limitations due to, but not limited to, their permeability (Pal, 2017) and inherent charge repulsion between zeolite framework and anionic species (Figueiredo and Quintelas, 2014). Nevertheless, zeolites are still extensively considered by researchers because their versatility allows them to be tailored to meet various industrial requirements (Figueiredo and Quintelas, 2014).

2.2.3 Molecular Sieve (MS)

Molecular sieves (MS) are types of zeolites that consist of sodium and calcium aluminosilicates (Armarego, 2017), so they have similar properties to zeolites. There are four main types of MS:

I. Type 3A Sieves: its pore size is around 3Å. It is suitable to dry liquids and gases such as acetone and ammonia. The material is supplied as beads or pellets.

II. Type 4A Sieves: its pore size is around 4Å. It is suitable to adsorb ethane molecules, and usually used to dehydrate many streams such as chloroform, diethyl ether, benzene, toluene, xylene, and ethyl acetate. 4A sieve is supplied as beads and pellets or powder.

III. Type 5A Sieves: its pore size is around 5Å. It is usually used to adsorb alkanes and higher n-alcohols.

IV. Type 13A Sieves: Its pore size is around 10Å. Due to the larger pore size, 13A can adsorb vast ranges of branched-chain and cyclic compounds.

Although molecular sieves are usually the preferred choice for adsorption processes, especially in the dehydration process, the perceptible degradation in the adsorption capability of regenerative molecular sieves is a serious problem for molecular sieve recycling (Zou *et al.*, 2013). In addition, the high capital and operating cost is another disadvantage of MS adsorbents (Mokhatab, Poe and Mak, 2019).

2.2.4 Activated Alumina (AA)

Activated alumina (AA), the adsorbent used in this study, is broadly utilized at different applications in petroleum and petrochemical industries due to its high mechanical strength and thermal stability (Thomas, 2019). AA possesses unique physical and chemical properties such as high surface area, variety of porosity sizes and wide spectrum of functional groups (Rabia, Ibrahim and Zulkepli, 2018). Furthermore, AA can be regenerated at a high temperature ranging between 300 °C up to 400 °C, and this makes AA economically more viable due to its efficiency in the regeneration and recycling process (Rabia, Ibrahim and Zulkepli, 2018).

Activated alumina is manufactured by dehydroxylating the aluminium (Azarfar *et al.*, 2016). Alumina is classified into four groups of aluminium compounds (Azarfar *et al.*, 2016):

I. Aluminium trihydroxides: its formula is $Al(OH)_3$. It is classified into two compounds: γ-$Al(OH)_3$ (gibbsite) and α-$Al(OH)_3$ (bayerite).

II. Aluminium oxides: its formula is AlOOH (bayerite). It comes in two different compounds:γ-AlOOH (boehmite) and α-AlOOH (diaspore).

III. Transition alumina: it has a large surface area and derived from $Al(OH)_3$ or AlOOH.

IV. Corundum Alumina (α-Al_2O_3): this is a thermally stable phase of aluminium oxide with a hexagonal close-packed oxygen sub-lattice.

The first usage of aluminium was in the water treatment in the beginning of the 1960's as a coagulant in water purification (Rabia, Ibrahim and Zulkepli, 2018). Since then, its composites such

as activated alumina have been developed to be widely used as a desiccant in different industries. However, AA is now applied in a wide range of applications in petroleum and petrochemical industries. In this regard, Jafari and Sabori (2011) have investigated the efficiency of a novel synthesised adsorbent, which is characterised by mixing Al_2O_3 and ZnO, in removing sulphur dioxide from sour natural gas, and comparing its performance with activated alumina and zinc oxide as separated adsorbents. Results have shown that the synthesised adsorbent proves to have better adsorption affinity than the activated alumina and zinc oxide as dependent adsorbents. Adsorption and catalytic oxidation of asphaltenes onto two activated alumina with different sizes was studied by Nassar, Hassan and Pereira-Almao (2011). They claimed that, on the basis of surface area, asphaltenes showed better affinity to nano-alumina than micro-alumina. They referred this result to a high dispersion degree of nanoparticles. However, it was noticed that only few and rare studies were performed to investigate the use of AA adsorbent to adsorb alcohols in the petroleum and petrochemical industries.

Not many studies have been performed to investigate the adsorption efficiency of single or multi fatty alcohols, also known as long chain alcohols, on the activated alumina. Fu and his team (1996) investigated the influence of the presence of 1-propanol, 1-pentanol and 1-decanol on n-decyl benzenesulfonate (n-DBS) adsorption isotherm onto the activated alumina adsorbent. Their study concluded with that the alcohol's chain length has a remarkable effect on the adsorption of n-DBS. The presence of 1-propanol decreases the adsorption of n-DBS, while n-DBS adsorption increases where 1-pentanol and 1-decanol exist. However, it is obvious this study investigated only the effects of different alcohol chains on the amount of surfactant adsorbed on the AA, and not the recyclability of the AA used. Recent studies conducted by Bosman (2019) and Groenewald (2019) were aimed at investigating the adsorption of binary and single long chain alcohols (C-6, C-8 and C-10) from n-decane solvent using different types of AA. Groenewald discussed single adsorption equilibrium, kinetics, and the effects of different factors on the adsorption process, as well as the regeneration of adsorbents and the influence of regeneration on the various AA adsorbents' efficiency. In term of chain length, Groenewald investigated the adsorbents' capacity for all these alcohols and reported that 1-hexanol proves better adsorption affinity onto the three different AA adsorbents. However, regeneration has been performed only for 1-hexanol, so the impact of the alcohol chain length on the regeneration efficiency cannot be obtained from her study (Groenewald, 2019). Bosman studied only the adsorption of single and binary components on the same three different adsorbents used by Groenewald (Bosman, 2019). Nevertheless, regeneration impact on the adsorbents' performance was not discussed by Bosman. Hence, the performance of activated alumina utilized to adsorb different 1-alcohols from n-decane throughout successive and longer

cycles of adsorption/regeneration was investigated in this research work at various regeneration temperatures, including at a lower temperature than that conducted by Groenewald in order to bridge the gap in her study. Moreover, the adsorption temperature in this study was carried out at 65 °C to widen the adsorption data of 1-alcohol from n-decane solvent. In another attempt to increase the adsorption data of the specific application investigated in this study, higher initial concentrations for single-component adsorption systems were investigated, and included their impact on the regenerated activated alumina adsorbent's performance which was discussed and compared to the respective binary-component adsorption systems. Table 2.1 summarizes the differences between the values of the variables taken into account in Bosman, Groenewald and this study.

Table 2.1: Variation in variables' values between Groenewald, Bosman, and current study

Variables	**Values of the Variables**		
	Groenewald (Groenewald, 2019)	**Bosman** (Bosman, 2019)	**Current Study**
Adsorption Temperature (°C)			
- Single-component adsorption system	25, 30, and 35	45	65
- Binary-component adsorption system	-	25 and 45	65
Initial Concentrations (mass%)			
- Single-component adsorption system	0 < x < 2	0.3 - 2	0.5 - 3.0
- Binary-component adsorption system	-	0.3 - 3.3	0.5 - 3.0
Regeneration Temperature (°C)			
- For adsorbents used in single-component adsorption system	205 and 185	-	205, 185, and 165
- For adsorbents used in binary-component Adsorption System	-	-	205, 185, and 165
Number of Adsorption/Regeneration Cycles			
- For adsorbents used in single-component adsorption system	8	-	10 cycles at 205 and 185 °C, and 15 cycles at 165 °C
- For adsorbents used in binary-component Adsorption System	-	-	10 cycles at 205 and 185 °C, and 15 cycles at 165 °C

2.3 Factors Affecting the Adsorption Process

The adsorption process is significantly influenced by a wide range of variables. These variables can be categorised into adsorbent properties, adsorbate properties and the adsorption operational conditions.

2.3.1 Adsorbent Properties

The properties of the adsorbents which affect the adsorption process include specific surface area, porosity, particle size and surface chemical functional groups.

2.3.1.1 Specific Surface Area

Adsorption capacity is significantly influenced by the adsorbents' specific surface area. Specific surface area is the surface area available for adsorption per mass of adsorbent (Kumar *et al.*, 2020). Brunauer-Emmett-Teller (BET) method is usually used to calculate the adsorbents' specific surface area (X. Li *et al.*, 2020). In the physical adsorption, specific surface area is particularly important since larger total surface area means more adsorptive sites that can be occupied by the adsorbate molecules (Le-Minh *et al.*, 2018). Therefore, a larger specific surface area is considered as an indicator for superior adsorption performance.

Activated alumina's specific surface area varies depending on the activated alumina's production techniques (Azarfar *et al.*, 2016). In the literature, it was found that the activated alumina's specific surface area ranges from 500 to 2000 m^2/g (Rabia, Ibrahim and Zulkepli, 2018).

2.3.1.2 Porosity

The porosity of adsorbents can be defined as the void volume ratio to the total volume that includes the void volume (Wang, Li and Xing, 2020). The adsorbent is supposed to be effective when it has a proper porous structure with a large contact area. Moreover, the porous surface should contain a large number of functional groups that help to enhance its adsorption selectivity and capacity (Chen *et al.*, 2016).

Based on the pore size, the pores of adsorbents can be classified into four categories: macroporous (> 50 nm), mesoporous (2–50 nm), micropores (< 2 nm) and narrow micropores (< 1 nm). Pore volume and size of adsorbents are usually measured by using the Barrett Joymer-Halenda (BJH) method, supported by the adsorption isotherm (X. Li *et al.*, 2020). Macroporous adsorbents are usually used to enhance molecules diffusion into the pores, while mesoporous and micropores adsorbents are suitable for medium and small adsorbates molecules, respectively (Thomas, 2019).

Furthermore, micropores offer principal adsorption sites, while the mesopores enhance the intraparticle diffusion which results in shortening the adsorption time (Zhang *et al.*, 2017).

Activated alumina is well known for its high adsorption capacity because of its large pore volume that can be utilized in various adsorption applications (Rabia, Ibrahim and Zulkepli, 2018). For instance, the alkaline treated hydrophilic alumina has a non-uniform pore distribution ranging from 20 to 500 Å, providing large pathways for the adsorbate's journey into the internal surfaces of the activated alumina structure (Mulgundmath *et al.*, 2012).

2.3.1.3 Particle Size

Particle size mainly affects the adsorption rate (Le-Minh *et al.*, 2018), and as a result, it affects the overall performance of the adsorption process (Karimi, Tavakkoli Yaraki and Karri, 2019). The removal of impurities requires diffusion of the adsorbates throughout the interior site of the adsorbent's particle structure, which leads to shortening/lengthening the time required to reach the adsorption equilibrium (Le-Minh *et al.*, 2018).

In general, there are two traditional shapes for adsorbents: i) Extrudate particles (needle shaped particles); and ii) Spherical particles (Belekar and Dhoble, 2018). Spherical adsorbents have been proven to have some benefits over extrudate adsorbents such as lower pressure drop (in the same range of mesh size), higher attrition resistance and better particle flow performance (Thomas, 2019).

2.3.1.4 Surface Chemical Functional Groups

Adsorbent's surface chemical functional groups are responsible for adsorption of adsorbates besides the morphology structure of the adsorbent. The nature of raw materials and modification or production methods like nano-casting technique, chemical, heating and electrochemical treatment methods are responsible for the chemical surface functional groups of the various adsorbents (Azarfar *et al.*, 2016; Zhang *et al.*, 2017).

The γ-Alumina is a unique activated alumina compound which is chemically closed to the hydroxyl (OH) groups because of the existence of OH groups and coordinated unsaturated (CUS) Lewis acid sites on the surfaces that make it a bi-functional support. Hence, γ-alumina attracts the chemical species with the OH groups such as alcohols, and it is open to be concurrently attacked by nucleophiles at the CUS sites (Azarfar *et al.*, 2016).

2.3.2 Adsorbate Properties

Adsorbates' properties such as molecular structure and weight, molecular polarity and boiling point have notable effects on the adsorption process.

2.3.2.1 Molecular Structure and Weight

Adsorption capacity is affected by the molecular size and shape of absorbents. Molecular size is defined by the molecule's cross-sectional area (Zhang *et al.*, 2017). Although smaller molecules are obviously more easily accessible to the adsorbent's active sites, the shape of the adsorbate's molecule also has an impact on the adsorption capacity which may be more crucial than the molecules' size.

In their investigation of VOCs adsorption onto novel carbon adsorbents, Xueyang Zhang et al. pointed out that the affinity of carbon adsorbent to adsorb *p*-xylene is higher than its affinity to adsorb *o*-xylene and *m*-xylene, although the *p*-xylene cross-sectional area is higher than the others (Zhang *et al.*, 2017). They suggested that it is due to the differences in the molecular shape that is derived from the different position of methyle side chain in the xylene molecule.

Physical adsorption is also affected by the molecular weights of the adsorbates. Adsorbents strongly tend to adsorb higher molecular weight components; however, they are limited practically since this often means having to increase the molecular size (Le-Minh *et al.*, 2018).

2.3.2.2 Molecular Polarity

Generally, polar adsorbates tend to be adsorbed by polar adsorbents, while non-polar adsorbates show higher tendency to get adsorbed by non-polar adsorbents. Neverthless, it may differ due to the existence of some polar inorganic impurities (Zhang *et al.*, 2017).

Activated alumina is a polar adsorbent with a strong affiliation to alcohols, as the alcohols are polar components as well. Thus, activated alumina can be considered as a viable alternative to purify the paraffin streams from the 1-alcohols (Bosman, 2019; Groenewald, 2019).

2.3.2.3 Boiling Point

Species at a higher boiling point have a higher tendency to be adsorbed by the adsorbents during the adsorption process, because of their rebound from the surface and expulsion from inside the adsorbents are less vigorous (Le-Minh et al., 2018). In other words, adsorbates having a higher boiling point which can easily be adsorbed due to stronger intermolecular forces (Xiang et al., 2020).

During the competitive adsorption process, adsorbates with lower boiling point may be easily replaced by those that having a higher boiling point (Zhang et al., 2017). Several reports reached the same conclusion including that of Wang et al. (2012) and Zhang et al. (2019) where they emphasized that the adsorbates with lower boiling points were displaced by species with higher boiling points in multi-adsorption systems.

2.3.3 Adsorption Operational Conditions

2.3.3.1 Temperature

Since adsorption is an exothermic process, the adsorption capacity is enhanced at lower temperature (Karimi, Tavakkoli Yaraki and Karri, 2019). Raising the adsorption temperature may, however, improve the molecular diffusion, and as a result, it enhances the adsorption kinetic rate. Furthermore, in higher temperature ranges, chemical adsorption may occur as a result of increasing the interaction energy between the adsorbates and the adsorbent (Zhang *et al.*, 2017).

As reported by Ramirez et al. (2004) Qian et al. (2015) and Mao et al. (2016), the adsorption capacity of organics increased when the temperature was decreased. The adsorption rate was compared at different temperatures by Reid and Thomas, Fletcher et al and Wang et al (Reid and Thomas, 2001; Fletcher, Yüzak and Thomas, 2006; Wang *et al.*, 2015) and they all concluded that the adsorption rate increased when the adsorption was carried out at higher temperatures.

To sum up, increasing the temperature inhibits the physical adsorption, while it improves the molecular diffusion and the potential of chemical adsorption.

2.3.3.2 Pressure

The pressure impact is more perceptible in the adsorption of gases, in particular for the physical adsorption, where the adsorption capacity and kinetic rate are proportional to the pressure. Although chemical adsorption is not much affected by the minor changes in the pressure, very high pressures are favourable for chemisorption (Anusha, 2013).

In this study, the pressure impact will not be discussed as the system investigated was in liquid phase and the experiments were performed only at atmospheric pressure.

2.3.4 Other Adsorption Conditions

Besides adsorbent properties, adsorbate properties and adsorption operational conditions, and other conditions such as the initial adsorbate concentration and co-existing adsorbates in multi-adsorption systems, can influence the adsorption process.

2.3.4.1 Initial Concentration

A wide range of studies have investigated the impact of initial concentration of adsorbates on the equilibrium of the adsorbent's loading. Guan et al. investigated the influence of initial concentration of Cu^{2+} on the adsorption performance of hydroxyapatite (Guan *et al.*, 2014). He reported that the removal of Cu^{2+} declined from 99.64% to 76.68% when its initial concentration was increased from 20 mg/L to 200 mg/L due to a lack of active sites on the hydroxyapatite surface at a high initial concentration of Cu^{2+}. On the other hand, the equilibrium loading on the hydroxyapatite surface increased by increasing the initial concentration of the adsorbate, as the mass transfer driving force was increased accordingly. In a recent study conducted by Zhao et al. (2020), they pointed out that the uptake of gold ions increased on the novel modified MOFs adsorbent's surface when the initial concentration of the adsorbate was increased in the solution.

To conclude, initial concentration of the adsorbate has a significant effect on the adsorption process. Equilibrium loading is increased if the initial concentration of the adsorbates is higher. On the contrary, the removal efficiency from the solution decreased by increasing the initial concentration at a constant adsorbent mass.

2.3.4.2 Adsorbate-Adsorbate Interaction

It is common in industry to have more than one impurity in the different streams. Purification processes then mainly aim to deal with and remove all these impurities. Therefore, conducting more research is important to understand the multicomponent adsorption mechanism in order to help choose a proper adsorbent for the corresponding applications. To the author's knowledge, only Bosman (Bosman, 2019) has investigated binary adsorption of 1-hexanol and 1-decanol from n-decane using activated alumina. However, she did not investigate the recyclability of the adsorbents used.

In a multicomponent adsorption process, there are three different types of interactions that can take place between the adsorbates (Girish, 2017):

I. Synergistic interaction: where the presence of multiple impurities enhances the adsorption of the targeted adsorbate.

II. Antagonistic interaction: where the presence of multiple impurities inhibits the adsorption of the targeted adsorbate.

III. Non-interaction: where the presence of multiple impurities has no impact on the adsorption of the targeted adsorbate.

The above three classifications can be investigated by making a comparison between the equilibrium loading of the targeted adsorbate in a multicomponent adsorption system, with its equilibrium loading in a single-component adsorption system, while keeping a constant initial concentration for the respective adsorbate using the following equation (Girish, 2017):

$$R_i = \frac{q_{e,i}}{q_e} \quad [2.2]$$

where R_i is a ratio of the equilibrium loading of an adsorbate (i) in a multicomponent adsorption system with its equilibrium loading in a single-component adsorption system; $q_{e,i}$ is the equilibrium loading of an adsorbate (i) in a multicomponent adsorption system, and q_e is the equilibrium loading of an adsorbate (i) in a single-component adsorption system.

The interaction is considered as synergistic when $R_i > 1$, antagonistic when $R_i < 1$ and non-interaction when $R_i = 1$.

2.4 Adsorption of Alcohols from Paraffins

Adsorption of alcohols from alkane solvents on Activated Alumina has scarcely been investigated. Bosman (2019) and Groenewald (2019), however, studied the adsorption of 1-alcohols from a n-alkane solvent. Both of them investigated the adsorption of 1-hexanol, 1-octanol and 1-decanol from n-decane solvents. Bosman investigated single and binary-component adsorption systems, while Groenewald discussed only single-component adsorption systems using activated alumina adsorbents. The systems were investigated at different adsorption temperatures and initial concentrations of the adsorbates.

Although Bosman and Groenewald investigated the adsorption of 1-alcohols from n-decane on different Activated Alumina adsorbents, recyclability of utilized adsorbents was studied only by Groenewald. To the best of knowledge of the author, no open data is available regarding the reusability of activated alumina used to adsorb binary 1-alcohols. This introduces a gap that would be bridged by this study. Moreover, expanding the adsorption temperature range could contribute to the data of these systems in particular.

2.5 Adsorption Equilibrium Modelling

The adsorption equilibrium is an essential thermodynamic property of the adsorption phenomenon to determine the efficiency of the separation process and to optimize the selection of adsorbent for a specific adsorption system (Sircar, 2020). Theoretical adsorption isotherms are usually used to describe the adsorption equilibrium at constant temperature (Kumar *et al.*, 2019). Different

adsorption isotherm models are described based on a simple physical demonstration of adsorption and desorption, while others are purely empirical models (Piccin, Dotto and Pinto, 2011).

For single-component adsorption isotherm systems, most of the reviewed studies (such as Nassar et al., 2011; Azarfar et al., 2016; Zhao et al., 2020) fitted Langmuir and Freundlich models to their experimental equilibrium data to verify which model better describes the systems studied. However, other equilibrium isotherm models were discussed like Brunauer–Emmett–Teller (BET) and Dubinin-Radushkevich (D-r) as reported in (Azarfar *et al.*, 2016; Zhao *et al.*, 2020). On the other hand, it was observed that the commonly used and discussed models for multi-component adsorption systems were extended from single adsorption models (Girish, 2017; Shukla *et al.*, 2019; Al-Ghouti and Da'ana, 2020; Laskar and Hashisho, 2020). Hence, the accuracy of single-component adsorption isotherms is crucial to the reliability of the multicomponent isotherms (Laskar and Hashisho, 2020).

2.5.1 Single-Component Adsorption Equilibrium Modelling

Langmuir, Freundlich and Sips Isotherms models have been discussed in this study for the single-component adsorption systems. Besides the simplicity of these models, they were chosen to study the adsorption behaviour because they provide the essential information required by the industry, such as the reversibility of the adsorption process.

2.5.1.1 Langmuir Isotherm Model (LM)

Langmuir isotherm model (LM) was developed first which describes the gas adsorption onto different types of adsorbents (Langmuir, 1918). According to the Langmuir theory, the adsorption process is based on a kinetic principle in which the rates of adsorption and desorption are equal for corresponding molecules (Al-Ghouti and Da'ana, 2020). The LM equation is denoted by Equation 2.3 (Laskar and Hashisho, 2020):

$$q_e = \frac{q_m K_L C_e}{1 + K_L C_e} \qquad [2.3]$$

where q_e and q_m are equilibrium and maximum adsorbent loading (g/g), respectively, K_L has a temperature-dependent Langmuir affinity coefficient (m^3/g), and C_e is an equilibrium adsorbate concentration in the bulk solution (mass%).

The LM is based on the following assumptions (Laskar and Hashisho, 2020; Torres-Perez *et al.*, 2020):

I. Adsorption is localized and occurs at definite and at a fixed number of sites.

II. Adsorption is monolayer, which means that each site can hold no more than one adsorbate molecule.

III. All adsorption sites are identical and equivalent to each other, i.e. homogenous energetic sites.

IV. There is no interaction between the adsorbed molecules, although they are located on adjacent sites.

Although the LM assumptions are rarely valid, the model is widely used to describe adsorption equilibrium mainly because of its simplicity in its solutions (Laskar and Hashisho, 2020).

2.5.1.2 Freundlich Isotherm Model (FM)

Freundlich isotherm model (FM), the first known adsorption isotherm (Freundlich, 1906), was basically an empirical model, which its description was afterwards based on the hypothesis that the reactive sites over the adsorbate are distributed exponentially with the heat of the adsorption process (Shukla et al., 2019; Yungui Li et al., 2020). The FM is not limited to the monolayer adsorption (Al-Ghouti and Da'ana, 2020) and applied to non-ideal and reversible multilayer adsorption on heterogeneous surfaces (Laskar and Hashisho, 2020; Y. Li *et al.*, 2020). The FM model is represented by Equation 2.4 (Laskar and Hashisho, 2020):

$$q_e = K_f C_e^{\frac{1}{n}} \qquad [2.4]$$

where K_f is Freundlich's capacity coefficient representing the adsorption affinity [(mg/g)/(mg/L)$^{1/n}$] and n is a dimensionless exponential constant related to the favourability of the adsorption. The adsorption is favourable when $0 < 1/n < 1$, and it is irreversible when $1/n = 1$. Both K_f and n parameters are dependent on temperature (Al-Ghouti and Da'ana, 2020).

The FM is based on the following assumptions:

I. Adsorption may occur in multilayers.

II. Adsorption may occur on heterogeneous sites with different levels of affinity and adsorption heats.

This model does not approach Henry's law at low loadings, is not suitable for low pressure systems, and is limited at high concentrations (Laskar and Hashisho, 2020). Nevertheless, the FM is widely investigated and used because the equation is adequate in describing a nonlinear adsorption system with a narrow range of adsorbate concentrations. It can be easily used due to the mathematical simplicity of the equation, and because it can describe the adsorption process on surface adsorption

sites which are energetically heterogeneous, a condition that is commonly found in adsorption systems (Proctor and Toro-Vazquez, 2009).

2.5.1.3 Sips Isotherm Model (SM)

Sips isotherm model (SM), a three-parameter model and sometimes referred to as Langmuir-Freundlich model, expresses the integration of Langmuir and Freundlich models (Awad *et al.*, 2020), thereby addressing the limitation of FM by exhibiting a finite limit at sufficiently high concentrations (Saadi *et al.*, 2015). As a result, this model is reduced to FM at a low adsorbate concentration, while it predicts the LM at a high concentration of adsorbate (Ayawei, Ebelegi and Wankasi, 2017). The SM is valid for predicting the heterogeneous adsorption systems without adsorbate-adsorbate interactions between the adsorbed molecules (Saadi *et al.*, 2015). The SM is denoted by the Equation 2.5 (Awad *et al.*, 2020):

$$q_e = \frac{q_m K_s C_e^{1/n_s}}{1 + K_s C_e^{1/n_s}} \qquad [2.5]$$

where K_s is Sips constant (L/g) and n_s is Sips model exponent that is often regarded as the heterogeneity factor which could stem from the adsorbent, the adsorbate, or from them both (Awad *et al.*, 2020). As reported by Saadi (Saadi *et al.*, 2015), the value of n_s is usually greater than unity, and the degree of the system's heterogeneity is increased with the increase of the value of n_s . On the other hand, the homogeneous adsorption system is represented when the value of n_s is equal or closer to 1, and subsequently, the Langmuir equation is then applicable to the adsorption system.

Although SM shares the same disadvantage with FM in that both models do not follow Henry's law at low pressures (Al-Ghouti and Da'ana, 2020), Sips model is considered as the most applicable isotherm model among the three-parameter monolayer adsorption isotherm models (Saadi *et al.*, 2015).

2.5.2 Multi-Component Adsorption Equilibrium Modelling.

In reality, most streams in oil & gas and petrochemical industries are associated with more than one impurity and the aim of the adsorption process is to remove all of them. Thus, understanding the mechanism of multi-adsorption is very important. Moreover, the influence of competitive interaction among the different components on the overall adsorption process should be considered (Girish, 2017). Therefore, single-component adsorption isotherm models are not compatible with the multi-component adsorption systems. There are many multi-component isotherm models which describe the multi-adsorption systems, however, only three models were incorporated in this study to discuss the binary-component adsorption systems.

2.5.2.1 The Extended Langmuir Isotherm Model (ELM)

The Extended Langmuir isotherm is the most simplistic model for multi-component adsorption (Shukla *et al.*, 2019). It was developed by Butler and Ockrent (1929) and has made the same assumptions as the Langmuir isotherm model for single components (Laskar and Hashisho, 2020).

The Extended Langmuir Isotherm Model for the two-component adsorption system is denoted by Equation 2.6 and 2.7 (Laskar and Hashisho, 2020):

$$q_{e,1} = \frac{q_{m,1} K_{L,1} C_{e,1}}{1 + K_{L,1} C_{e,1} + K_{L,2} C_{e,2}} \quad [2.6]$$

$$q_{e,2} = \frac{q_{m,2} K_{L,2} C_{e,2}}{1 + K_{L,1} C_{e,1} + K_{L,2} C_{e,2}} \quad [2.7]$$

where $q_{e,1}$ and $q_{e,2}$ are the equilibrium adsorbent capacities for component 1 and 2, respectively; (mg/g), $C_{e,1}$ and $C_{e,2}$ are equilibrium adsorbates concentration of components 1 and 2, respectively, in the bulk solution (mass%); $q_{m,1}$ and $q_{m,2}$ are maximum equilibrium adsorbent capacities for component 1 and 2, respectively; and (mg/g), $K_{L,1}$ and $K_{L,2}$ are respective Langmuir affinity coefficients of components 1 and 2 which are obtained from their corresponding single adsorbate adsorption isotherms (m^3/g).

The parameters of Equation 2.6 and 2.7 are calculated from the respective single-component adsorption systems for each component at the same operational conditions, which suggests that there is no competition between the different types of adsorbed components. Thus, these equations were extended further by Kurniawan et al. (Kurniawan *et al.*, 2012) to include fractional loading of each adsorbed molecule onto the adsorbent. The proposed equation is denoted by Equation 2.8:

$$q_{e,i} = \frac{q_{max,bin}\, K_{L,i(bin)}\, C_{e,i}}{1 + \sum_{j=1}^{N} K_{L,j(bin)} C_{e,j}} \quad [2.8]$$

$$q_{max,bin} = q_{1,sin}\Theta_1 + q_{2,sin}\Theta_2 \quad [2.9]$$

$$K_{L,1(bin)} = K_{L,1(sin)} e^{\frac{-\Theta_2}{\Theta_1}} \quad [2.10]$$

$$K_{L,2(bin)} = K_{L,2(sin)} e^{\frac{-\Theta_1}{\Theta_2}} \quad [2.11]$$

where Θ_1 and Θ_1 are constants and represent fractional loading of each adsorbed molecule, $q_{max,bin}$ is a constant of the total maximum adsorbed species (component 1 and 2), $K_{L,1(bin)}$ and $K_{L,2(bin)}$ are Langmuir constants of adsorptivity of the respective adsorbates in the binary-component adsorption system. From Equation 2.8 through 2.11, it can be observed that the amount of adsorbed species in

binary systems is expected to be less than the those adsorbed in single systems (Equation 2.9), and the adsorption potential in binary systems is expected to be less when compared to the respective single systems (Equation 2.10 and 2.11).

2.5.2.2 The Extended Freundlich Isotherm Model (EFM)

EFM was originally developed by Fritz and Schlunder (1981), and the evaluation of correlating factors was modified by McKay and Al-Duri (1991) by reducing the extensive calculation procedure in 1991. The EFM assumes that the adsorbed molecules interact with each other in heterogeneous systems (Girish, 2017). The EFM is denoted by Equation 2.12 and 2.13 (Girish, 2017):

$$q_{e,1} = \frac{K_{f,1} C_{e,1}^{\left(\frac{1}{n_1}\right)+x_1}}{C_{e,1}^{x_1} + y_1 C_{e,2}^{z_1}} \qquad [2.12]$$

$$q_{e,2} = \frac{K_{f,2} C_{e,2}^{\left(\frac{1}{n_2}\right)+x_2}}{C_{e,2}^{x_2} + y_2 C_{e,2}^{z_2}} \qquad [2.13]$$

where $K_{f,1}$ and $K_{f,2}$ are Freundlich constants for adsorbates 1 and 2, respectively, which are obtained from the respective single-component adsorption systems, the constants x_1, y_1, z_1 and x_2, y_2, z_2 are obtained from the set of experimental values of $q_{e,1}$ vs $C_{e,1}$ and $q_{e,2}$ vs $C_{e,2}$, respectively, by minimizing the error in the non-linear regression analysis (Girish, 2017), and n_1 and n_2 are obtained from the experimental data of individual Freundlich isotherms.

2.5.2.3 The Extended Sips Isotherm Model (ESM)

The extended Sips isotherm model is applicable only to the heterogeneous systems (Al-Ghouti and Da'ana, 2020). The ESM is presented by Equation 2.14 (Girish, 2017):

$$q_{e,i} = \frac{q_{m,i} K_{s,i} C_{e,i}^{1/n_{s,i}}}{1 + \sum_{j=1}^{N} K_{s,j} C_{e,j}^{1/n_{s,i}}} \qquad [2.14]$$

where the parameters $q_{m,i}$ and $K_{S,j}$ are obtained from the experimental data measured from the single-component Sips isotherm for the corresponding adsorbates, while $n_{s,j}$ is determined by fitting the model into multicomponent adsorption data (Girish, 2017). Similar to the single-component Sips isotherm, when n_s value is greater than 1, Freundlich isotherm is approached, while when n_s value is equal to or closer to 1, the model is reduced to Langmuir isotherm (Girish, 2017).

2.6 Adsorption Kinetic Modelling

Adsorption kinetics is the measurement of adsorption uptake with respect to time at given operational conditions, and is applied to measure the adsorbate's diffusion through the adsorbent's pores (Saha and Grappe, 2017). In order to showcase any adsorption processes of inherent mechanisms, it is necessary to estimate the best suitable adsorption rate expression by using the adsorption kinetic modelling methodology, which is also used to determine the adsorption rate (Karimi, Tavakkoli Yaraki and Karri, 2019; Zou *et al.*, 2019). What is more, the adsorption kinetic modelling is a method to determine whether the adsorption is chemisorption or physisorption (Zou *et al.*, 2019).

Various studies (Banerjee and Chattopadhyaya, 2017; Liu *et al.*, 2020; Xiang *et al.*, 2020) have pointed out that the adsorption rate is affected by the contact time between the solutions and the adsorbents. At the beginning of adsorption, the adsorption rate happens rapidly and slows down over time until the equilibrium phase is reached. However, studies such as (Zou *et al.*, 2019) suggest that the adsorption mechanism may vary with the porous structure at different adsorption times, while Nayakasinghe et al. (2017) propose that the adsorption kinetics of different alcohols on silicate adsorbent vary according to molecular size. In their study of toxic dye and tartrazine removal from aqueous solutions by a developed low-cost agricultural by-product adsorbent, Banerjee and Chattopadhyaya (2017) reported that a higher temperature resulted in a faster adsorption rate. Based on these studies, it can be concluded that the adsorption kinetic is governed by many factors: properties of adsorbates, adsorbents and the adsorption operational conditions.

2.6.1 Types of Adsorption Kinetic Modelling

The adsorption kinetic models are classified into adsorption reaction and diffusion models (Karimi, Tavakkoli Yaraki and Karri, 2019). The main difference between the two types is that the adsorption reaction models, such as the Pseudo-First and Second-Order and Elovich Models, were developed based on the prevailing reaction kinetics of the system, whereas adsorption diffusion models, such as Intra-Particle Diffusion Model (Weber-Morris), are based on the adsorption stages described in Section 2.1.1 (Karimi, Tavakkoli Yaraki and Karri, 2019).

According to the literature, adsorption reaction models have been widely applied to study the adsorption kinetics. However, they cannot describe the physical behaviour well and, consequently, the mass transfer and rate-controlling steps cannot be investigated by using these adsorption reaction models only. Hence, it is necessary to consider diffusion models when investigating physical diffusion in the adsorbents (Senthil Kumar *et al.*, 2012; Safwat and Matta, 2018; Wang and Guo, 2020).

In this work, the adsorption kinetics were studied using PseudoFirst and Second-Order Models, the Elovich Model, and Intra-Particle Diffusion Model (Weber-Morris) as they are simple to implement, and they provide useful preliminary information about the adsorption kinetics.

2.6.1.1 Pseudo-First-Order Model (PFO)

The PFO model was first represented by Lagergren in 1898 for adsorption of malonic acid and oxalic acid on the charcoal adsorbent and it is perhaps the first model to describe the liquid-solid adsorption systems based on solid capacity (Y. HO, 2004). The PFO model assumes that the adsorption rate is proportional to the available unoccupied sites (Zou *et al.*, 2019; Zhao *et al.*, 2020).

The Pseudo-First-Order Model equation is denoted by Equation 2.15 (Wang and Guo, 2020):

$$q_t = q_e\,(1 - e^{-K_1 t}) \qquad [2.15]$$

where q_t is the adsorbent loading at the corresponding time, t, and K_1 is Pseudo-First-Order rate constant (min^{-1}).

Pseudo-First-Order Model assumes the following (Wang and Guo, 2020):

I. The adsorbates initial concentration is very high;

II. The adorption process has mainly taken place in an early stage; and/or,

III. The adsorbent has few active sites for adsorption.

2.6.1.2 Pseudo-Second-Order Model (PSO)

Although the PSO was first proposed in the middle of the 80's, it became more popular in 1999 when it was developed by Ho and McKay (1999). It was applied earlier for adsorbing gas onto solids, and in recent years it has been widely used to describe the adsorption of pollutants from aqueous solutions (Ho, 2006).

The PSO model assumes that the adsorption rate is constant with the time and that the adsorbed amount at equilibrium determines the total number of occupied sites. Therefore, it is considered as a special kind of Langmuir kinetics (Zou *et al.*, 2019). This model is mainly fitted to the chemisorption; however, it can be used for the physisorption systems as well (Tian *et al.*, 2017). The model equation is denoted by Equation 2.16 (Wang and Guo, 2020):

$$q_t = \frac{q_e^2 K_2 t}{1 + q_e K_2 t} \qquad [2.16]$$

where K_2 is Pseudo-Second-Order rate constant (mg/g·h).

The advantage of the PSO model is that the equilibrium loading and the initial adsorption rate can be estimated not only from the experiments, but it can also be calculated from the model (Ho, 2006).

In their study, Wang and Guo (Guo and Wang, 2019) ended up concluding that the PSO can exhibit three conditions:

I. If the initial concentration of adsorbate is low;

II. If the adsorption has taken place at the last stage; and/or,

III. If the adsorbent is abundant with active sites.

2.6.1.3 Elovich Model (EM)

The EM was first established by Zeldowitsch in 1934, when it was used to describe the rate of adsorption of carbon monoxide on manganese dioxide (Qiu *et al.*, 2009). The basic hypotheses of EM are: (i) the activation energy increased with adsorption time, and (ii) the adsorbent's surface is heterogeneous (Wang and Guo, 2020). The EM model is typically used to model chemisorption processes (Karimi, Tavakkoli Yaraki and Karri, 2019). The EM model can be represented by Equation 2.17 (Safwat and Matta, 2018).

$$q_t = \frac{1}{ß}\ln(1 + \alpha ß t) \qquad [2.17]$$

where $ß$ (mg/g) and α (mg/g.min) are the surface coverage and initial adsorption rate constants, respectively.

2.6.1.4 Intra-particle Diffusion Model (IPDM)

One of the widely investigated diffusional models was deduced by Weber and Morris (W&M) in 1963 to describe the internal diffusion of the adsorbates inside the pores of the adsorbents (Wang and Guo, 2020). The W&M is denoted by Equation 2.18 (Senthil Kumar *et al.*, 2012).

$$q_t = K_{Ip}\sqrt{t} + \Theta \qquad [2.18]$$

where K_{IP} is intra-particle diffusion constant rate, and Θ is a constant related to the boundary layer thickness. The greater value of Θ, the greater effect the boundary layer has on the adsorption process (Senthil Kumar *et al.*, 2012).

As reported by Safwat and Matta (2018), the plot of q_t vs $\sqrt{t}$ of the intra-particle diffusion model may be divided into three linear portions: (i) the first portion is usually ascribed to a boundary layer

diffusion step (film diffusion); (ii) the second portion is attributed to intra-particle diffusion; and (iii) the third portion is ascribed to the final equilibrium stage. The plot of q_t vs $\sqrt{t}$ is a straight line; however, the intra-particle diffusion is a slow process that makes Equation 2.18 develop a curvature plot (William Kajjumba *et al.*, 2019). Therefore, Equation 2.18 should be applied at different points to determine the three different portions (William Kajjumba *et al.*, 2019). Should the extension of the straight-line pass through the origin, the sole rate-controlling step is governed by the intra-particle diffusion. Otherwise, the sole rate-controlling step is governed by multiple mechanisms together with the intra-particle diffusion (Senthil Kumar *et al.*, 2012; Wang and Guo, 2020).

2.7 Regeneration of Adsorbents

The regeneration technique is a frequently used recovery process of saturated adsorbents using feasible methods (Momina, Shahadat and Isamil, 2018). The regeneration of adsorbents aims mainly at reusing the spent adsorbents for several adsorption cycles due to environmental and economic concerns, as well as to valorise the desorbed species for other applications (Khas and Delhi, 2013; Khalil *et al.*, 2020). In addition, regeneration performance and reusability are important to assess the feasibility of adsorbents (Liu *et al.*, 2020; Su *et al.*, 2020). The regeneration efficiency (RE) can be determined by Equation 2.19 (Shah, Pascaline and Alappat, 2014):

$$RE = \left(\frac{q_n}{q_0}\right) * 100 \qquad [2.19]$$

where q_n and q_0 are the total adsorption capacities for the cycle number n and the initial total adsorption capacity, respectively.

2.7.1 Regeneration Methods

A wide range of regeneration methods are typically used in different industries such as thermal, pressure swing, desorbent displacement, purge with inert gases, vacuum, microwave, ultrasound, chemical, oxidative, ozone regeneration and bio-regeneration (Cavalcante, 2000; McQuillan, Stevens and Mumford, 2018; Momina, Shahadat and Isamil, 2018). Combined methods such as thermochemical regeneration and electrochemical are well known in the industry as they have produced better results (Momina, Shahadat and Isamil, 2018). However, the most common regeneration techniques used in industry are pressure swing, chemical and thermal regeneration methods.

2.7.1.1 Pressure Swing Regeneration Method

The pressure swing regeneration method is typically a cyclic batch process (Cavalcante, 2000). The regeneration of adsorbents using this method is achieved by decreasing the system pressure to the

partial pressure of the adsorbate in the fluid phase (Cavalcante, 2000; Grande, 2012). Pressure swing regeneration is more suitable and widely used in the gaseous adsorption systems (Gabelman, 2017). Normally, this method is used for bulk separation processes and where the separated species are quite important for reuse purposes (Grande, 2012; Thomas, 2019).

The pressure swing regeneration method is generally associated with lower energy consumption when compared to other technologies (Grande, 2012). However, it exhibits limitations for low adsorbed amounts and for strongly bonded adsorbates which have adsorbed to active sites where the desorption process requires very low pressure (Cavalcante, 2000).

2.7.1.2 Chemical Regeneration Method

Chemical regeneration methods use solvents and/or chemical species to remove adsorbates from the adsorbents, or use chemicals that behave as oxidants in under-supercritical or subcritical conditions to decay the adsorbed molecules (Momina, Shahadat and Isamil, 2018; Momina, Shahadat and Ismail, 2020). This method is governed by the pH of the solution, oxidation rate and degradation by complexion (Momina, Shahadat and Isamil, 2018). Hence, the proper choice of solvent, which shows higher affinity for the adsorbates, is crucial for this method (Gabelman, 2017).

Although chemical regeneration is a cost-effective and a widely used method, the surface properties of adsorbents can be modified or destroyed by the decomposition of adsorbents and may lead to pores being blocked which result in a severe drop in the adsorbent's capacity (McQuillan, Stevens and Mumford, 2018; Momina, Shahadat and Isamil, 2018; Nunes *et al.*, 2020). Furthermore, a secondary treatment is usually required in order to achieve a high recovery of the separated molecules (McQuillan, Stevens and Mumford, 2018). Above all, the solvent may remove many adsorbates making the residual more toxic than the effluent initially treated (Nunes *et al.*, 2020).

2.7.1.3 Thermal Regeneration Method

Similar to the pressure swing method, thermal regeneration is normally operated in a cyclic batch mode where at least two adsorption columns are required: one under adsorption process, while the other one is performing a regeneration cycle (Cavalcante, 2000). It is typically used for eliminating strongly adsorbed molecules by breaking the bonds formed between the adsorbate and adsorbent through heating up the system to a suitable temperature (Cavalcante, 2000; Momina, Shahadat and Isamil, 2018). This method is used mainly when a highly purified stream is required (Thomas, 2019). Thermal regeneration is usually associated with other methods such as inert purge or low pressures (Cavalcante, 2000).

Thermal regeneration techniques require high energy consumption (Cavalcante, 2000; McQuillan, Stevens and Mumford, 2018; Momina, Shahadat and Isamil, 2018). Most of the time, this leads to a change in surface morphology which may result in a significant drop in the adsorption capacity (Momina, Shahadat and Isamil, 2018). What is more, thermal regeneration at high temperatures may enhance the chances of the chemisorption process during the regeneration cycle, and cause a further drop in the total adsorption capacity (Dutta *et al.*, 2019).

2.7.2 Thermal Regeneration of Activated Alumina

Various studies have been conducted and have discussed the impact of the thermal regeneration method on the performance of various types of activated alumina applied to adsorb different species (Abd-Elrahman *et al.*, 2011; Chen and Ahn, 2011; Auta *et al.*, 2013; Rafique *et al.*, 2013; Auta and Hameed, 2014; Wasti and Ali Awan, 2016; Abou-Ziyan *et al.*, 2017; Hu *et al.*, 2017; Neubauer *et al.*, 2017; Groenewald, 2019). In all these studies, regenerated activated alumina showed consistent performance over consecutive cycles.

Chen and Ahn (2011) studied the performance of two types of mesoporous alumina (MA) used to capture carbon dioxide from the air. For 5 successive cycles, both types demonstrated stable efficiency when thermal regeneration was implemented at 100 °C and 200 °C, despite a sudden decline in adsorption capacity in the second cycle. A slightly higher performance was observed at a higher regeneration temperature though. The stability of the performance of activated alumina after the notable drop in its capacity in the second cycle was also reported by Auta and Hameed (2014). Auta and Hameed investigated the elimination of carbon dioxide from nitrogen gas using modified activated alumina, as well as the performance of the applied adsorbent over 13 adsorption/regeneration cycles. Thermal regeneration at 110 °C was applied to the saturated adsorbents, and the efficiency dropped by 6.4% in the second cycle, whereafter the efficiency remained stable throughout the next cycles. The abrupt drop in the second cycle was ascribed to an amount of chemisorbed carbon dioxide which was retained after the regeneration cycle. A study conducted by Rafique et al. (2013) revealed that the activated alumina performance utilized to purify drinking water from fluoride was up to 85% at the fifth adsorption cycle when the exhausted adsorbent regenerated at 450 °C for 30 minutes.

However, and to the best of author's knowledge, one study investigated the thermal regeneration of AA which was utilized to adsorb 1-alcohols from n-alkane solvents. This study was carried out by Groenewald (Groenewald, 2019). Groenewald discussed the regeneration of three AA adsorbents used to adsorb 1-hexanol from n-decane. The initial concentration of the system investigated was 1.5 mass%. The regeneration experiments were carried out at 185 °C and 205 °C for the duration of

1 hour. A fairly consistent performance over 7 cycles was observed for the three adsorbents, whereafter a drastic decline in the adsorption loading was reported in the eighth cycle. The efficiency of adsorbents was higher at the greater regeneration temperature of 205 °C.

After a comprehensive literature review, and to the author's knowledge, no open data was found that investigated the thermal regeneration effects on the activated alumina utilized to adsorb binary 1-alcohols from n-alkane solvents, which introduced a lacuna that will be filled by this study. Thermal regeneration of AA adsorbents applied in a single-component adsorption system was discussed in this study though. The reason for this is to make a comparison between the impact of the thermal regeneration of the AA adsorbent applied in single-component and binary-component adsorption systems. Moreover, the influence of the thermal regeneration temperature on the AA adsorbents used in systems with different initial concentrations could further contribute to the data of these specific systems as there are no open data that considers the influence of different initial concentrations on the regeneration behaviour of the systems concerned. Furthermore, the regeneration of adsorbents utilized to adsorb 1-alcohols from n-decane solvents at the adsorption temperature of 65 °C was not found in the literature, so this study will try to bridge this gap. In addition, no comprehensive studies were done at the three different temperatures to assess the regeneration behaviour of the system. Thus, regeneration temperatures at 205 °C, 185 °C and 165 °C were considered in this research work.

Chapter 3 : Materials and Methods

3.1 Overview

In this chapter, the necessary information on materials and methods applied in this study are discussed. To begin with, the materials and chemicals used in the study are highlighted. The equipment design and specifications of the adsorption and regeneration experiments are then presented. In addition, the experimental design and procedure of the adsorption and regeneration experiments are discussed. The last part of this chapter presents the procedures of sample preparation and analysis, as well as the repeatability experiment and data processing.

3.2 Materials

One type of AA adsorbent was used in this study. The physical specifications of the utilized adsorbent are summarized in Table 3.1. The adsorbent's physical characterization was obtained by a Micrometrics® BET analyser using nitrogen adsorption-desorption isotherms at 77.438 K. Brumauer-Emmett-Teller (BET) method was used to determine the surface area and average pore diameter, while the total pore volume was obtained by using desorption data and Barrett-Joyner-Halenda (BJH) formula. The particle size is given in the specification sheet received by the supplier.

Table 3.1: Physical properties of utilized activated alumina

Adsorbent	BET Surface Area (m^2/g)	Total Pore Volume (cm^3/g)	Particle Size (mm)	Average pore diameter (Å)
Activated Alumina	354.3556	0.478588	3.2	52.099

The chemicals used for the adsorption experiments are listed in Table 3.2. These chemicals were chosen because they are relevant to the petrochemicals and surfactant industry, and they are within an acceptable price for this study. Above all, these chemicals have a potential to provide better understanding of the adsorption behaviour of 1-alcohols in an n-alkane solvent.

Table 3.2: List of chemicals used in adsorption experiments

Name	Formula	CAS Number	Purity	Manufacturer
n-decane	$C_{10}H_{22}$	124-18-5	≥ 99%	Sigma-Aldrich
1-decanol	$C_{10}H_{22}O$	*112-30-1*	≥ 98%	Sigma-Aldrich
1-hexanol	$C_6H_{14}O$	111-27-3	≥ 99%	Sigma-Aldrich

The chemicals used in the sample analysis are given in Table 3.3.

Table 3.3: List of chemicals used in samples analysis

Name	Formula	CAS Number	Purity	Manufacturer
1-pentanol	$C_5H_{12}O$	71-41-0	≥ 99%	Sigma-Aldrich
Methanol	CH_3OH	*67-56-1*	≥ 99.9%	Sigma-Aldrich

3.3 Experimental Design

To achieve the objectives of this study, two sets of experiments were carried out: adsorption and regeneration experiments. Adsorption experiments were conducted to measure the equilibrium and kinetic data. Separate adsorption experiments were not carried out to measure equilibrium and kinetic data, as the same runs were used to obtain both sets of data. The regeneration experiments were carried out to obtain the regeneration efficiency throughout multiple adsorption/regeneration cycles.

In general, adsorption equilibrium and kinetic data can be obtained by either batch method, sometimes referred to as static, or dynamic method which is sometimes called continuous or flow technique (Khalil *et al.*, 2020). The batch bench-scale experiment method is known for its simplicity and can provide better understanding of the adsorption mechanism and adsorbate's behaviour on the pores and surfaces of adsorbents (Sanciolo *et al.*, 2014; Iftekhar *et al.*, 2018). Therefore, the batch bench-scale method was chosen for this study. Subsequently, the batch technique was used for the regeneration experiments as well.

3.3.1 Adsorption Experimental Setup

The components of the adsorption experimental setup are shown by schematic diagram 3.1. Photos of the real setup are provided in Appendix A (Section A.1.5). The setup consisted of a water bath where the required temperature was maintained using a water heater. Schott bottles were used to contain the solutions used in this study. The caps of these bottles were adjusted to have a sampling point and a hook to hold a mesh basket into which the adsorbents were put. The bottles were maintained in the water bath by a lid in which the bottles were mounted. Underneath the water bath, and throughout the experiments, a magnetic stirring plate was used to keep moving the magnetic stirrers inside the Schott bottles at a fixed speed to ensure the homogeneity of the mixtures to be investigated.

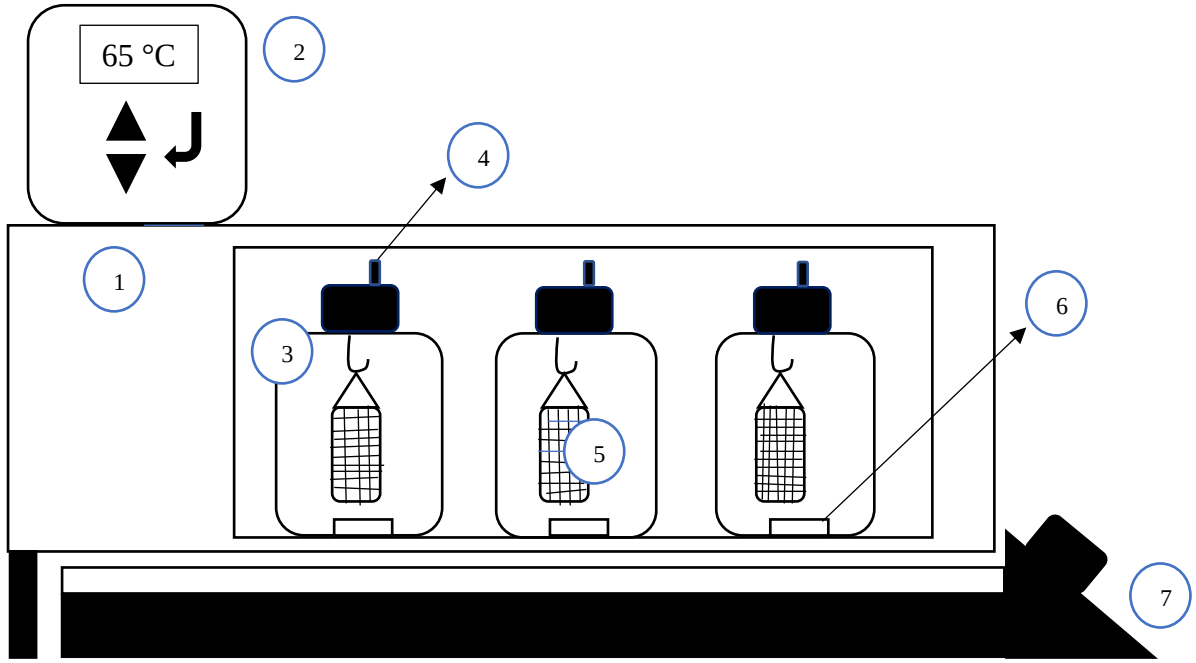

Figure 3.1: Schematic diagram of adsorption experimental setup ((1) Water bath. (2) Heater with circulation pump. (3) 250 mL Schott bottle. (4) Sampling point. (5) Mesh basket. (6) Magnetic stirrer. (7) Magnetic stirrer plate.)

3.3.2 Regeneration Experimental Setup

The regeneration setup is denoted by Figure 3.2. A thermal regeneration technique, combined with purge gas flow, was used to reactivate the spent adsorbents utilized in the preceding adsorption experiments. The setup consisted of three columns with beds into which the exhausted adsorbents were loaded. A nitrogen gas cylinder was connected to the entrance of these columns. The columns and the nitrogen gas were heated up using electric wires. The temperature was controlled using a temperature control system. A heat exchanger located downstream of the columns was used to cool down the mixture of the hot gas and remove amounts of adsorbates. The removed organics were then trapped in an organic trap (for liquid) and an activated carbon trap (for vapour).

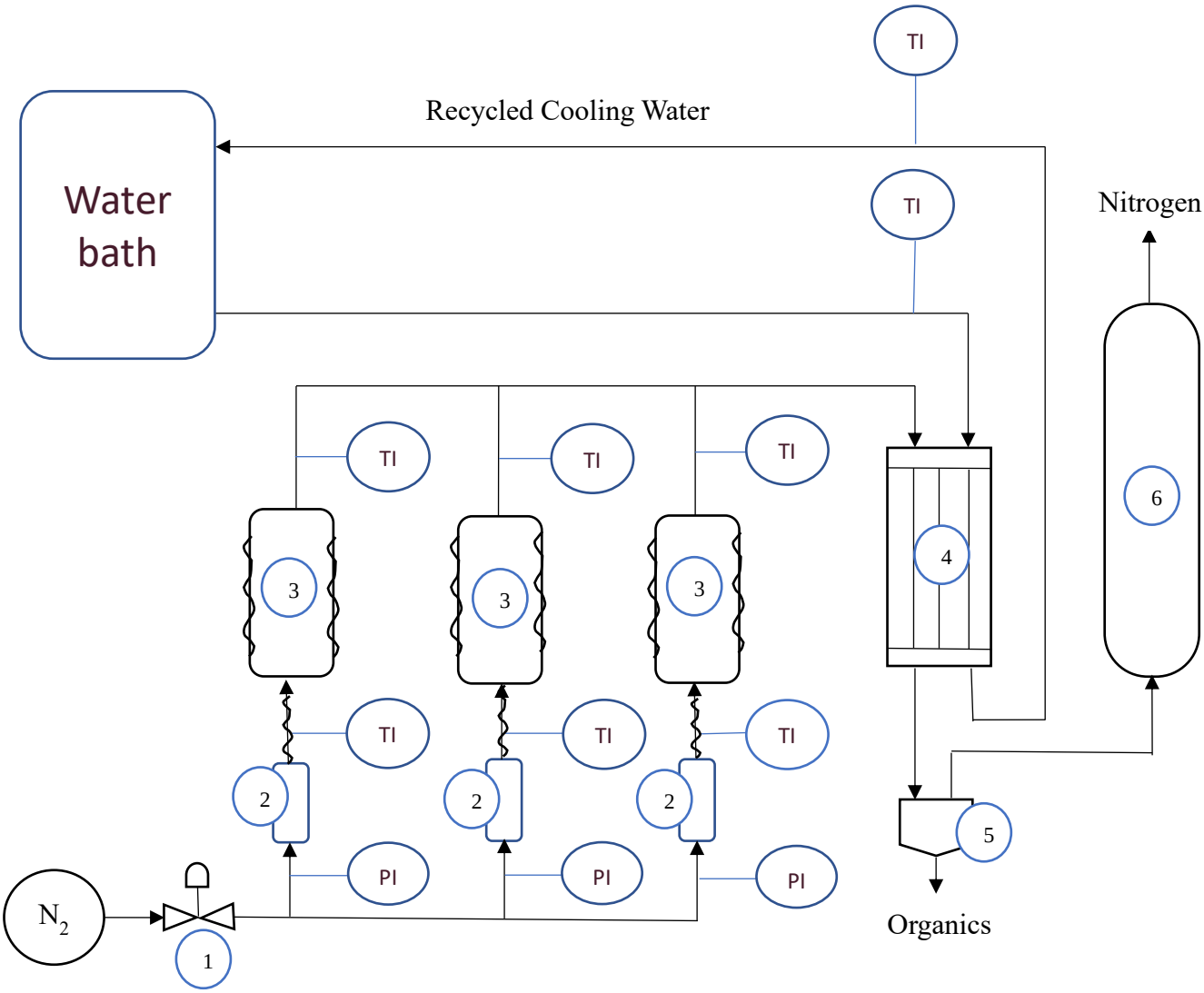

Figure 3.2: Simplified scheme of the regeneration experimental setup ((1) Manual valve. (2) Flowmeter. (3) Regeneration columns. (4) Heat exchanger. (5) Organic liquid trap 1. (6) Organic solid trap 2.)

3.4 Experimental Procedure

Experimental procedures for adsorption and regeneration experiments, including samples preparation, are discussed in this section. More details are provided in Appendix A (Sections A.1.2, A.1.3 and A.1.4).

3.4.1 Adsorption Experimental Procedure

Firstly, the adsorbent was prepared by leaving it in a heated oven (at 120 °C) over night. This was done to evaporate and remove possible adsorbed moisture and other volatiles from the adsorbent. The following day, the water bath was filled with water and the water heater was set to the desired

temperature of 65 °C. The heater was switched on and the water bath was covered at the top using foil to prevent water from evaporating. Meanwhile, a solution at a volume of 200mL was prepared using a digital weight scale. First an empty 250 mL Schott bottle, together with a magnetic stirrer in each bottle, was weighed. The solution was then prepared by adding first the solvent (n-decane) followed by the adsorbates (1-decanol and/or 1-hexanol). The weights of each component were recorded. The required weights of each component for the 200mL solution were estimated by considering the density of these components. A detailed procedure of the calculations done to determine the required weights of each component to prepare the 200mL solution is provided in Appendix A (A.1.2). The same procedure was repeated for each system with a different adsorbate initial concentration that ranged from 0.5 to 3.0 mass%. Every adsorption run contained six solutions and the initial concentration of adsorbates were typically 0.5, 1.0, 1.5, 2.0, 2.5 and 3.0 mass%. The Schott bottles, which contained the solution, were mounted in a stainless-steel lid. Once the heated water had reached the desired temperature, the foil was removed and the Schott bottles containing the mixture were immersed in the hot water. The stirrer plate was then switched on at 410 rpm and the solutions were left to reach the specific adsorption temperature. Once the mixtures reached the required desired temperature, the adsorbent was removed from the oven and 10 g of the AA adsorbent was weighed for each system and added to the mesh basket. These were then carefully lowered into the respective bottles. The system was left to reach the equilibrium stage before switching off the experiment.

Samples for equilibrium and kinetic data were taken from the same runs since no separate runs were carried out to measure the equilibrium or kinetic data. The specific sampling times varied between the different systems, because different systems reached equilibrium at different times. The single 1-hexanol adsorption system and binary adsorption system reached the equilibrium stage after three hours, while the single 1-decanol adsorption system reached the equilibrium stage after five hours. This was identified by a preliminary experiment, where all systems were allowed to run for 8 hours. More details are provided in Appendix A (Section A.1.1).

Samples for kinetic data were taken at 0, 15, 30, 60, 120, 180, 195 and 210 minutes for n-decane + 1-hexanol and the binary-component adsorption systems (n-decane + 1-decanol + 1-hexanol). For the n-decane + 1-decanol system, the samples were taken at 0, 15, 30, 60, 120, 300, 315 and 330 minutes. For equilibrium data, the data were measured from the samples taken at 0, 180, 195 and 210 for n-decane + 1-hexanol and the binary-component adsorption systems, and at 0, 300, 315 and 330 minutes for n-decane + 1-decanol system. The samples were taken through sample ports in the bottles' caps using a pipette, and transferred into dedicated 4mL glass vials which were then marked accordingly. Each sample volume was 400µL.

3.4.2 Regeneration Experimental Procedure

After completing the adsorption experiment, the adsorbents were transferred into dedicated tubes and well isolated for the regeneration cycle on the following day to remove the adsorbates and prepare the adsorbent for the next adsorption run. The regeneration was affected by the duration time, purging gas flow rate and the regeneration temperature. The purging gas flow rate and contact time were kept constant, and the regeneration temperature was varied to examine the influence of different temperatures on the adsorbent's performance throughout successive adsorption/ regeneration cycles. The duration time did not include the heating up time that was needed to reach the desired temperature. Due to time constraints caused by COVID-19, only three temperatures, one type of adsorbent and one duration time was investigated in this study, as examining one regeneration temperature impacted on one type of adsorbent for 10 cycles which took around 3 months for the three systems.

Based on Groenewald's study (Groenewald, 2019), the duration time was 1 hour, the flow rate of the nitrogen was 0.011 m^3/h, and the regeneration temperatures were chosen to be 205 °C and 185 °C for the adsorbents used in the three systems. Another round of experiments at the regeneration temperature of 165 °C were carried out for the adsorbents applied on the single 1-hexanol adsorption system as well as for the binary-component adsorption system. Although the regeneration temperature is recommended to be 30 °C higher than the highest boiling point in the investigated systems (Groenewald, 2019), as the highest boiling point was 230 °C (1-decanol), it was decided to not conduct the regeneration experiments at temperatures beyond 205 °C. This decision was taken for safety concerns to avoid the auto-ignition of n-decane, which has a low auto-ignition temperature (200 °C). The regeneration temperature 205 °C was safe though, as it was successfully examined by Groenewald.

The regeneration procedure was initially prepared by opening the regeneration columns from the top, while ensuring that the outlet valve on the downstream of the activated carbon trap was open. The adsorbents used in the adsorption experiment were weighed and their weights were recorded, then they were poured carefully into the inserts. The inserts, including the wet adsorbents, were loaded in the regeneration columns and the columns were well sealed. The nitrogen gas cylinder valve was opened, and the nitrogen gas was left to flow through the system for 15 minutes before starting the heating process to eliminate the oxygen from the regeneration setup to avoid any risk of explosion. Meanwhile, the control box was switched on, a USB was inserted into an HIM screen to start logging the procedure, the desired temperature was set in the control system, and the cooling system was switched on. After 15 minutes, the heating up process was started, and the system was

left to reach the required temperature. Once the regeneration temperature was reached, the system was left for 1 hour before starting the shutdown procedure.

At the shutdown procedure, the heating was switched off and the flow gas was maintained through the system until the system had cooled down to 40^0C. Afterwards, the gas cylinder's outlet valve was closed, and the cooling system was switched off once the gas flow reached 0 m^3/h. Thereafter, the columns were opened from the top and the inserts were taken off. The regenerated adsorbents were then weighed, and their new mass was recorded.

3.4.3 Gas Chromatography Analysis Procedure

The 400 µL samples taken from the adsorption experiments were analysed by a Gas Chromatography instrument (GC) to determine the concentration of each component in the samples. The GC was calibrated before analysing the samples. Due to COVID-19 constraints, all GC calibration and analysis procedures were carried out by the lab analysis team. Only the preparation of samples for GC analysis was conducted by the author.

The samples taken from adsorption experiments were prepared for GC analysis. An empty 2µL glass vial was weighed on a digital scale, and then the scale was tared. 100µL of the samples were added to the empty vial and its weight was recorded. 30µL of an internal standard, which was 1-pentanol, was added to the vial and its mass was recorded as well. The mixture was diluted by adding 1000 µL of methanol, and 100µL of the mixture was transferred into another 2µL glass vial, which was then diluted by adding 1000 µL of the methanol. The latter vial was marked and sent into GC lab for analysis. The same procedure was followed to prepare all samples for the three systems.

3.5 Repeatability Experiments

The adsorption experiment procedure mentioned in 3.4.1 was duplicated for the three systems investigated to examine the reliability of the data extracted. Figures 3.3 and 3.4 represent results pertaining to repeatability experiments for the single and binary systems, respectively.

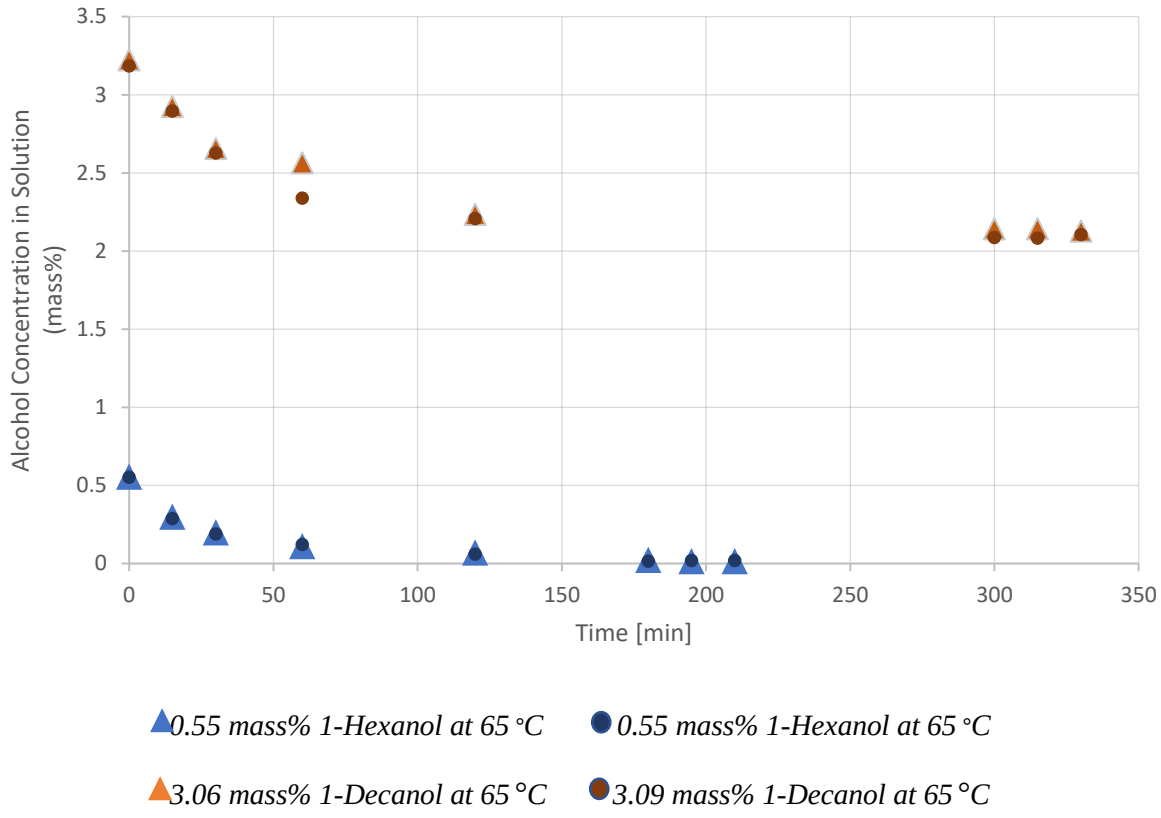

Figure 3.3: The change in alcohols' concentration in solution with time during repeatability experiments for single-component adsorption systems (T = 65 °C)

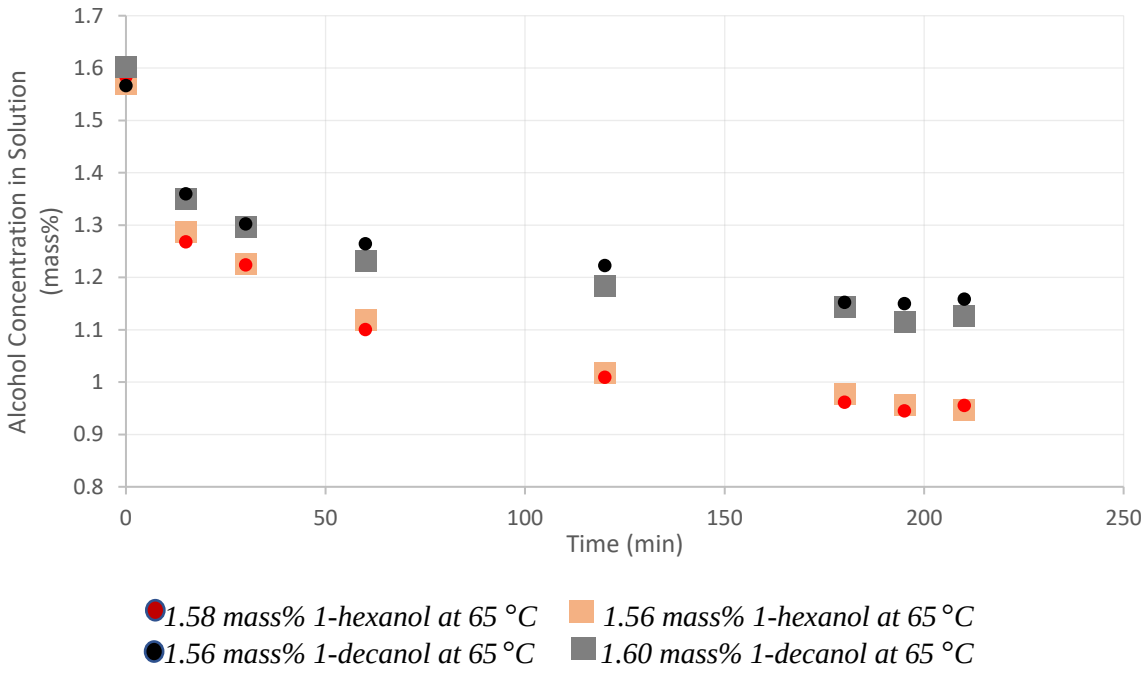

Figure 3.1: The change in alcohols' concentration in solution with time during repeatability experiments for binary-component adsorption systems (T = 65 °C)

In single adsorption repeatability experiments, an average of 96.64% of 1-hexanol was removed when the initial concentration of 1-hexanol was 0.55 mass%, while the percentage of eliminated 1-decanol was 34.78% at the initial concentration 3.10 mass%. On the other hand, the repeatability experiments of binary adsorption at the initial concentration of 1.60 mass% of each alcohol component, the removal percentages for 1-hexanol and 1-decanol were 39.29 mass% and 28.05 mass%, respectively. The standard deviation for single adsorption experiments was 0.02% for 1-hexanol and 1-decanol. The standard deviation for binary adsorption removal was 0.66% and 2.26% for 1-hexanol and 1-decanol, respectively. Thus, the reliability of the data extracted was deemed acceptable.

3.6 Uncertainty Analysis

Uncertainty analysis was based on the GC results, pipettes, and the scales used in this research work. The amount of uncertainty measured composed of uncertainty obtained from repeated experimental runs, GC repeat samples, repeated measurement of volumes using the pipettes, and repeated measurement of sample weights and the adsorbents using different scales. The different types of pipettes were filled to their maximum capacities with the chemical considered in this study and the volumes were weighed five times. One of these samples was weighed five times to estimate the uncertainty of the scale used in preparing the samples for the GC analysis. A same mass of adsorbent, on other hand, was weighed five times to obtain the uncertainty of the scale used to measure the adsorbent's mass. The adsorption experiment at one initial concentration was repeated five times for each system. The uncertainty parameter of each system was calculated using t-test with a significance level of 0.05 and the standard error of five duplicate measurements, considering all repeated experiments explained above (GC, scale, pipettes, etc). For the binary-component adsorption system, the uncertainty was determined for each concentration for each component separately, as well as for the binary mixture. A detailed methodology can be found in Appendix D.

3.7 Data Processing

All raw data measured in this study can be found in Appendix B. The calculation methodologies pertaining to the chapters of results are available in the corresponding appendices, as indicated in each chapter, including the methodologies followed to determine the concentration at any time t and the adsorbent loading q.

Due to the vast amount of data measured in this work, only selected graphs were chosen to be presented in the body of this thesis.

Chapter 4 : Adsorbent Characterisation

4.1 Overview

This chapter discusses the physical properties and chemical composition of the activated alumina adsorbent used in this study. The information provided in this chapter will ultimately aid in understanding the findings in subsequent chapters of results, such as the thermal regeneration effect in the physical and chemical compositions.

4.2 Physical Properties

4.2.1 Surface Area and Pore Volume

The low-pressure gas adsorption (LPGA) method, using nitrogen gas as an adsorptive medium, was used to determine the surface area as well as the pore volume of the adsorbent applied. This was carried out with 3Flex Version 4.00 instrument from the Micromeritics Instrument Corporation. Surface area, pore volume and pore size are summarized in Table 4.1.

It can be observed that the utilized adsorbent is mainly mesopores, since the micropore volume was determined to be approximately 24% of the total pore volume per Horvath-Kawazoe method, while the mesopores volume constitutes around 76% of the total pore volume. As a result, the macropore volume was estimated to contribute to less than 1% of the total pore volume. On the other hand, the micropore structure determined by Density Functional Theory Model (DFT) was found to be responsible for approximately 74% of the total surface area. The average adsorption pore diameters, as determined using the BET method, was 52.099 Å and the average micropore diameters, as estimated using the Horvath-Kawazoe method, was 9.678 Å.

Table 4.1: LPGA results for blank activated alumina applied in this study

Properties	Values
Surface Area	
Single point surface area (m^2/g)	348.1471
BET surface area (m^2/g)	354.3556
BJH Adsorption cumulative surface area of pores between 10 Å and 4000 Å width (m^2/g)	329.0827
BJH Desorption cumulative surface area of pores between 17 Å and 3000 Å width (m^2/g)	395.1454
Pore Volume	
Single point adsorption total pore volume (cm^3/g)	0.461539
Single point desorption total pore volume (cm^3/g)	0.462162
BJH adsorption cumulative pore volume (cm^3/g)	0.400857
BJH desorption cumulative pore volume (cm^3/g)	0.478588
Pore Size	
Adsorption average pore diameter (Å)	52.099
Desorption average pore diameter (Å)	52.169
BJH adsorption average pore width (Å)	48.724
BJH desorption average pore width (Å)	48.447

Figure 4.1 illustrates the adsorption-desorption isotherm obtained from the LPGA analysis. The adsorption-desorption isotherms for the utilized adsorbent seem to resemble Type IV BET isotherms. Referring to IUPAC (Rouquerol *et al.*, 1994), this exhibits multilayer adsorption of the nitrogen gas with capillary condensation at high pressures. In addition, H2 hysteresis is presented in Figure 4.1, suggesting that the adsorbent's pore sizes are not well defined (Rouquerol *et al.*, 1994; Androutsopoulos and Salmas, 2000).

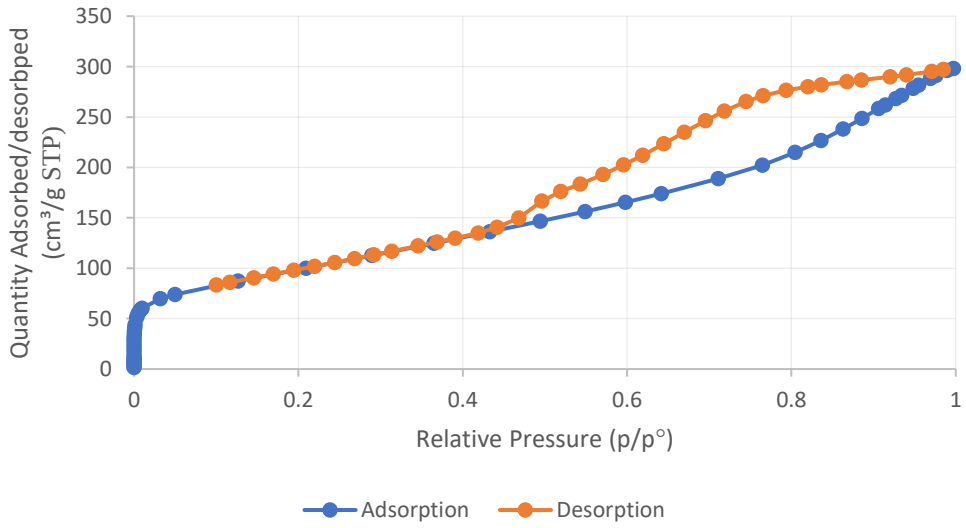

Figure 4.1: BET adsorption-desorption isotherms for utilized activated alumina

Figure 4.2 depicts the Barrett-Joyner-Halenda (BJH) pore size distributions. It can be observed that the utilized adsorbent predominantly consists of mesopores structure.

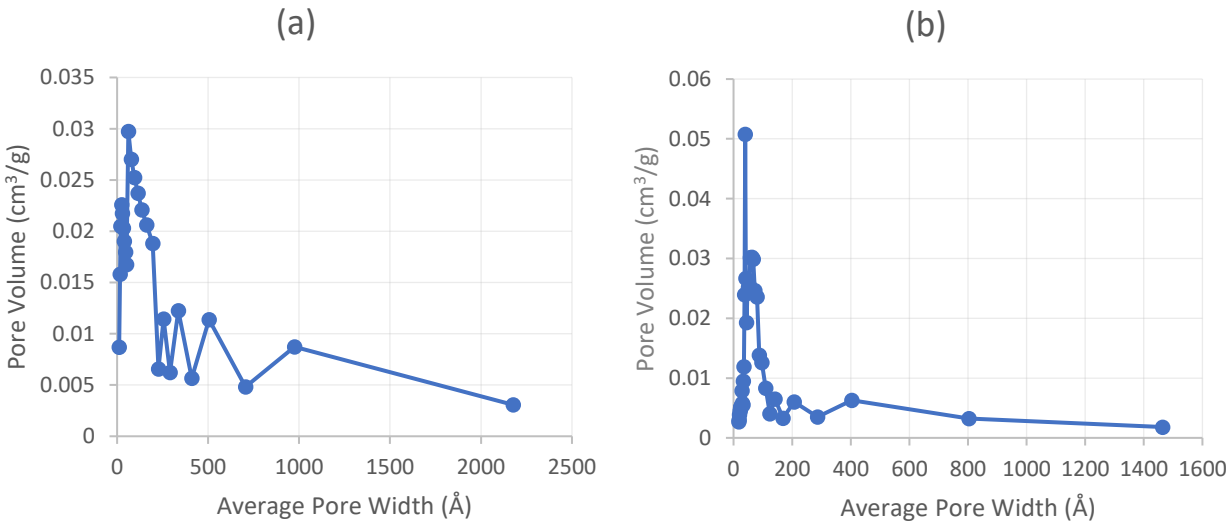

Figure 4.2: BJH pore size distributions (a) adsorption, (b) desorption

4.2.2 Pore Structure

The pore structure of the applied activated alumina adsorbent was investigated using scanning electron microscope (SEM) manufactured by Carl Zeiss Microscopy, Germany. In order to illustrate the change in pore structure throughout the adsorbent, Figure 4.3 denotes two sets of SEM images: one set closer to the external surface, while the second set is more towards the centre.

The outer part of the adsorbent tends to be less dense than the inner part. As a result, the macropores and mesopores are situated more to the surface of the adsorbent, while the smaller mesopores and micropores are situated more towards the centre of the adsorbent. Therefore, macropores and mesopores are aptly called transport pores, where the molecules would have been passed through to reach the adsorbent's micropore structure.

(a) (b)

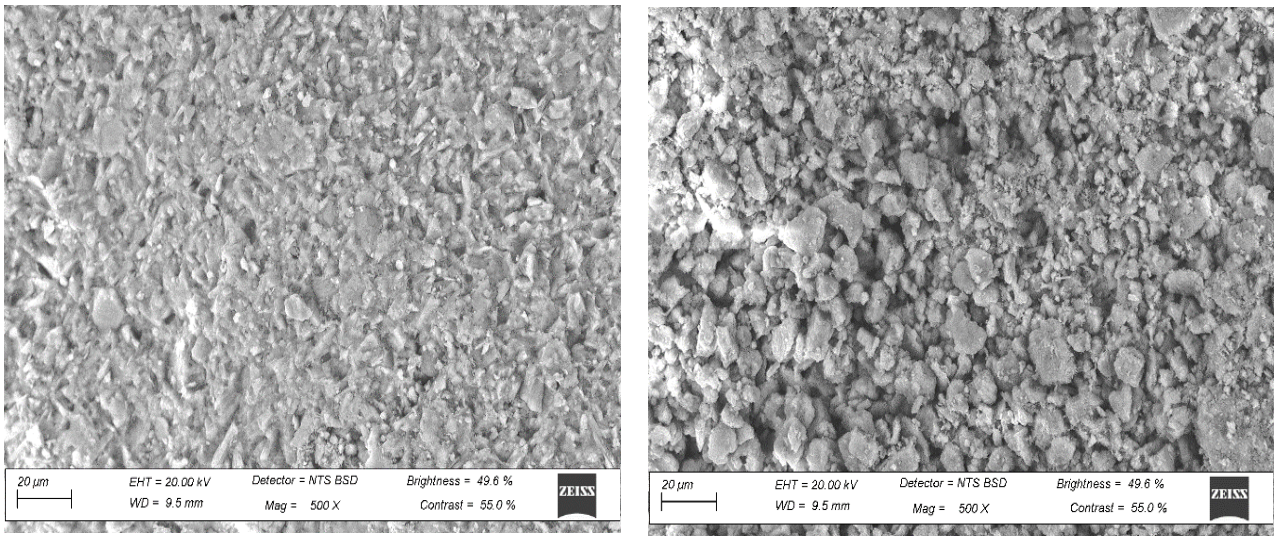

Figure 4.3: SEM image of fresh activated alumina indicating –
(a) cross-sectional image of the centre; and (b) the outer part of the adsorbent

SEM magnification images represented by Figure 4.4, which are granular in structure and the agglomeration of spherical particles can be observed. As indicated in 2.3.1.3, spherical morphology exhibits higher attrition resistance and better flow performance.

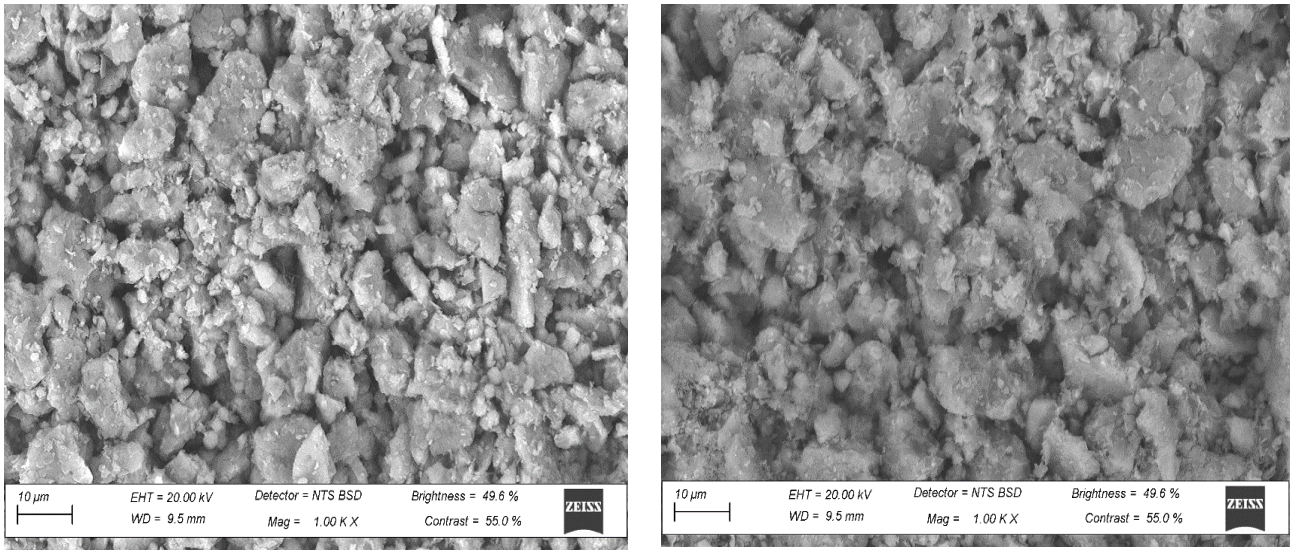

Figure 4.4: Different SEM images of the freshly activated alumina closer to the outer parts of the adsorbent bead

4.3 Chemical Properties

4.2.1 Adsorbent Composition

The fresh adsorbent was chemically quantified by Energy Dispersive X-ray Spectroscopy (EDX) Oxford Instruments®. The chemical composition of the utilized activated alumina adsorbent in this study can be found in Table 4.2.

Table 4.2: EDX results for the freshly activated alumina used in this study

Element (mass%)	Adsorbent
	Activated Alumina
Oxygen (O)	56.96
Aluminium (Al)	33.26
Carbon (C)	7.30
Silica (Si)	1.30
Sodium (Na)	1.20

The majority of the adsorbent is comprised of oxygen and aluminium, as the combined amount of oxygen and aluminium in the applied adsorbent was determined to be approximately 90 mass% of the total chemical composition. The silica, on the other hand, was found to be slightly higher than the sodium element, which together form the lesser composition of the utilized adsorbent.

4.4 Chapter Summary

The objectives of this chapter include the investigation of the physical and chemical properties of the activated alumina applied in this study.

The analysis proved that the adsorbent utilized is mainly mesoporous. SEM images show that the pores of the adsorbent seem to have a granular structure. In addition, oxygen and aluminium were found to form the majority of the adsorbent applied. The change in the physical and chemical properties of the regenerated adsorbent at different temperatures will be discussed and compared to the fresh properties of the adsorbent. This will help to understand the change in the adsorbent's performance in the various systems investigated in this study.

Chapter 5 : Adsorption Experimental Results

5.1 Overview

Objective (I) of this study is addressed in this chapter. This chapter investigates the experimental adsorption data obtained from the first adsorption cycle. The adsorption ability of the applied activated alumina to adsorb 1-hexanol and 1-decanol from single-component and binary systems is compared at different initial concentrations, as well as the possible competitive interaction between the adsorbates in the binary systems.

5.2 Experimental Measurements

In this study, various data sets were measured to obtain the change in adsorbates' concentration in the bulk solutions over time. The adsorbed amount of adsorbates onto the activated alumina surface and pores was determined as a function over time and the adsorbent loading of each respective system. The parameters used in this chapter to investigate the data and results include normalized adsorbate concentrations (C_t/C_0) and adsorbent loading (q_t). The reader is referred to Appendix C for the outline methodology for the calculations of these parameters.

Three different systems were investigated: two single-component adsorption systems and one binary-component adsorption system. For each system, the adsorption experiments were carried out at 65 °C using six different initial adsorbate concentrations.

5.2.1 Single-Component Adsorption System

Figure 5.1 shows the concentration decay profiles of 1-hexanol and 1-decanol at three initial concentrations. From these figures, it can be noted that the amount of 1-hexanol and 1-decanol adsorbed is relatively similar at a longer equilibrium time for 1-decanol adsorption. For the system represented by Figure 5.1b, the 1-hexanol eliminated from the n-decane solvent was approximately 58%, while the 1-decanol removed at similar conditions was 59.5%. When the initial concentration was doubled, it can be observed from Figure 5.1c that the percentage of 1-hexanol and 1-decanol removed was approximately 33.5% and 34%, respectively. Although the results were relatively close, the adsorbent exhibited marginally better performance in the equilibrium phase when 1-decanol was adsorbed. This is possibly owed to the higher boiling point of 1-decanol, since the boiling point of 1-decanol and 1-hexanol are 233 °C and 157 °C, respectively (Ashok *et al.*, 2019). Moreover, the adsorption temperature of 65 °C is relatively high, thus the 1-decanol would exhibit higher stability than the 1-hexanol at equilibrium stage due to its stronger intermolecular forces. More studies were concluded with similar findings. For instance, Zhang et al. investigated the

adsorption of different volatile organic compounds (VOCs) onto porous minerals (Zhang *et al.*, 2019). Zhang and his co-researchers reported that the VOCs with a higher boiling point achieved the highest adsorption capacity on all porous materials investigated in their work.

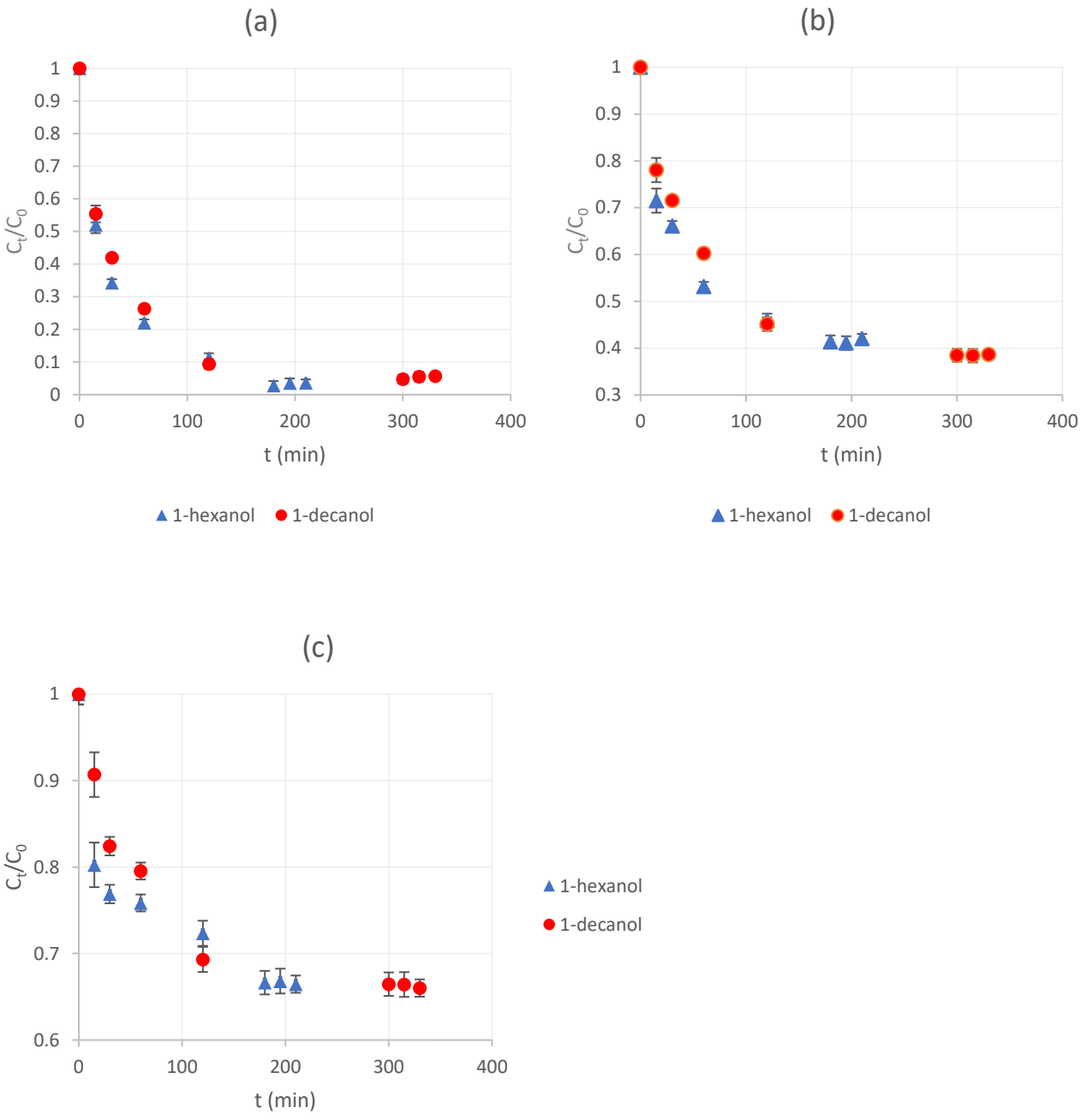

Figure 5.1 Comparison of adsorption ability to adsorb single components 1-hexanol and 1-decanol at 65 °C and different initial concentrations (a) initial concentration is 0.5 mass%; (b) initial concentration is 1.5 mass%; and (c) initial concentration is 3.0 mass%

Furthermore, it can be observed from Figure 5.1 that the amount of 1-hexanol adsorbed, before reaching the equilibrium stage, appeared to be higher than for 1-decanol, which means the 1-hexanol adsorption rate was faster than the 1-decanol at the beginning of the adsorption experiment,

in particular during the first 100 minutes. Presumably, the 1-hexanol adsorption rate was faster in the beginning due to its smaller size compared to the 1-decanol. According to Zhang et al, the species with smaller size have easier access onto active sites than the larger species (Zhang *et al.*, 2017). This is expected also because most of the applied adsorbent's surface pores are micropores, as discussed in Section 4.2.1.

Table 5.1 encapsulates the equilibrium loading of the activated alumina adsorbent for the single-component adsorption systems at the given conditions. The equilibrium loading is presented in different units using the adsorbates' molecular weights, as well as the surface area presented in Table 4.1.

Table 5.1 : Equilibrium adsorbent loadings at T = 65 °C

Adsorbates	Activated alumina loading at different initial concentration		
	0.5 mass%	1.5 mass%	3.0 mass%
1-hexanol			
mg/g	78	123	157
mg/m²	0.220	0.347	0.443
mmole/g	0.763	1.204	1.537
mmole/ m²	0.002	0.003	0.004
1-decanol			
mg/g	78	132	159
mg/m²	0.220	0.372	0.449
mmole/g	0.492	0.834	1.004
mmole/ m²	0.001	0.002	0.003

Although the equilibrium loading for the systems presented in Table 5.1 show a larger mass of 1-decanol adsorbed than 1-hexanol, the number of 1-hexanol molecules per unit surface area and mass of adsorbent is greater than those of the 1-decanol's at the respective systems, which means more 1-hexanol molecules were adsorbed by the activated alumina adsorbent applied than the 1-decanol molecules at the similar initial concentration. This can be ascribed to the shorter carbon chain and size of the 1-hexanol molecule compared to the 1-decanol molecules.

Further discussion in this section investigates the impact of initial concentration as well as the alcohol chain length on the single adsorption results.

5.2.1.1 Initial Concentration Impact on Single-Component Adsorption Systems

It was observed that the initial concentration had a significant impact on the loading of the adsorbent. As discussed in Chapter 2 (Section 2.3.4.1), the uptake of the adsorbates is increased by increasing the initial concentration of the adsorbates. This can be ascribed to the increased driving force, which increases by increasing the initial concentrations required for the adsorbates to transfer through the film, diffuse from the film onto adsorbent surface, and eventually to diffuse into the porous structure of the adsorbent (Özbay *et al.*, 2013). Meanwhile, the removal efficiency decreased under similar conditions as discussed in 5.2.1. This drop in the efficiency may be attributed to the saturation of active sites available to interact with the adsorbates (Özbay *et al.*, 2013). The initial concentration impact on the adsorption capacity is described in Figure 5.2.

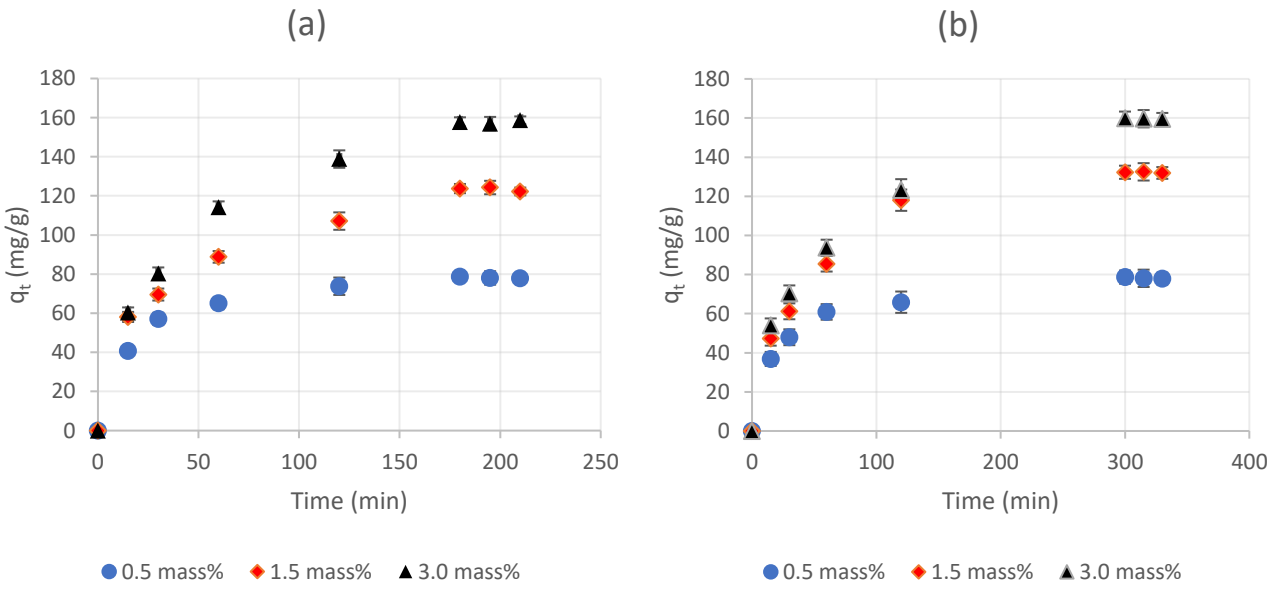

Figure 5.2: Time profiles for the single-component adsorption of – (a) 1-hexanol (b) 1-decanol concentrations

As can be seen in Figure 5.2, the increase in equilibrium adsorbent loading for the 1-hexanol dropped down from 33.3% between initial concentrations of 0.5 and 1.0 mass% to 4.7% between initial concentrations of 2.5 and 3.0 mass%. On the other hand, the equilibrium adsorbent loading for 1-decanol began to plateau at an initial concentration higher than 2.0 mass%, and thereafter the equilibrium adsorbent loading was almost nothing (Figure 5.3b). A marginal increase in the equilibrium adsorbent loading was exhibited when the initial concentration of the 1-hexanol was increased beyond 2.5 mass% (Figure 5.3a).

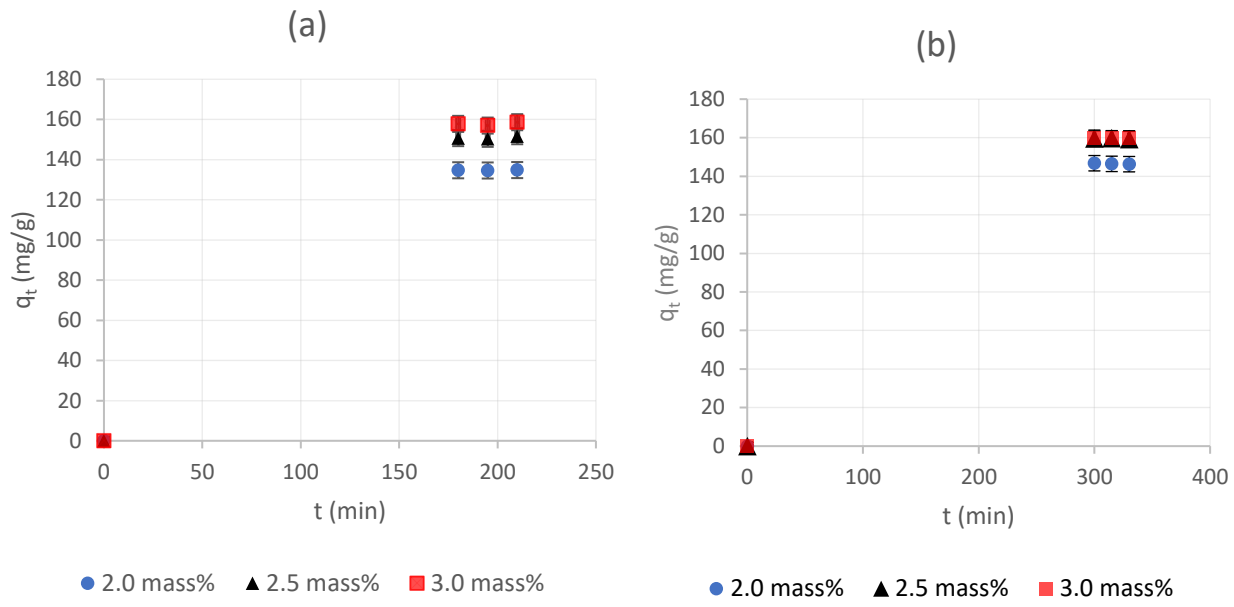

Figure 5.3 : Equilibrium loading at different adsorbate's initial concentration for (a) 1-hexaol; and (b) 1-decanol at 65 °C

The findings obtained for the single-component adsorption systems in this study concur with the results reported by previous works. Majumder (2018) found that the activated alumina adsorbent equilibrium loading increased significantly when increasing the initial concentration of arsenic in the water, while the removal percentage decreased as the initial concentrations were increased. Wadie and Al-Khawaja used activated nano-alumina in their study to remove cadmium and silver at different initial concentrations ranging between 25 to 200 mg/L from aqueous solutions (Wadie and Al-Khawaja, 2018). They reported that an increase in adsorption capacity was observed by increasing the initial cadmium and silver concentrations in the aqueous solutions, and the elimination efficiency decreased inversely by increasing the initial concentration of the adsorbates in the systems investigated. This is expected, as increasing the initial concentration increases the driving force between the adsorbates and the adsorption media, and subsequently a higher equilibrium loading can be achieved. On the other hand, the active sites on the adsorbent's pores and surface are limited, and as a result, the ratio of active sites decreases as the adsorbate's initial concentration increases. Therefore, the removal percentage declines when the adsorbate's initial concentration is increased (Özbay *et al.*, 2013).

5.2.1.2 Alcohol Chain Length Impact on Single-Component Adsorption Systems

The length of the alcohol chain exhibited almost no influence on the equilibrium loading; however, the equilibrium loading for 1-decanol is slightly higher than 1-hexanol. Presumably, this is attributed to the higher weight of 1-decanol resulting from its longer chain compared to the 1-hexanol. However, 1-hexanol shows a slightly higher adsorption rate at the beginning of the

adsorption process as seen in Figure 5.1. This may be ascribed to the 1-hexanol shorter carbon chain length. A shorter carbon chain length and a smaller size adsorbate have easier access into the adsorbent's morphology, as discussed in 2.3.2.1 and 5.2. This can obviously be seen in Figure 5.4, where the adsorbed molecules of 1-hexanol and 1-decanol are depicted. Although the equilibrium loading of 1-decanol inclines to be slightly greater than 1-hexanol, and regardless the initial concentrations of the adsorbates, the number of 1-hexanol molecules adsorbed in the equilibrium stage seemed to be greater than the molecules of 1-decanol adsorbed from the respective systems. Moreover, the 1-hexanol's molecular adsorption rate per unit surface area of adsorbent was notably higher than 1-decanol.

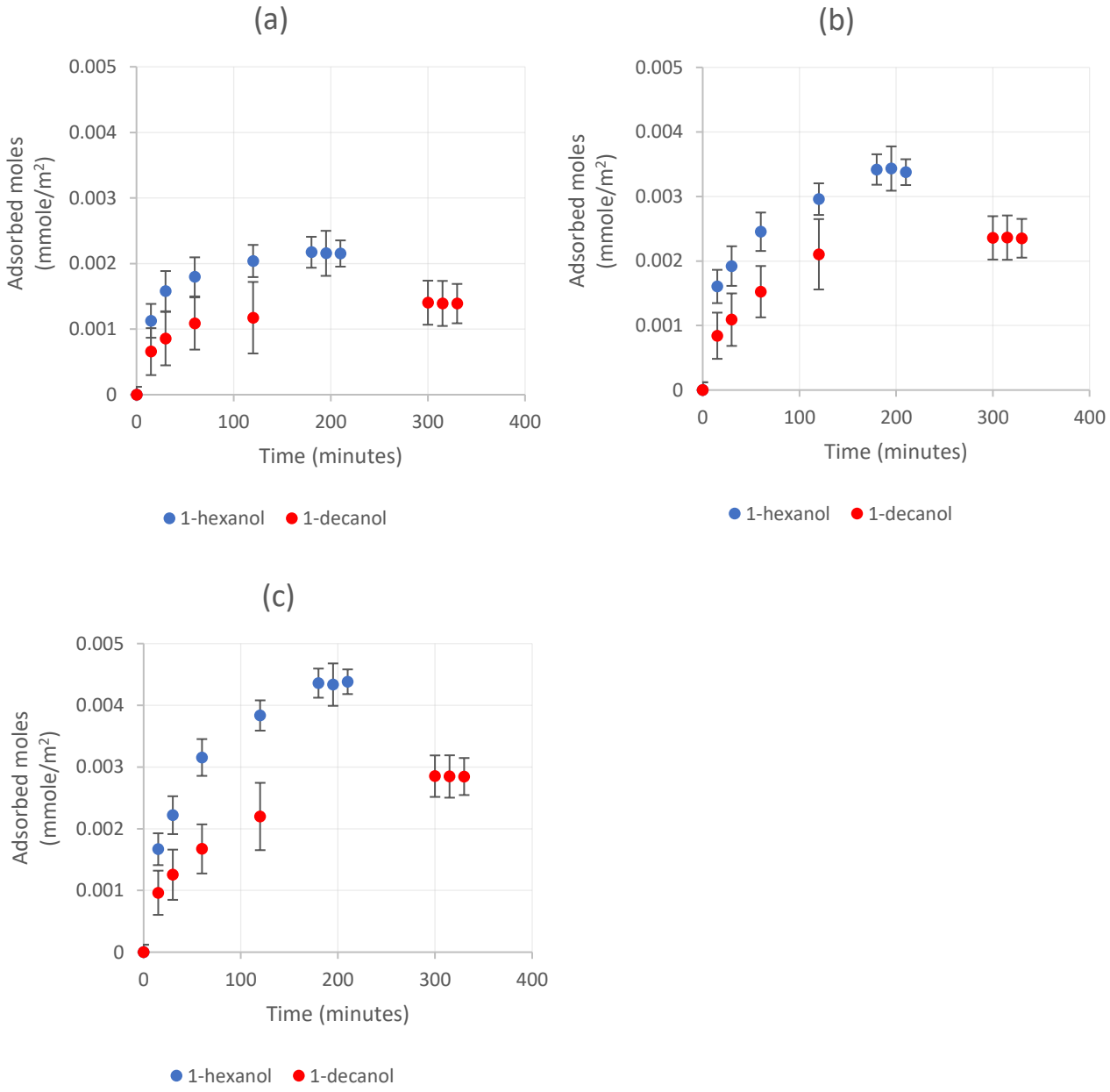

Figure 5.4: Time profiles for the moles of 1-hexanol and 1-decanol adsorbed from single-components adsorption systems at (a) C_0 = 0.5 mass%; (b) C_0 = 1.5 mass%; and, (c) C_0 = 3.0 mass%

Some of the above findings obtained from this work are contradictory to those reported by Bosman and Groenewald (Bosman, 2019; Groenewald, 2019). Bosman and Groenewald reported that the single-component adsorption systems resulted in better adsorption of shorter chain 1-alcohols at the equilibrium time on various types of activated alumina. This might be attributed to the lower adsorption temperatures considered by Bosman and Groenewald (25 °C – 45 °C). Owing to its greater intermolecular forces, 1-decanol might exhibit higher stability than 1-hexanol at the higher adsorption temperature carried out in this study, which resulted in larger equilibrium loading. Nevertheless, the initial adsorption rate at the beginning of adsorption experiments obtained by Bosman and Groenewald was similar to the findings determined in this study.

5.2.2 Binary-component Adsorption System

For the binary-component adsorption system, the influence of the initial concentration, the 1-alcohols chain length, and interaction effect between the adsorbates were investigated.

5.2.2.1 Initial Concentration Impact on Binary-component Adsorption systems

Similar to the single-component adsorption system, the equilibrium adsorbent loading in the binary-component adsorption systems was proportional to the initial concentration of 1-alcohols. The equilibrium adsorbent loading began to plateau at a total initial concentration greater than 2.0 mass% as can be seen Figure 5.5.

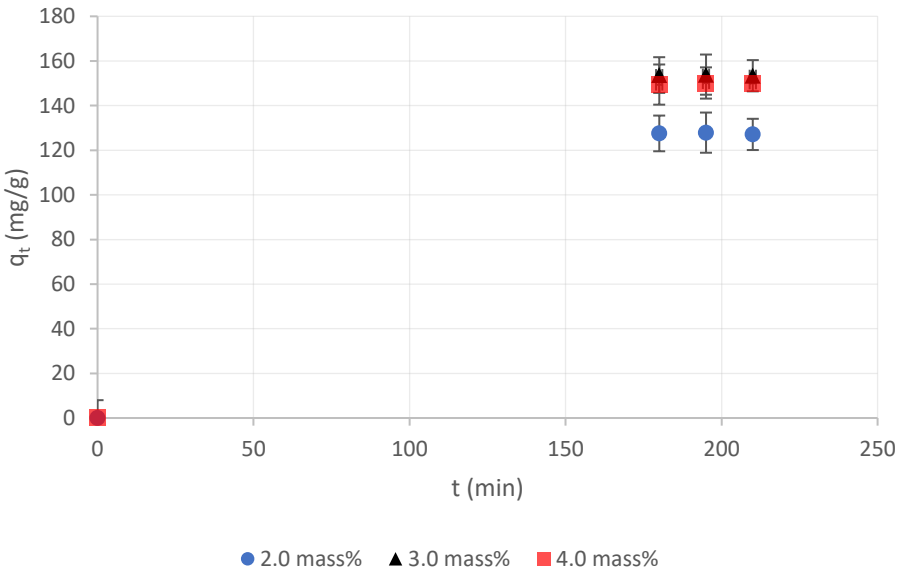

Figure 5.5: Equilibrium loading for binary-component adsorption system of 50:50 mass ratio mixture at different adsorbates' initial concentration at 65 °C

Besides the saturation of the adsorbent's active sites, the plateau may be ascribed to the interaction between the adsorbed 1-alcohols. Cai and Sohlberg (2003) investigated the adsorption of different alcohols on activated alumina. They indicated that the chemisorption of 1-alcohols on activated alumina is influenced by the orientation of adsorbed alcohols when they become close to the active sites. When two adsorbates are adjacent to one another on an active site, on some occasions only one adsorbate will be dehydrogenated and the two adsorbates will start repelling each other. Similar behaviour is also expected in the single-component adsorption systems.

5.2.2.2 Alcohol Chain Length Impact on Binary-component Adsorption Systems

As expected, the adsorbent exhibited higher affinity to adsorb the shorter chain alcohol, which was 1-hexanol. This can be seen in Figure 5.6 and 5.7 where the preference for 1-hexanol was pronounced at different initial concentrations. As discussed in Section (5.2.1.2), smaller size molecules have easier access to the active sites, and are thus faster and more easily adsorbed onto these active sites. During a competitive adsorption of 1-hexanol and 1-decanol, and at similar initial concentration of both components in the binary-component systems, a higher mass of 1-hexanol was adsorbed in the equilibrium stage (Figure 5.6.a and 5.6.b). Consequently, more molecules of 1-hexanol were adsorbed than 1-decanol in the respective systems (Figure 5.7.a, 5.6.b, and 5.7.c).

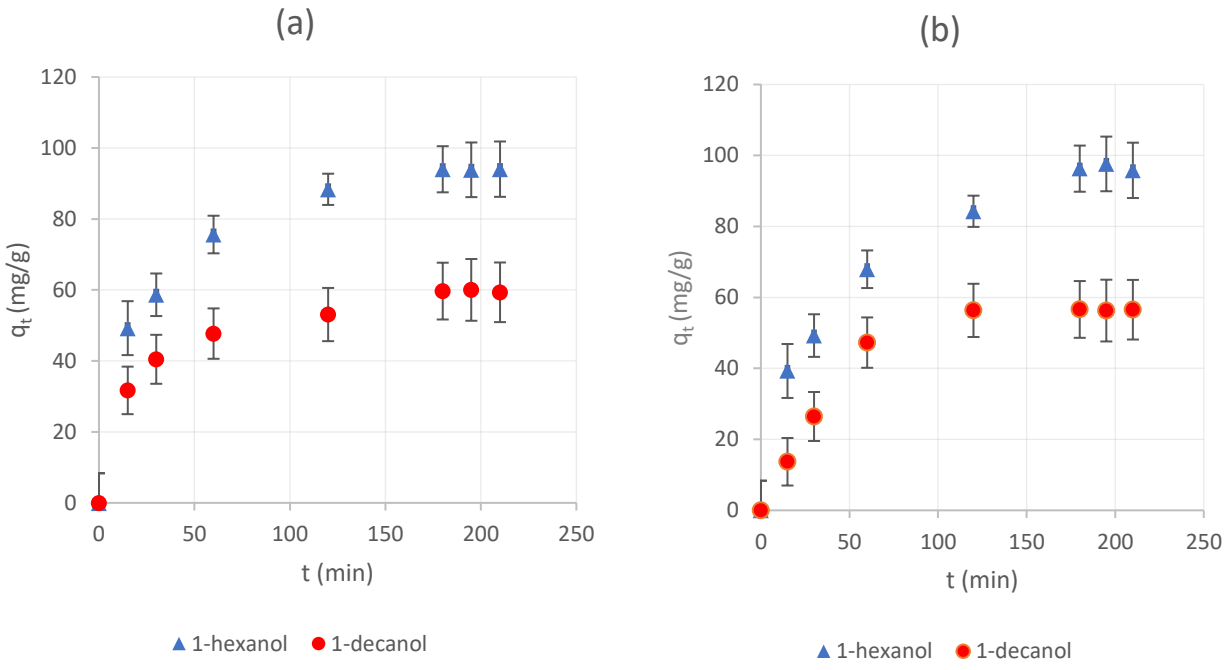

Figure 5.6: Time profiles of the binary-component adsorption system of a 50:50 mixture at (a) total initial concentration 3.0 mass% (T = 65 °C), and (b) total initial concentration 6.0 mass% (T = 65 °C)

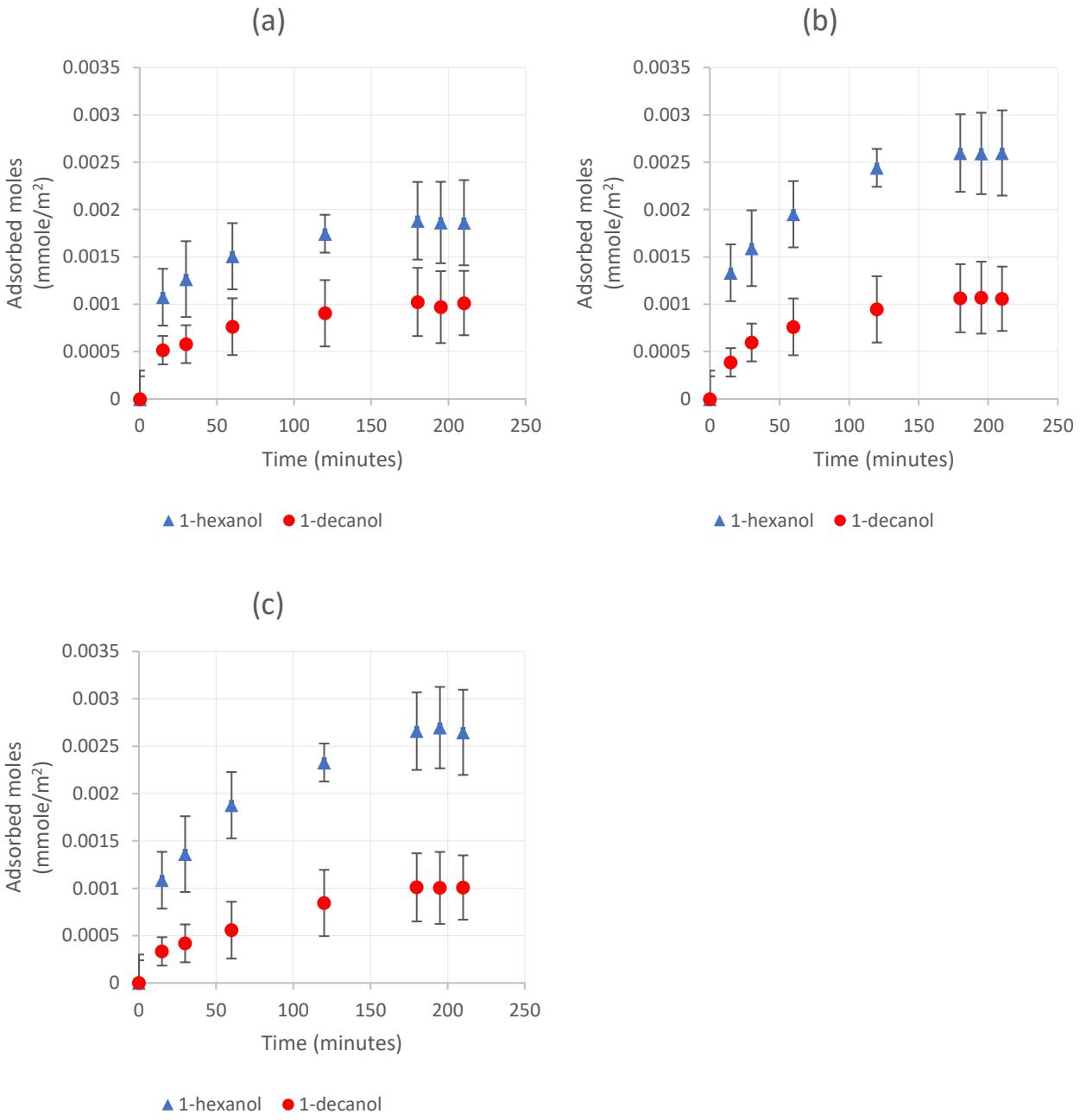

Figure 5.7: Time profiles for the moles of 1-hexanol and 1-decanol adsorbed from binary-component adsorption systems of a 50:50 mixture at (a) C_0 = 0.5 mass%; (b) C_0 = 1.5 mass%; and, (c) C_0 = 3.0 mass%

The above finding is aligned with the previous study conducted by Bosman (Bosman, 2019), and contrary to that of Wang et al. (2012). Wang et al. reported that the adsorption tendency of n-decane on beaded activated carbon over n-heptane is likely due to n-decane's greater and longer carbon chain length. According to Wang et al, a longer carbon chain length and a higher boiling point result in greater interaction between the adsorbent and adsorbate. Nevertheless, this seemed to not be the case in this study for the binary-component adsorption system, as the size of the adsorbed molecules may have a major impact on the adsorption process more than the boiling point.

5.2.2.3 Adsorbate-Adsorbate Interaction Impact on Binary-component Adsorption Systems

In a multicomponent adsorption process, there are three different types of interactions that can take place between the adsorbates: synergistic interaction, antagonistic interaction, and non-interaction (Girish, 2017). As discussed in 2.3.4.2, the interaction parameter is represented by R_i (Equation 2.1), which is the ratio of the binary-component equilibrium adsorbent loading to the single-component equilibrium adsorbent loading. The interaction is considered synergistic when $R_i > 1$, antagonistic when $R_i < 1$ and non-interaction when $R_i = 1$.

The interaction for the binary-component adsorption system investigated in this study was found to be antagonistic as can be observed in Figure 5.8. It was also observed that the interaction parameter corresponding to 1-hexanol is closer to the unity than of that corresponding to 1-decanol. As a result, the presence of 1-hexanol was likely to have a perceptible impact on the adsorption of 1-decanol, whereas the presence of 1-decanol exhibited less influence on the adsorption of 1-hexanol. Moreover, the adsorption of 1-decanol was more adversely affected at higher initial concentrations, which suggests an increased competition between the respective adsorbates at greater initial concentrations. These findings were expected since they were reported by Bosman (Bosman, 2019). Bosman is, to the best of the author's knowledge, the only one who investigated the adsorption of multiple 1-alcohols from a paraffin solvent by the activated alumina adsorbents, but at an adsorption temperature of only 45 °C.

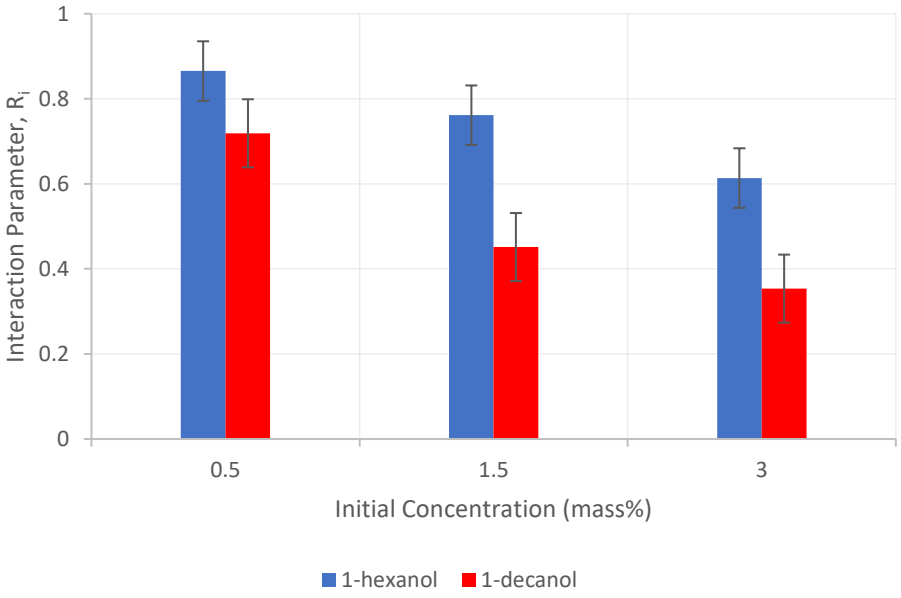

Figure 5.8: Comparison of the interaction parameters corresponding to 1-hexanol and 1-decanol in a binary component system at a different initial concentration (T = 65 °C)

The antagonistic interaction is generally attributed either to direct competition for adsorption sites or blocked pores (Lin et al., 2015). In mesopores materials, the reduction in adsorbent equilibrium loading for the fresh adsorbents due to blocked pores can be observed in adsorption systems that contain molecules of heavier weight (Lin et al., 2015). The weight of adsorbates investigated in this study is considered low, since their molecular weight is lower than 200 g/mol (Yang *et al.*, 2010). Hence, the antagonistic interaction can be ascribed to the direct competition for adsorption sites.

5.3 Chapter Summary

The objective of this chapter was to discuss and characterise the adsorption behaviour by measuring the data of adsorption experiments. This was achieved by measuring data for a single 1-hexanol adsorption system, a single 1-decanol adsorption system, and a binary-component adsorption system, using one type of activated alumina adsorbent at one adsorption temperature, 65 °C. The variation in adsorbates' initial concentrations and the impact of the carbon chain length of alcohols on the adsorption ability of the adsorbent were discussed. Moreover, possible interaction between the adsorbates in the binary-component adsorption system was investigated as well.

When the initial concentration of alcohols is higher, the activated alumina adsorbent was found to adsorb higher amounts of alcohols in all systems investigated. However, this increase in the total capacity was not infinite within the initial concentrations range investigated in all systems studied.

At similar initial concentrations, the adsorbent exhibited a higher affinity to adsorb higher mass of 1-decanol than 1-hexanol in their respective single-component adsorption systems during the equilibrium time. In contrast, the adsorbent proved to have a higher tendency to adsorb more molecules of 1-hexanol than 1-decanol in the corresponding binary systems. In both single and binary systems, the adsorption rate of 1-hexanol at the beginning of the adsorption experiments was higher than 1-decanol.

In the binary systems, the interaction between the alcohols proved to be antagonistic. 1-hexanol, however, showed a higher impact on the 1-decanol adsorption than vice versa.

Ultimately, this chapter discussed the adsorption data measured, and investigated the ability of a commercially applied activated alumina adsorbent to adsorb 1-alcohols for a paraffin solvent. The effect of various factors, including the variation in the initial concentration, 1-alcohols carbon chain length, as well as adsorbate-adsorbate interaction in the binary system was discussed, and the objective (I) of this study was fulfilled accordingly.

Chapter 6 : Adsorption Equilibrium Modelling

6.1 Overview

The aim of this chapter is to address objective (II.a). This will be done by applying different equilibrium isotherm models to single and binary-component adsorption systems investigated in this study to identify the most suitable models for the correlation of the adsorption data measured. Adsorption equilibrium modelling, on the other hand, is important to predict the reversibility of the adsorption process.

6.2 Isotherm Modelling

A non-linear minimisation method was applied for equilibrium isotherm modelling. To determine the isotherm parameters for each system, the Solver Add-in function in Microsoft Excel® was used together with the Hybrid fractional error function (HYBRID) which is denoted by Equation 6.1 (Saadi *et al.*, 2015):

$$\text{HYBRID} = \frac{100}{n-p}\sum_{i=1}^{n}\left(\frac{\left(q_{e,exp}-q_{e,calc}\right)_i^2}{q_{e,exp}}\right)_i \qquad [6.1]$$

where,

n = Number of data points;

p = Number of regression parameters in specific model;

$q_{e,exp}$ = Experimentally determined adsorbent loading at equilibrium (mg/g); and,

$q_{e,calc}$ = Model calculated adsorbent loading at equilibrium (mg/g).

The HYBRID error function was chosen among the wide range of error functions because it was developed to be employed for low concentration systems. It also accounts for the degree of freedom relating to the system by subtracting the number of model parameters from the number of data points measured as a divisor in Equation 6.1 (Saadi *et al.*, 2015).

For each model, the correlation coefficient (R^2) and Marquardt's Percentage Standard Deviation (MPSD) (Kumar, Porkodi and Rocha, 2008) were calculated and compared to identify the model that best fits the measured data. The correlation coefficient and the MPSD are denoted by Equation 6.2 and 6.3, respectively.

$$R^2 = \frac{\sum(q_{e,calc}-\overline{q_{e,\text{exp}}})^2}{\sum(q_{e,calc}-\overline{q_{e,\text{exp}}})^2+\sum(q_{e,calc}-q_{e,exp})^2} \qquad [6.2]$$

$$\text{MPSD} = 100\left(\sqrt{\frac{1}{n-p}\sum_{i=1}^{n}\left(\frac{\left(q_{e,exp}-q_{e,calc}\right)_i}{q_{e,exp}}\right)_i^2}\right) \quad [6.3]$$

The suitable models should present a high correlation coefficient (closer to 1) and a low MPSD value (closer to 0).

6.3 Single-component Adsorption

Three different adsorption isotherm models were discussed in this section. These models were investigated for the first adsorption cycle only. The investigated models are summarized in Table 6.1.

Table 6.1: Single-component adsorption isotherm models

Isotherm Models		
Langmuir Isotherm (LM)	$q_e = \frac{q_m K_L C_e}{1 + K_L C_e}$	[2.3]
Freundlich Isotherm (FM)	$q_e = K_f C_e^{\frac{1}{n}}$	[2.4]
Sips Isotherm (SI)	$q_e = \frac{q_m K_s C_e^{1/n_s}}{1 + K_s C_e^{1/n_s}}$	[2.5]

6.3.1 Single-component Adsorption Results

The correlation coefficient, together with the MPSD, was determined in order to identify the most suitable model for each system, as the correlation coefficient results for the 1-decanol adsorption system were very similar. The raw data of the single-component adsorption systems used for the equilibrium modelling is available in Appendix B (Section B.1.1). The isotherm model parameters for the single adsorption of 1-hexanol and 1-decanol on the utilized adsorbent are summarized in Table 6.2.

According to the correlation coefficients and MPSD values for each system, the Langmuir model seemed to be the least suitable model among the isotherm models investigated. The Freundlich model was most suitable for the 1-hexanol adsorption system, whereas the 1-decanol adsorption system exhibited preference for the Sips model. It is very important to notice that the results

obtained from this study may be valid only for the range of initial concentrations considered during the experimental work.

Table 6.2 : Equilibrium isotherm model parameters for the adsorption of a single alcohol from n-decane onto activated alumina adsorbent at 65 °C

Isotherm Parameters	1-hexanol	1-decanol
Langmuir Isotherm		
q_{max} ($mg.g^{-1}$)	152	156
K_L ($mL.mg^{-1}$)	1729	2023
R^2	0.79	0.87
MPSD (%)	29.0	15.1
Freundlich Isotherm		
n (-)	6.2	5.9
K_F ($mg.g^{-1}$)($mL.mg^{-1}$)$^{1/n}$	289	314
R^2	0.98	0.99
MPSD (%)	5.5	2.2
Sips Isotherm		
q_{max} ($mg.g^{-1}$)	387	387
K_S (mL.mg-1)$^{1/n}$	1.58	1.86
n (-)	4.4	4.0
R^2	0.96	0.99
MPSD (%)	5.0	2.1

The Langmuir constant K_L, which indicates the binding energy between the adsorbates and adsorbents (Y. Li et al., 2020), increases with an increase in the alcohol's chain length at the adsorption temperature investigated. This may explain the higher affinity of the adsorbent applied towards adsorbing the higher molecular weights of 1-alcohols at 65 °C. Similarly, the Sips constant *Ks* is slightly higher for 1-decanol than the 1-hexanol system, suggesting that the adsorbent had a stronger interforce with 1-decanol than 1-hexanol. All these findings are concordant with those reported in Section 5.2.1.

The *n* parameters determined for the Freundlich Model were markedly greater than 1, which indicated a favourable adsorption process (Al-Ghouti and Da'ana, 2020). In addition, *n* parameters obtained for the Sips model were observed to be greatly distanced from unity. Thus, the adsorption data were considered to fit the Freundlich model better than the Langmuir model (Lee *et al.*, 2012).

Table 6.3 compares the parameters obtained by Groenewald, Bosman and this study. The higher values of K_L determined by this study compared to those reported by Groenewald and Bosman can be attributed to a higher binding energy which resulted from the higher adsorption temperature

conducted in this study. Since adsorption at higher temperatures requires higher binding energy, it might be an indication for possible chemical adsorption (Saeed and Ahmed, 2006).

The values of q_{max} estimated in this study are greater than those determined by Groenewald and Bosman, although a similar mass of adsorbent was used to investigate the adsorption process. This is to be expected as the size of adsorbent in this study was smaller than the size of the adsorbents used by Groenewald and Bosman This means more beads were applied in this study, and as a result, a higher surface area was available for the adsorption process. While *n* values of the Freundlich Model do not show a discernible trend, the *n* values of Sips Model estimated by this study is remarkably greater than those reported by Bosman. This might indicate that the physical adsorption is more favourable in this study. Groenewald did not apply the Sips model in her work.

6.3.2 Single-component Adsorption Discussion

As discussed in Section 6.3.1, the 1-hexanol and 1-decanol systems were inclined to follow the Freundlich and Sips models, respectively, at 65 °C using an activated alumina adsorbent. This was obtained by applying the correlation coefficient and MPSD methods for both systems. Moreover, the models studied were visually fitted onto experimental data for further investigation. In Figure 6.1, it can be clearly observed that the Langmuir model was the least suitable.

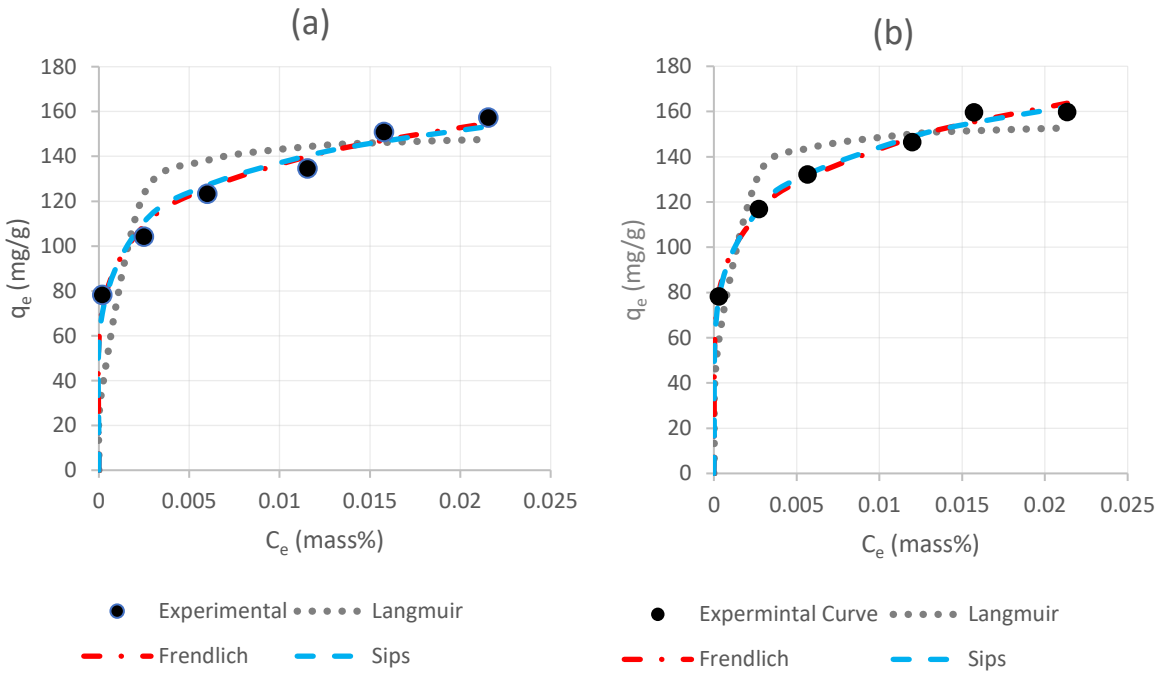

Figure 6.1: Equilibrium models on the single-component adsorption of (a) 1-hexanol, and (b) 1-decanol onto the activated alumina adsorbent at 65 °C

Table 6.3: Equilibrium isotherm model parameters for the adsorption of a single alcohol from n-decane onto activated alumina obtained by Groenewald, Bosman and current study

Isotherm Parameters	Current Study		Groenewald (Groenewald, 2019)						Bosman (Bosman, 2019)			
	65 °C		25 °C		30 °C		35 °C		25 °C		45 °C	
	1-hexanol	1-decanol	1-hexanol	1-decanol	1-hexanol	1-decanol	1-hexanol	1-decanol	1-hexanol	1-decanol	1-hexanol	1-decanol
Langmuir Isotherm												
q_{max} ($mg.g^{-1}$)	152	156	99.86	99.29	87.87	80.79	124.16	97.77	100	89.5	127	146
K_L ($mL.mg^{-1}$)	1729	2023	3	3	198	4	2	4	3.66	2.98	3.52	2.18
R^2	0.79	0.87	0.986	0.989	0.999	0.989	0.935	0.909	1.0	0.86	0.99	0.99
Freundlich Isotherm												
n (-)	6.2	5.9	5.35	5.37	9.78	7.56	3.82	7.46	5.72	6.12	5.1	4.33
K_F ($mg.g^{-1}$)($mL.mg^{-1}$)$^{1/n}$	289	314	19.72	19.1	37.82	24.84	13.10	29.25	73.4	64.7	91.2	94.4
R^2	0.98	0.99	0.933	0.986	0.992	0.945	0.999	0.727	1.0	0.86	0.96	0.96
Sips Isotherm												
q_{max} ($mg.g^{-1}$)	387	387	-	-	-	-	-	-	118	103	118	133
K_S (mL.mg-1)$^{1/n}$	1.58	1.86	-	-	-	-	-	-	1.77	1.76	7.44	3.90
n (-)	4.4	4.0	-	-	-	-	-	-	1.8	1.72	0.64	0.61
R^2	0.96	0.99	-	-	-	-	-	-	1.0	0.86	1.0	1.0

Initially, the Langmuir Model underpredicts, thereafter overpredicts and finally continues to plateau below the experimental data. Although the patterns of the Freundlich and Sips models are virtually indistinguishable, the Freundlich Model was found to be slightly superior with correlation coefficients (R^2) and MPSD of 0.98 and 5.5%, respectively, for the 1-hexanol system. The Sips Model was the best fit for the experimental data for the 1-decanol system with R^2 and MPSD of 0.99 and 2.1%, respectively. The *n* parameter in the Freundlich and Sips models were significantly greater than unity, however less than 10 for both systems, which suggests a favourable physical adsorption and that the adsorbed 1-alcohols are reversible (Do, 1998). As a result, only weak chemisorption may take place in both systems, since chemisorption is an irreversible process (Sevim *et al.*, 2021). The reversibility of adsorbed 1-alcohols is discussed in further detail in Chapter 8.

Since the Freundlich Model exhibited the best fit to the experimental data, it suggests that the adsorption occurred in multilayer and is more energetically heterogeneous than homogenous (Laskar and Hashisho, 2020; Y. Li *et al.*, 2020). Nevertheless, it cannot indicate the source of the heterogeneity. The heterogeneity or homogeneity of adsorption can be ascribed either to the adsorbent's morphology, or the energetic properties of the adsorbate and/or adsorbent (Do, 1998).

6.4 Binary-component Adsorption

As discussed in Section 2.5.2, multiple component adsorption equilibrium isotherms use parameters from corresponding single models with multiple model parameters regressing from the multiple component adsorption data to predict the best fit for the measured data obtained from the multiple component adsorption systems. However, only the binary-component isotherm parameters are provided in this section, and the reader is referred to Section 6.3.1 for the single-component adsorption isotherm parameters. Similar to the single-component adsorption systems, adsorption isotherm models were applied to the first experiment of the binary-component adsorption system. The Extended Langmuir, Extended Freundlich and Extended Sips Models were investigated in this section. Table 6.4 summarises the isotherm models applied to the binary-component adsorption system being investigated.

Table 6.4: Binary-component adsorption isotherm models

Isotherm Models		
Extended Langmuir Isotherm Model (ELM)	$q_{e,i} = \frac{q_{i,\max\,(bin)}\, K_{L,i(bin)}\, C_{e,i}}{1 + \sum_{i=1}^{N} K_{L,i(bin)} C_{e,i}}$	[2.8]
Extended Freundlich Isotherm Model (EFM)	$q_{e,1} = \frac{K_{f,1} C_{e,1}^{\left(\frac{1}{n_1}\right)+x_1}}{C_{e,1}^{x_1} + y_1 C_{e,2}^{z_1}}$	[2.12]
Extended Sips Isotherm Model (ESM)	$q_{e,i} = \frac{q_{m,i} K_{s,i} C_{e,i}^{1/n_{s,i}}}{1 + \sum_{j=1}^{N} K_{s,j} C_{e,j}^{1/n_{s,j}}}$	[2.14]

6.4.1 Binary-component Adsorption Results

The correlation coefficient (R^2) is used to predict the most suitable model for the binary-component adsorption system being investigated. The raw data of the binary-component adsorption systems used for the equilibrium modelling is available in Appendix B (Section B.1.2). The different parameters of the isotherm models for the binary adsorption of 1-hexanol and 1-decanol onto the applied adsorbent are summarized in Table 6.5.

The Extended Freundlich Isotherm Model (EFM) was observed to be the best model overall for the description of the binary-component system being investigated, as it showed the height correlation coefficient, followed by the The Extended Sips Model (ESM). Although the Extended Langmuir Model (ELM) was the least suitable model that described the binary system's data, its parameters can give some insight into the adsorption behaviour. The fractional coverage parameter, Θ, identified by the ELM was greater for 1-hexanol, the shorter chain alcohol investigated in this study. This was expected and it exhibited a slight preference of adsorption shorter chain alcohols by the adsorbent utilized. This means the majority of adsorbent surface was covered by the shorter chain 1-alcohols.

In addition, it can be observed that the *n* values for the ESM for both adsorbates are appreciably greater than the unity; however, not as great as in the single-component adsorption system. This may suggest that the behaviour of the system being investigated was slightly less inclined toward the Sips Model than the single-component adsorption system. The *n* values also suggest a formation of multilayer adsorption and the adsorption was inclined to be energetically heterogeneous (Saadi *et al.*, 2015). For visual comparison, parity plots are illustrated in Figure 6.2.

Table 6.5: Equilibrium isotherm model parameters for the adsorption of a binary alcohol from n-decane onto activated alumina at 65 °C

Isotherm Parameters	**1-hexanol + 1-decanol**
Extende Langmuir Isotherm (ELM)	
Θ_1	0.61
Θ_2	0.39
$q_{max,binary}$ (mg.g^{-1})	153.4
$K_{L1,binary}$ (mL.mg^{-1})	361
$K_{L2,binary}$ (mL.mg^{-1})	1068
R_1^2	0.85
R_2^2	0.47
Extended Freundlich Isotherm (EFM)	
x_1	0.0008
y_1	0.75
z_1	0.095
x_2	0.52
y_2	0.300
z_2	0.099
R_1^2	0.92
R_2^2	0.50
Extended Sips Isotherm (ESM)	
n_1 (-)	3.2
n_1 (-)	2.1
R_1^2	0.87
R_2^2	0.50

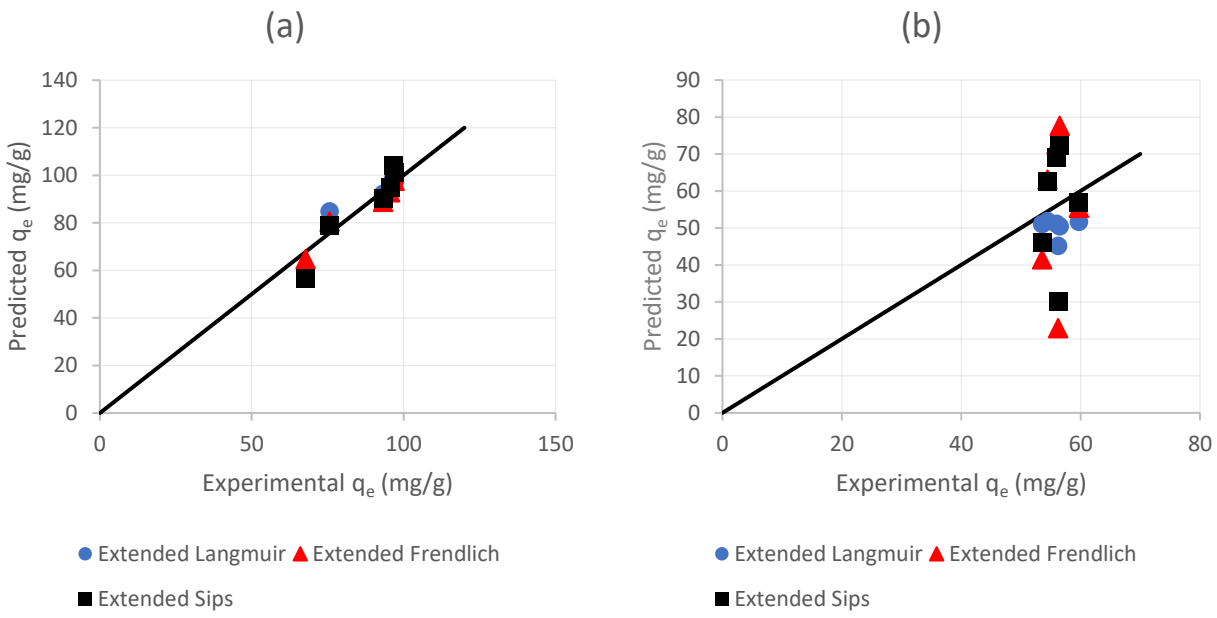

Figure 6.2: Predicted vs experimental equilibrium adsorbent loadings for the comparison of different isotherm models for the adsorption of a) 1-hexanol; and, b) 1-decanol in a binary 1-octanol + 1-decanol mixture onto activated alumina at T=65 °C

6.4.2 Binary-component Adsorption Discussion

The EFM exhibited better correlation of the equilibrium adsorption data for the binary-component system being investigated in this study. The EFM correlation coefficient was 0.92. This may suggest that there was an interaction between the adsorbates in the solid phase (Girish, 2017) and, to some extent, the adsorption was not entirely homogenous (Saadi *et al.*, 2015). However, these assumptions cannot be verified with certainty as the EFM has six regression parameters, which is more than the others, and thus is expected to be mathematically more compatible to the 1-alcohols uptake data than the ELM and ESM. Hence, EFM may not be used to investigate the equilibrium behaviour of the system being investigated, and rather used only for the correlation of the 1-alcohols uptake data determined from the binary system being studied.

On the other hand, the single-component regression parameters for LM (for a single-component adsorption system) were greater than those determined by ELM (for a binary-component adsorption system). This was expected and can be ascribed to the competitive behaviour in the binary-component adsorption system, and a consequent decrease in affinity towards the corresponding adsorbates.

Similar to the ELM parameters, the *n* values for ESM were observed to be slightly greater in the single-component adsorption system. Presumably, the *n* values were less in the binary systems due

to the possible interaction between the adsorbates in the solid phase. As a result, the multilayer adsorption behaviour in the binary system was inclined to be less than in the single system.

In general, the multiple component adsorption isotherm models investigated in this study may not provide a good correlation of the uptake of the data of 1-alcohols. This is due to the incorporation of single-component isotherm regression parameters for the modelling of the uptake data obtained from the binary-component adsorption system. This can suggest that the interaction parameters used in the binary-component models were not capable enough to correct the single-component adsorption data. Consequently, it may not well describe the competitive behaviour in the binary system being investigated.

6.5 Chapter Summary

The objective of this chapter was to determine the best equilibrium isotherm model that describes the equilibrium uptake data. Besides characterisation of the adsorption behaviour of the systems being investigated in this study, estimating the parameters of various isotherm models can help predict the regeneration behaviour of the respective systems. For instance, the parameters can determine if the adsorption is physical (reversible) or chemical (irreversible).

For the single systems, the Freundlich and Sips models exhibited the best fit for 1-hexanol and 1-decanol, respectively, whereas the Extended Freundlich Model proved to be the most suitable model for the binary system. However, the multiple component adsorption isotherm models investigated in this study showed poor correlation coefficients, and thus assumed to have poor correlation of the uptake data.

According to the parameters of the isotherm model being investigated, the adsorption in single and binary systems were inclined to be multilayer and heterogeneous. The parameters also revealed that the adsorption was more likely to be physisorption, with possibly only weak chemisorption. Therefore, a reversible process was suggested.

To sum up, the objective (II.a) of this study was addressed by identifying the most suitable isotherm models for both single and binary-component adsorption systems by modelling equilibrium measured data using different isotherm models.

Chapter 7 : Adsorption Kinetic Modelling

7.1 Overview

The objective of this chapter is to fulfil objective (II.b) of this study. This will be achieved by identifying the most suitable kinetic models that can well describe the kinetic uptake data obtained from the single and binary systems, as well as by determining the adsorption rate-limiting step in the different systems used in this research study. In addition, kinetic modelling is significant to understand the nature of the adsorption mechanism, which can provide more insight into the reversibility of the adsorption process.

7.2 Kinetic Models

As discussed in Section 2.6.1, the adsorption kinetic models are classified into adsorption reaction and diffusion models. The reaction models cannot well describe the mass transfer mechanism due to their lack of physical meaning, and because they assume the adsorption process is controlled only by the adsorption reaction on the adsorbent's surface (at the liquid/sold interface) (Simonin, 2016; Wang and Guo, 2020). On the other hand, the diffusional models suggest that the adsorption at the liquid/solid interface is instantaneous, and as a result, the intra-particle and external diffusion are the sole rate-controlling steps (Wang and Guo, 2020).

In this study, four models were applied to the kinetic data obtained from the three systems investigated: three reaction models and one diffusional model. A summary of these models is available in Table 7.1.

Table 7.1: Adsorption kinetic models

Adsorption Kinetic Models		
Reaction Kinetic Models		
Pseudo-First-Order Model (P1)	$q_t = q_e\,(1 - e^{-K_1 t})$	[2.15]
Pseudo-Second-Order Model (P2)	$q_t = \frac{q_e^2 K_2 t}{1 + q_e K_2 t}$	[2.16]
Elovich Model (EM)	$q_t = \frac{1}{ß}\ln(1 + \alpha ß t)$	[2.17]
Diffusional Kinetic Model		
Intra-particle Diffusion Model (Weber & Morris) (IPDM)	$q_t = K_{Ip}\sqrt{t} + \theta$	[2.18]

7.3 Kinetic Modelling

Similar to isotherm modelling in Chapter 6, non-linear minimization of Hybrid fractional error function (HYBRID) using the Solver Add-in function in Microsoft Excel® was applied to determine the adsorption parameters of the kinetic models. The most suitable models for the data extracted from the systems being investigated were identified by comparing the correlation coefficients (R^2) and Marquardt's Percentage Standard Deviation (MPSD) of each model.

For single-component adsorption systems, the parameters of the models were determined and compared at three various initial concentrations and at one adsorption temperature (T = 65 °C). Similarly, the parameters of the models for the binary-component adsorption system were calculated and compared to single-component adsorption systems at the corresponding conditions.

7.3.1 Single-component Adsorption Results

The parameters for the kinetic models obtained for the single systems are provided in Table 7.2. The correlated coefficients (R^2) were relatively close, with an exception for the 1-decanol + n-decane system where the initial concentration of 1-decanol was 0.5 mass%. The Pseudo-Second-Order (PSO) and Elovich Models (EM) exhibited slightly higher R^2 and lower *MPSD* values than the Pseudo-First-Order Model (PFO), with slight preference to EM. However, the predicted equilibrium loadings determined by PFO were more comparable to the experimental values than those estimated by PSO.

In addition, the rate constant of PFO, K_1, was observed to have fairly similar values for both systems; however, the 1-hexanol adsorption system exhibits slightly larger values of K_1. The rate constant of PSO, K_2, for both systems was notably larger at 0.5 mass%, the lower adsorbate's initial concentration investigated in this study. Collectively, the K_2 value was slightly greater for the 1-hexanol adsorption system than the 1-decanol system at different initial concentrations.

The initial adsorption rate constant of EM, α, exhibited lower values as the initial concentration increased. A similar trend was observed for the 1-decanol system. However, the 1-hexanol system showed greater values of α at the corresponding initial concentration. Interestingly, α value was remarkably higher at a very low initial concentration, 0.5 mass%, which thereafter decreased slightly between 1.5 and 3.0 mass%. For both systems, the extent of the surface coverage constant, *ß*, was mostly constant for the systems with the respective initial concentrations.

Table 7.2: Adsorption kinetic model parameters for the single-component adsorption systems onto activated alumina at T = 65 °C

Single System	**1-hexanol**			**1-decanol**		
Initial Concentrations (mass%)	**0.5**	**1.5**	**3.0**	**0.5**	**1.5**	**3.0**
$q_{e,exp}$ *(mg.g^{-1})*	78.20	123.42	157.37	78.21	132.23	159.74
Reaction Models						
Pseudo-First-Order Model (PFO)						
$q_{e,cal}$ *(mg.g^{-1})*	76.82	121.42	156.83	77.76	132.04	159.26
K_1 *(min^{-1})*	0.038	0.029	0.024	0.032	0.020	0.017
R^2	0.95	0.97	0.99	0.93	0.99	0.99
MPSD (%)	9.2	13.8	10.1	11.7	12.5	17.2
Pseudo-Second-Order Model (PSO)						
$q_{e,cal}$ *(mg.g^{-1})*	84.91	138.27	186.00	84.13	149.64	183.07
K_2 *(mg.g^{-1}·min^{-1})*	0.00076	0.00031	0.00015	0.00057	0.00017	0.00011
R^2	0.99	0.99	0.98	0.98	0.99	0.98
MPSD (%)	2.1	8.3	5.3	4.9	7.0	10.1
Elovich Model (EM)						
ß (mg.g^{-1})	0.07	0.038	0.026	0.072	0.034	0.027
α (mg.g^{-1}.min^{-1})	22.3	13.8	11.6	15.64	9.92	9.25
R^2	0.98	0.99	0.99	0.98	0.99	0.99
MPSD (%)	5.1	4.2	3.4	4.8	6.7	5.5
Diffusional Model						
Intra-Particle Diffusion Model (Weber & Morris) (IPDM)						
K_{IP} *(mg.g^{-1}.min$^{-0.5}$)*	2.7	6.86	7.89	4.91	4.89	6.13
Θ (mg.g^{-1})	42.39	32.55	54.66	21.68	47.56	54.39
R^2	0.99	0.99	1.00	0.99	1.00	0.99
MPSD (%)	1.9	2.4	0.3	2.5	0.14	1.8

For the Intra-Particle Diffusion Model (Weber & Morris) (IPDM), the intercept parameter, *Θ*, had positive values for all systems being investigated. Although there was no discernible relationship observed between *Θ* and the initial concentration of 1-alcohols, the values of *Θ* were, to some extent, closed for all single-component adsorption systems being investigated. On the other hand, the intra-particle diffusion constant, K_{IP}, increased by increasing the initial concentration of 1-hexanol, while the K_{ip} value for the 1-decanol system was almost constant at the initial concentration 0.5 and 1.5 mass%, and increased slightly when the initial concentration was increased to 3.0 mass%. Similar to *Θ*, no discernible pattern was observed between the K_{IP} and the carbon chain length of the 1-alcohols.

Table 7.3 illustrates some kinetic results obtained by Groenewald and Bosman.

Table 7.3: Kinetic results reported by Groenewald and Bosman studies

Kinetic Parameters	Groenewald (Groenewald, 2019)												Bosman (Bosman, 2019)							
	25 °C				30 °C				35 °C				25 °C				45 °C			
	1-hexanol		1-decanol		1-hexanol		1-decanol		1-hexanol		1-decanol		1-hexanol		1-decanol		1-hexanol		1-decanol	
	0.51	1.39	0.51	1.52	0.30	1.71	0.53	1.37	0.48	1.55	0.53	1.60	0.51	1.39	0.51	1.34	0.43	1.59	0.53	1.63
Pseudo-First-Order Model (PFO)																				
$q_{e,cal}$ $(mg.g^{-1})$	55.44	86.11	52.58	91.64	42.04	95.11	53.71	67.79	59.68	102.99	58.15	85.73	60.7	94.1	57.4	80.3	58.7	118	66.1	118
K_1 (min^{-1})	0.025	0.017	0.017	0.014	0.028	0.007	0.017	0.016	0.022	0.017	0.016	0.011	0.02	0.01	0.01	0.01	0.01	0.03	0.03	0.01
R^2	0.94	0.95	0.96	0.96	0.85	0.98	0.97	0.98	0.93	0.88	0.95	0.97	0.97	0.97	0.98	0.97	0.98	0.96	0.96	0.97
Pseudo-Second-Order Model (PSO)																				
$q_{e,cal}$ $(mg.g^{-1})$	64.79	106.60	64.25	115.62	47.62	131.03	65.91	84.73	70.45	127.79	72.41	111.99	69.3	113	68.8	98.7	66.2	126	78.7	132
K_2 $(mg.g^{-1}{\cdot}min^{-1})$	0.0004	0.0001	0.0003	0.0001	0.0007	0.00004	0.0003	0.0002	0.0003	0.0001	0.0002	0.00008	0.0003	0.0001	0.0002	0.0001	0.0002	0.0003	0.0004	0.00009
R^2	0.98	0.98	0.99	0.99	0.99	0.98	0.99	0.99	0.98	0.94	0.98	0.97	0.99	0.98	1.00	0.99	0.97	0.98	0.96	0.99
Elovich Model (EM)																				
$ß$ $(mg.g^{-1})$	-	-	-	-	-	-	-	-	-	-	-	-	0.07	0.04	0.07	0.05	0.01	0.06	0.08	0.05
α $(mg.g^{-1}.min^{-1})$	-	-	-	-	-	-	-	-	-	-	-	-	3.77	3.77	2.34	2.82	5.16	30.70	9.56	10.40
R^2	-	-	-	-	-	-	-	-	-	-	-	-	1.00	0.99	1.00	0.99	0.95	0.97	0.95	0.95
Intra-Particle Diffusion Model (Weber & Morris) (IPDM)																				
K_{IP} $(mg.g^{-1}.min^{-0.5})$	2.92	5.1	2,76	4.28	1.98	4.47	2.31	4.86	3.18	6.07	2.74	4.36	2.07	5.14	1.94	3.92	1.35	2.44	1.99	3.90
Θ $(mg.g^{-1})$	9.71	4.79	6.37	6,27	10.75	0.00	8.12	0.00	9.27	5.96	9.08	13.71	24.6	4.68	21.7	7.42	33.5	71.8	29.9	31.5
R^2	0.99	0.96	0,98	0.99	0.93	0.97	0.96	0.99	0.98	0.99	0.96	0.88	0.99	0.99	0.99	0.99	0.98	0.93	0.98	1.00

In general, the PSO rate constant, K_2, and the initial adsorption mass rate constant of EV, α, predicted by this study was inclined to be larger than those reported by Groenewald and Bosman in the corresponding systems. This can be attributed to the higher adsorption temperature investigated in this study, as the adsorption mass rate is proportional to the temperature (Zhang *et al.*, 2017). On the other hand, the intercept parameters of IPDM estimated by this study are remarkably larger than those determined by Groenewald, while there is no discernible trend observed between the values predicted by this study and Bosman's research work. This irregular trend of intercept parameters can be ascribed to the heterogeneity of the adsorbent's structure (Al-Ghouti *et al.*, 2009).

7.3.2 Single-Component Adsorption Discussion

As outlined in Table 7.2, all models being investigated exhibited high and relatively close R^2 values, typically higher than 0.90. This may suggest that the experimental adsorption kinetic data can be well described by all models investigated in this study (Simonin, 2016).

Comparing PFO with PSO, PSO had slightly greater R^2 and lower MPSD values, in particular at the lowest initial concentration investigated in this study, 0.5 mass%. This is expected as PSO is assumed to provide a better correlation of experimental data for systems with low initial concentration than PFO (Ho and Mckay, 1999). Thus, the single-component adsorption systems investigated in this study can be considered to be second order processes. This finding concurs with previous studies which investigated the elimination of 1-alcohols from an n-alkane solvent conducted by Bosman and Groenewald (Bosman, 2019; Groenewald, 2019). Nonetheless, the EM exhibited a marginal preference to the experimental data than the PSO according to the R^2 and *MPSD* determined.

Figure 7.1 illustrates some results represented in Table 7.2 for visual comparison between the adsorption reaction kinetic models. From Figure 7.1, it can be observed that the 1-hexanol and 1-decanol systems reached the equilibrium phase at $t \geq 180$ and $t \geq 300$ minutes, respectively, and the experimental data can be better described by PSO and EM, with a slight preference to EM, whereas PFO was less adequate in describing the uptake data. EM seemed to fit the initial data well ($t \leq 30$ minutes). PFO, on the other hand, under predicted the initial uptake data in the first 15 minutes, overpredicted the data at $t \geq 30$ minutes, which thereafter levelled off to just below the experimental equilibrium loading for both illustrated systems.

The Figure 7.1 also showed the quite rapid adsorption of 1-alcohols at an early stage of the process, which slowed down afterwards when approaching the equilibrium stage. This can be attributed to vast active sites available at the beginning of the process, and as time passed, the active sites available decreased due to occupied binding sites (Liu *et al.*, 2020; Zhao *et al.*, 2020).

As discussed in Section 7.3.1, K_2 exhibited higher values for the 1-hexanol system than the 1-decanol system. This suggests that the shorter carbon chain 1-alcohols were adsorbed faster onto the adsorbent's surface than the longer carbon chain 1-alcohols. The initial adsorption rate of the PSO, *h* (mg/g.min), can be calculated as per Equation 7.5 (Sonawanea and Shrivastava, 2011):

$$h = q_e^2 K_2 \qquad [7.5]$$

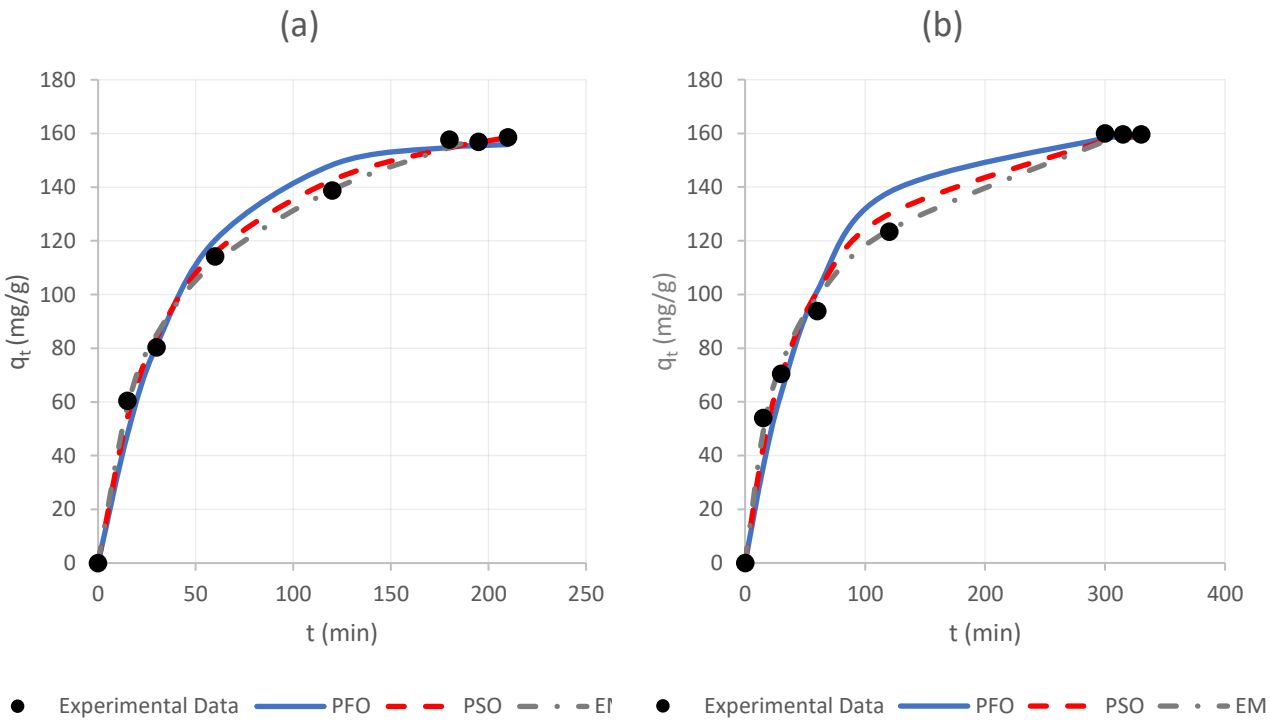

Figure 7.1: Kinetic adsorption models for the adsorption of (a) 1-hexanol; and, (b) 1-decanol onto Activated Alumina adsorbent at initial concentration 3.0 mass% and T = 65 °C

It can be observed from Table 7.4 that the initial adsorption rate identified by PSO decreased marginally as the initial concentration increases. The 1-hexanol system, however, exhibited a slightly greater initial adsorption rate constant. This finding is in agreement with many previous works including the research work on water defluoridation using activated alumina adsorbent (Kumari, Behera and Meikap, 2019). This study reported that the initial adsorption rate predicted by PSO decreased as the adsorbates' initial concentration increased. Presumably, this may be explained by the repulsive interaction between the molecules on the binding sites. Cai and Sohelberg studied adsorption of various alcohols on an activated alumina adsorbent and reported that when, for instance, two alcohol species lie on an adjacent binding site, a possible interaction occurs between

those molecules, and as a result, one molecule will be eliminated from the respective binding site (Cai and Sohlberg, 2003). Increasing the initial concentration would increase this kind of competition on the adsorbent's surface and result in slowing down the initial adsorption rate.

Table 7.4: Initial adsorption rate obtained by Pseudo-Second-Order Model for all investigate single-component adsorption system

	1-hexanol			1-decanol		
Initial Concentrations (mass%)	**0.5**	**1.5**	**3**	**0.5**	**1.5**	**3**
h	5.39	5.12	5.09	4.02	3.81	3.73

Furthermore, the initial adsorption rate constant determined by EM, α, was notably greater for the shorter carbon chain length 1-alcohol, namely 1-hexanol, which concurred with the abovementioned findings of h values from this study, and the results discussed in Section 5.2.1.2. This may be attributed to the fact that shorter carbon chain alcohols have smaller size, and consequently, they have easier access into porous media (Zhang *et al.*, 2017). Moreover, the α values followed the same pattern of *h*, as they were found to decrease as the initial concentration of 1-alcohols increased. This finding complies with several previous reports including the study pertaining to the adsorption of nickel and copper from aqueous solutions by nanoparticle activated alumina (Fouladgar, Beheshti and Sabzyan, 2015). Again, this can be attributed to the increased competitive nature between the adsorbates at a higher initial concentration.

As discussed in Section 2.6.1, reaction models alone cannot describe the physical behaviour of the adsorption process well. From Table 7.2, the intercept parameter of IPDM determined for all systems investigated, Θ, exhibited positive values, which suggests the internal particle diffusion may not be the only rate-limiting step. In other words, the adsorption of 1-alcohols may be affected by the external diffusion as well (film diffusion) (Senthil Kumar *et al.*, 2012; Wang and Guo, 2020). This can also be explained by the visual comparison depicted in Figure 7.2.

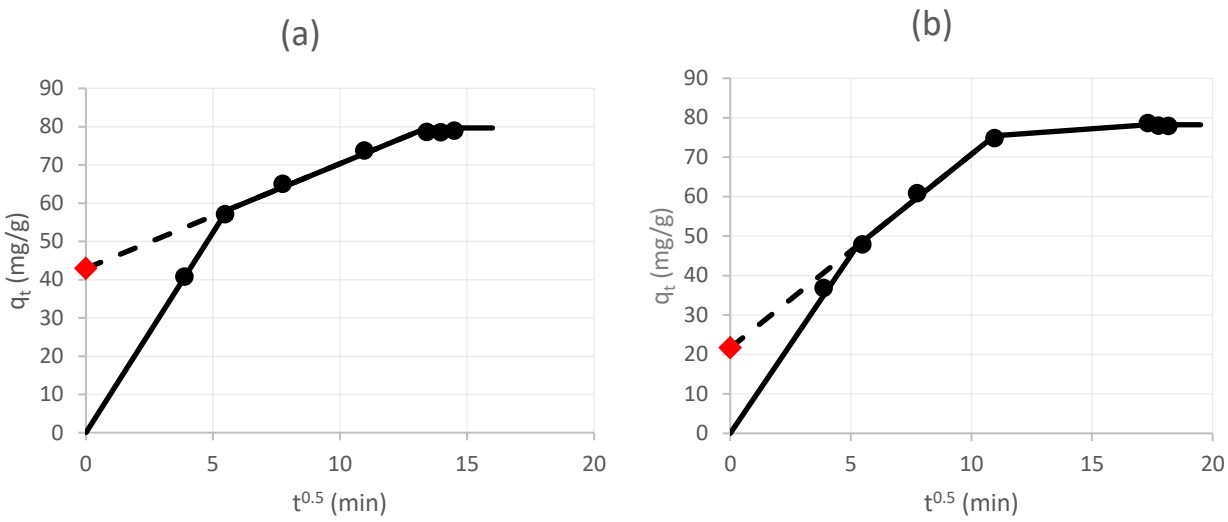

Figure 7.2: Intra-particle diffusion model (IPDM) (Weber-Morris) plot for single-component adsorption system for the adsorption of (a) 1-hexanol; and, (b) 1-decanol at initial concentration = 0.50 mass% and T = 65 °C

As discussed in Section 2.6.1.4, the IPDM Equation can develop a curvilinear trend, and thus, the curvature plot may be divided into two or three portions. Both single-component systems investigated in this study exhibited a similar curvilinear trend, which typically followed the trend illustrated in Figure 7.2, where typically three portions can be observed for each system: (i) the first portion between 0~30 minutes which suggests external diffusion (film diffusion); (ii) the intra-particle diffusion portion that took place between 30~180 minutes and 30~120 for 1-hexanol and 1-decanol, respectively, and eventually, (iii) reaching the equilibrium phase. Collectively, the external diffusion was found to be faster than the intra-particle diffusion. This is expected, in particular at the beginning of the adsorption process (Plazinski and Rudzinski, 2009). Nevertheless, the positive values of the interception of the extension of intra-particle diffusion portion, the red point illustrated in Figure 7.2, would suggest that the rate-limiting step was simultaneously influenced by the film diffusion.

To summarise, the single-component adsorption systems investigated in this study could be dependent on intra-particle and external diffusion (film diffusion), as well as on the reaction adsorption on the adsorbent's surface. This finding substantiates the findings of Bosman (Bosman, 2019). Groenewald, on the hand, reported that 1-alcohols adsorption from an n-alkane solvent onto different types of activated alumina adsorbents was significantly limited by the intra-particle diffusion step, and in some cases was limited by the surface reaction step (Groenewald, 2019). However, Ho and Mckay (1999) pointed out that neither the diffusional nor the surface reaction models can experimentally identify the rate-limiting step well.

7.3.3 Binary-component Adsorption Results

The various adsorption kinetic models provided in Table 7.1 were applied to the binary system investigated in this study. The experimental kinetic data of each component in the binary system was fitted into each reaction model to determine the models' parameters for each component in the mixture, whereas the adsorption data of the total mixture was used to determine the diffusional model parameters.

Table 7.5 and 7.6 summarise the parameters of the reaction and diffusional models applied to the binary-component adsorption system, respectively. The adsorbates' concentration mass fraction is 50:50. It can be observed from Table 7.4 that the R^2 value for all systems investigated was higher than 0.90. However, PFO indicated less suitability to the experimental data measured among the applied models as it proved lower and higher values of R^2 and *MPSD*, respectively, whereas PSO and EV exhibited higher R^2 and lower *MPSD* values, with the main preference to EV. The predicted equilibrium adsorbent loading determined by PFO was notably closer to the experimental loading than those obtained by PSO.

For PSO and PFO, K_2 and K_1 values decreased by increasing the initial concentration of both adsorbates. However, K_2 and K_1 values were slightly greater for 1-hexanol than 1-decanol in all the respective adsorbates' initial concentrations. A similar trend was observed as well for α and $ß$ parameters of the EV model; however, they showed a constant value at the lower initial concentration investigated for the binary-component system (0.56 and 0.58 mass% of 1-hexanol and 1-decanol, respectively).

Table 7.5: Reaction kinetic models' parameters for the binary-component adsorption systems onto Activated Alumina at T = 65 °C

1-hexanol + 1-decanol System	**1-hexanol**			**1-decanol**		
Initial Concentrations (mass%)	**0.56**	**1.70**	**3.18**	**0.58**	**1.69**	**3.18**
$q_{e,exp}$ *(mg.g^{-1})*	67.66	93.97	96.57	56.22	59.68	56.48
Reaction Models						
Pseudo-First-Order Model (PFO)						
$q_{e,cal}$ *(mg.g^{-1})*	66.68	93.57	96.49	56.07	59.37	60.04
K_1 *(min^{-1})*	0.039	0.032	0.024	0.030	0.025	0.014
R^2	0.90	0.95	0.97	0.93	0.97	0.96
MPSD (%)	11.7	13.6	12.8	14.2	8.5	18.2
Pseudo-Second-Order Model (PSO)						
$q_{e,cal}$ *(mg.g^{-1})*	72.48	104.24	113.52	62.74	69.83	77.27
K_2 *(mg.g^{-1}·min^{-1})*	0.00087	0.00043	0.00024	0.00067	0.00041	0.00018
R^2	0.97	0.98	0.99	0.97	0.99	0.97
MPSD (%)	5.2	5.1	7.6	8.7	2.8	14.2
Elovich Model (EM)						
ß (mg.g^{-1})	0.08	0.05	0.04	0.08	0.06	0.06
α (mg.g^{-1}.min^{-1})	22.2	12.61	7.41	8.07	4.52	2.53
R^2	0.98	0.99	0.99	0.98	0.99	0.97
MPSD (%)	1.5	3.6	4.7	5.0	2.4	14.4

Table 7.6: Diffusional kinetic model's parameters for the binary-component adsorption systems onto activated alumina at T = 65 °C

Binary System	**1-hexanol + 1-decanol**		
Initial Concentrations (mass%)	**1.14**	**3.39**	**6.36**
Diffusional Model			
Intra-Particle Diffusion Model (Weber & Morris) (IPDM)			
K_{IP} *(mg.g^{-1})*	5.93	7.89	9.12
Θ (mg.g^{-1}.min$^{-0.5}$)	46.01	50.65	30.28
R^2	0.98	0.99	0.99
MPSD (%)	3.10	3.06	2.04

As can be seen in Table 7.6, the intra-particle diffusion constant increased slightly as the initial concentration of adsorbates increased. On the contrary, no discernible trend was observed for the intercept parameter when the adsorbates' initial concentration was varied.

7.3.4 Binary-component Adsorption Discussion

As discussed in Section 7.3.3, the values of the correlated coefficients for all models applied to binary-component adsorption systems were greater than 0.90, which suggests that the binary system can be described by all models investigated in this study (Simonin, 2016). As in single-component adsorption systems, EV may be considered as the most suitable reaction model for the uptake of kinetic data since it exhibited higher and lower R^2 and *MPSD*, respectively, showing marginal preference to the PSO.

The reaction models applied for binary systems at the total initial concentrations of 1.70 and 1.69 mass% for 1-hexanol and 1-decanol, respectively, are depicted in Figure 7.3. From Figure 7.3, it can be observed that the system equilibrium phase was reached at $t \geq 180$ minutes. In general, PSO and EM appeared to fit the experimental data fairly well. In contrast, the PFO seemed to be the least suitable model to describe the systems, which was the case for all binary systems investigated. As shown, PFO underpredicted the experimental data at an early stage of the adsorption process, whereafter it over predicted the data towards the end of the adsorption experiment. This trend was also observed for the other two systems.

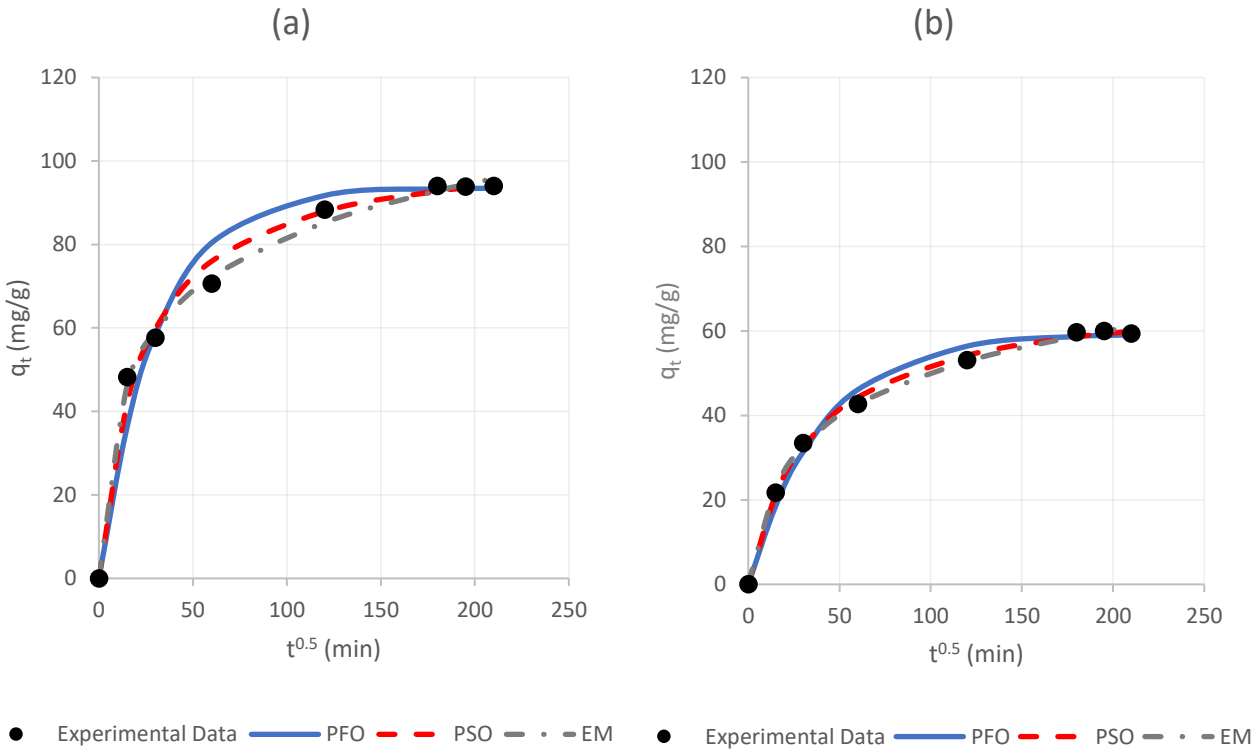

Figure 7.3: Kinetic reaction models for the adsorption of (a) 1-hexanol (initial concentration = 3.18); and, (b) 1-decanol (initial concentration (3.18) in a binary-component adsorption system onto activated alumina adsorbent at T = 65 °C

Similar to the single-component adsorption systems, it can be observed from Figure 7.3 that the adsorption rate was quite rapid at the beginning of the experiment, and slowed down afterwards when it approached the equilibrium stage. As indicated in section 7.3.2, the availability of active sites declines as time passes, and the adsorption rate decreases accordingly (Liu *et al.*, 2020; Zhao *et al.*, 2020).

The adsorption rate constant, K_2, obtained by PSO seemed to be higher for 1-hexanol than 1-decanol in the binary system. This is expected as the shorter carbon chain 1-alcohols tend to be adsorbed faster due to their smaller size (Zhang *et al.*, 2017). Table 7.7 denotes the initial adsorption rate, $h_{i,b}$, obtained by PSO using Equation 7.5, where it can be observed that the initial adsorption rate decreased gradually by increasing the adsorbates' initial concentration. Again, the $h_{i,b}$ indicated greater values for the shorter chain 1-alcohol.

Table 7.7: Initial adsorption rate obtained by Pseudo-Second-Order Model for all investigate binary-component adsorption systems

Binary System	**1-hexanol**			**1-decanol**		
Initial Concentrations (mass%)	**0.56**	**1.70**	**3.18**	**0.58**	**1.69**	**3.18**
$h_{i,b}$	4.81	4.67	3.14	2.64	2.01	1.06

By increasing the initial concentration of the adsorbates, the $h_{i,b}$ pattern complies with the initial uptake rate determined by EM, α. These findings are in agreement with those obtained for single-component adsorption systems. It was also noted that both initial adsorption rate parameters for PSO and EM were significantly greater for single systems than the binary systems at the corresponding initial concentration of adsorbates. This suggests that the competition between the different kinds of molecules on the adsorbent's surface in the binary system is higher than the competition between similar molecules (same types of alcohols) in single-component adsorption systems. In addition, the initial adsorption rate obtained by PSO and EM exhibited a remarkable variation between 1-decanol and 1-hexanol in binary system (higher values for 1-hexanol) compared to those estimated from the corresponding single-component adsorption systems. This suggests that the influence of 1-hexanol on the 1-decanol uptake in the binary system was notably less than the effect of 1-decanol on the 1-hexanol adsorption onto the activated alumina adsorbent used in this study. This finding substantiates the findings in section 5.2.2.3 where the interaction effect of both adsorbates in binary systems was discussed.

Figure 7.4 illustrates the IPDM applied to the experimental data of the binary systems studied in this research work. The interception of the extension of the intra-particle diffusion portion (the red

point) indicates that the external diffusion has an influence on the adsorption process. This finding concurs with the findings discussed regarding single-component adsorption systems in Section 7.3.2, which suggests that the diffusional behaviour of components in binary systems tend to follow their behaviour in corresponding single adsorption processes.

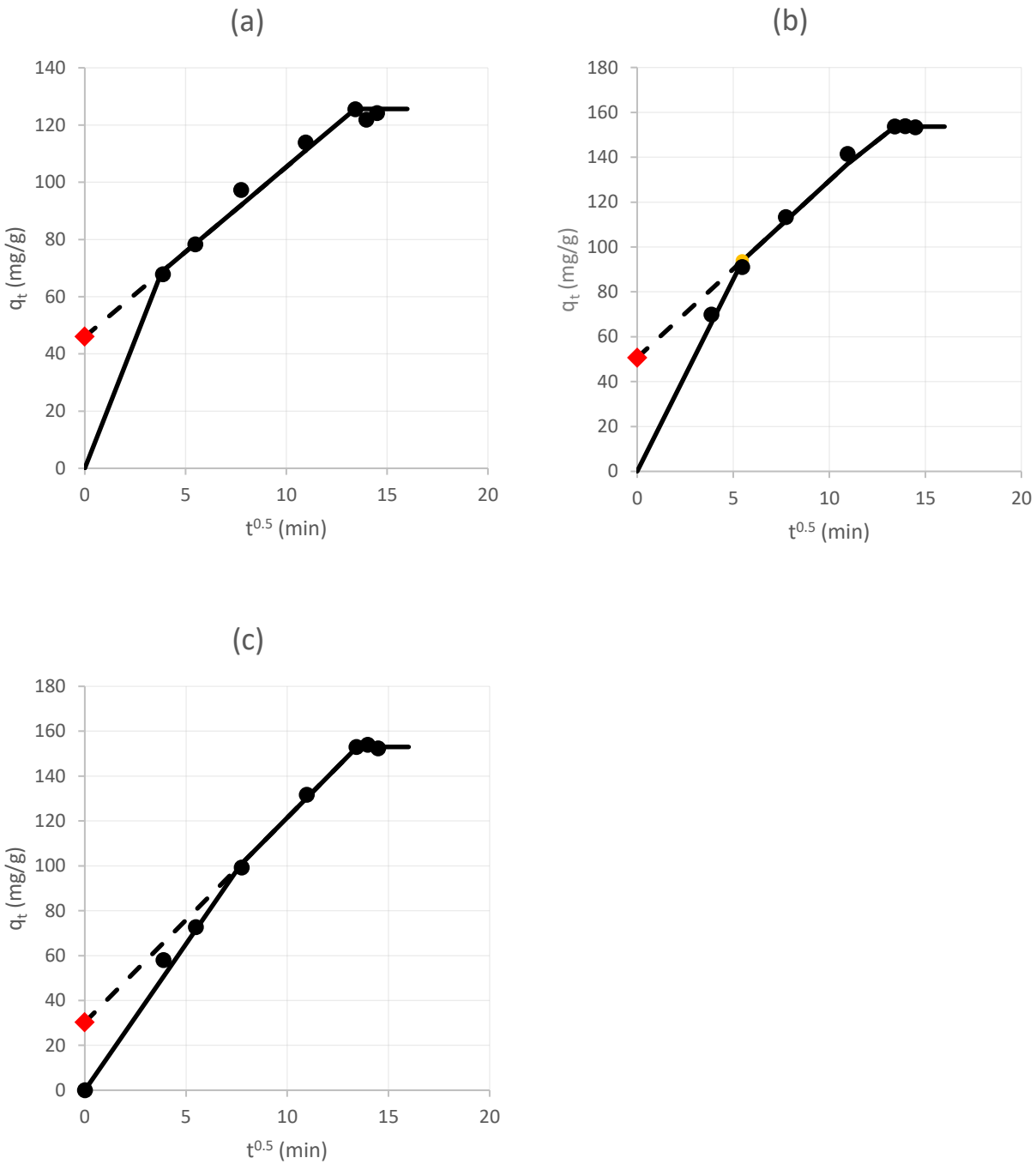

Figure 7.4: Intra-particle diffusion model (IPD) (Weber-Morris plot) for the binary-component adsorption systems at (a) initial concentration 1.14 mass% ; (b)) initial concentration 3.39 mass%; and, (c) 6.36 mass% at T = 65 °C

Interestingly, the external diffusion duration seemed to increase by increasing the initial concentration of the adsorbates. The external diffusion took place between 0 ~ 15 minutes at the initial adsorbates' concentration of 1.14 mass% (Figure 7.4.a), 0 ~ 30 minutes at the initial adsorbates' concentration of 3.39 mass% (Figure 7.4.b), and 0 ~ 60 minutes when the adsorbates' initial concentration was 6.36 mass% (Figure 7.4.c). However, the intra-particle diffusion duration seemed to be much longer than the external adsorption in all systems, which is expected for the same reasons discussed in Section 7.3.2. No discernible trend was observed for the intercept parameter by increasing the initial adsorbates' concentration, which is in agreement with the single-component adsorption system. On the contrary, an increase in the intra-particle diffusion constant was displayed by increasing the initial adsorbates' concentration. Presumably, this may be attributed to the increased driving force by increasing the initial adsorbates' concentrations, while the irregular trend of the intercept parameter can be ascribed to the heterogeneity of the adsorbent's structure (Al-Ghouti *et al.*, 2009). This finding would be of great support to those discussed in Section 6.4.2 where the Extended Freundlich Model was found to be the most suitable model to describe the equilibrium data for the binary systems investigated in this study, suggesting that the adsorption was inclined to be more heterogeneous than homogenous (Laskar and Hashisho, 2020; Y. Li *et al.*, 2020).

7.4 Chapter Summary

To better understand the adsorption behaviour, this chapter aimed at determining the most suitable kinetic model for the measured kinetic data obtained from the single and binary systems. This was done by applying three adsorption reaction models, as well as one intra-particle model, to the measured data and to the kinetic uptake data.

The alcohols showed similar behaviour in both single and binary systems as the Elovich Model, a reaction model which exhibited the best fit to the kinetic experimental data among the reaction models investigated in this study. The parameters obtained by the reaction models suggest that the initial adsorption rate was enhanced by decreasing the alcohols' initial concentrations. A shorter chain length alcohol, namely 1-hexanol, proved to have a faster initial adsorption rate. The initial adsorption rate was found to be lower in binary systems than in the respective single systems. Moreover, the parameter obtained by the Pseudo-Second-Order Model may suggest a possibility of chemical adsorption, and to some extent, may lead to non-desorbed molecules during the regeneration cycles. Intra-Particle Diffusional Model (IPDM) proved to have good correlation for the kinetic data. As a result, it was assumed that the adsorption rate-limiting step is governed by the

intra-particle and external diffusion, as well as by adsorbate-adsorbent reaction on the adsorbent's surface.

In conclusion, the most suitable kinetic models were identified through applying various models to the measured kinetic data, and thus the objective (II.b) was achieved and successfully fulfilled.

Chapter 8 : Thermal Regeneration Results and Discussion

8.1 Overview

This chapter addresses the objective (III) of this study. The objective of this chapter is therefore to investigate the thermal regeneration impact on the applied activated alumina adsorbent's performance in both single and binary systems throughout consecutive cycles using three different regeneration temperatures, 205 °C, 185 °C and 165 °C. To begin with, the equilibrium adsorbent loading will be compared for 10 adsorption/regeneration cycles at 205 °C and 185 °C for the adsorbents utilized in the three systems, whereafter the same comparison will be conducted for the adsorbents used for 15 cycles of single 1-hexanol adsorption and binary adsorption at the regeneration temperature 165 °C. Afterwards, the change in the structure and chemical composition of the regenerated adsorbents at various temperatures after the last regeneration cycle will be compared and discussed. The regeneration temperature profile will be discussed at the end of this chapter.

8.2 Experimental Measurements

Various data sets were measured to determine the change in the adsorbent's performance throughout different cycles. Degradation in the adsorbent's efficiency was determined by considering the regeneration efficiency (*RE*). The parameters used in this chapter are the equilibrium adsorbent loading of the first adsorption experiment (q_0) and the equilibrium adsorbent loading obtained from the successive cycles (q_n). These parameters will be investigated for the single and binary systems. Each system will be investigated at three different initial concentrations and three different regeneration cycles.

8.3 Results of Regeneration Temperature 205 °C and 185°C

Regeneration temperatures 205 °C and 185 °C were applied on the three systems for 10 adsorption/regeneration cycles. In this section, the impact of the regeneration temperatures 205 °C and 185 °C on the applied adsorbent is briefly discussed.

8.3.1 Results and Discussion for Single-component adsorption systems

The variation in adsorption capacity over the ten adsorption cycles at two different temperatures, 205 °C and 185 °C, is presented in Figure 8.1. A notable drop in equilibrium loading was observed after the first adsorption cycle at both regeneration temperatures for both systems: 1-hexanol and 1-decanol systems. At a regeneration temperature of 205 °C, the equilibrium loading afterwards was almost stable until the third adsorption cycle, whereafter it dropped again and became constant in

the subsequent cycles, 4 through 9, before it dropped slightly at the tenth adsorption cycle (Figure 8.1.a). On the other hand, the adsorption capacity seemed to have a stable trend over the nine consecutive adsorption cycles at the lower regeneration temperature, 185 °C (Figure 8.1.b). Presumably, the drop in the adsorbent's mass may be attributed to the change in the adsorbent's structure after the regeneration process. At a higher regeneration temperature, a greater change is expected in the adsorbent's morphology (Momina, Shahadat and Isamil, 2018). Therefore, the higher regeneration temperature investigated in this study seemed to have greater impact on the total adsorption capacity.

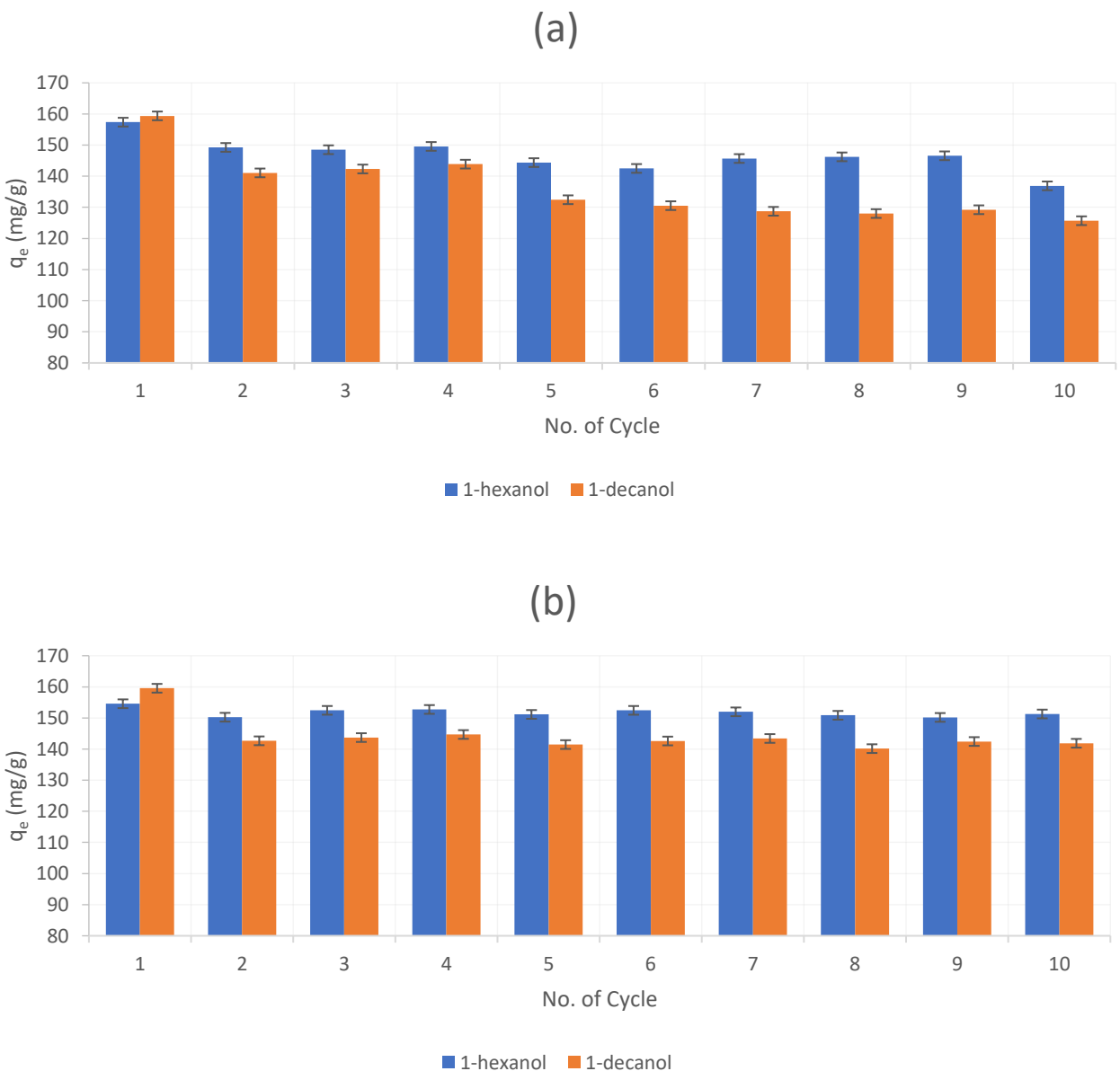

Figure 8.1: Degradation of equilibrium adsorbent loading over 10 successive adsorption cycles at (a) T = 205 °C, and (b) T = 185 °C (initial concentration 3.0 mass%)

Interestingly, the regenerated adsorbent exhibited a higher affinity to adsorbing a greater mass of 1-hexanol than 1-decanol throughout the successive cycles, although the mass of 1-decanol adsorbed by the fresh adsorbents at the first cycle was remarkably higher than 1-hexanol at the given systems. As discussed in Section 5.2.1, 1-decanol may exhibit higher stability than the 1-hexanol at the equilibrium phase due to its higher intermolecular forces (Zhang *et al.*, 2019). This might also lead to a lesser amount of the strongly physiosorbed 1-decanol molecules being desorbed during the regeneration process. As a result, the successive 1-decanol adsorption cycles may be more affected by those strongly physiosorbed molecules left during the regeneration cycle.

The regeneration efficiency (*RE*) was calculated using Equation 2.19 represented in Section 2.7. The *RE* for the 1-hexanol system is depicted in Figure 8.2. The *RE* at a lower initial concentration, 0.5 mass% (Figure 8.2.a), did not show a stable trend from the second cycle through the tenth cycle, whereas it exhibited more stable patterns at an initial concentration of 3.0 mass%. The *RE* was notably greater at the lower regeneration temperature of 185 °C. At an initial concentration of 0.5 mass%, the *RE* decreased to 83% and 91% at the regeneration temperature of 205 °C and 185 °C, respectively, in the last cycle (Figure 8.2.a). On the other hand, and at an initial concentration of 3.0 mass%, the *RE* declined to 87% at 205°C, while it was almost constant at 97% throughout all the cycles at 185 °C.

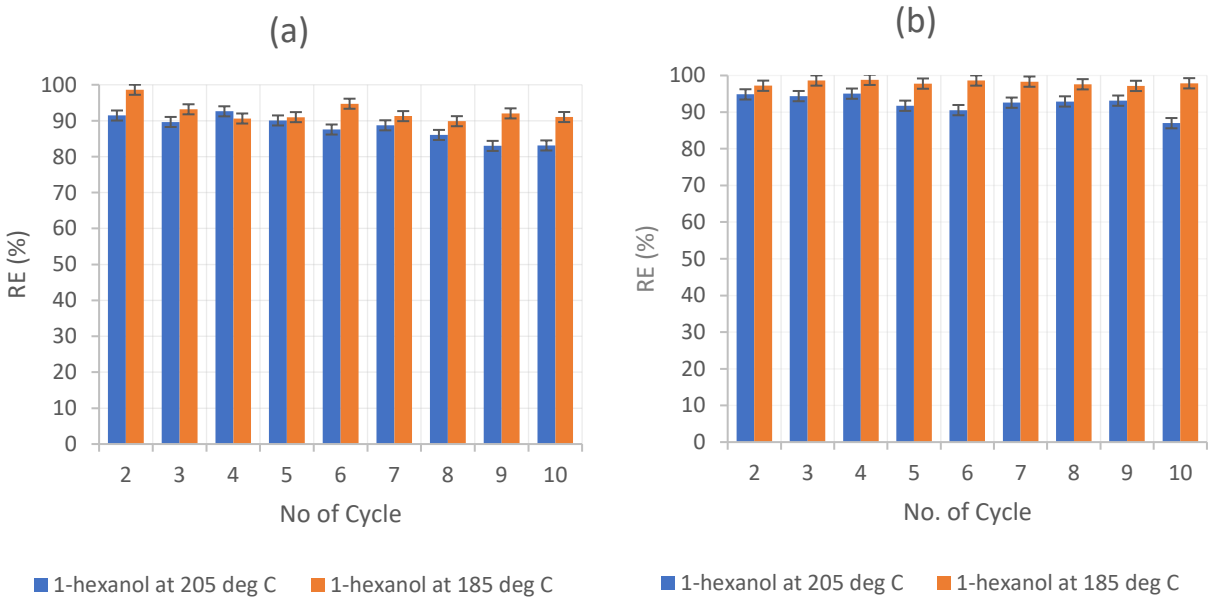

Figure 8.2: Regeneration efficiency for 1-hexanol system throughout nine regeneration cycles at different regeneration temperatures and at (a) initial concentration 0.5 mass%, and (b) initial concentration 3.0 mass%

Figure 8.3 illustrates the *RE* for the 1-decanol adsorption system at two various initial concentrations and two regeneration temperatures. As for the 1-hexanol system, the *RE* was greater

at the lower regeneration temperature investigated. At the initial concentration of 0.5 mass%, the *RE* dropped in the tenth cycle to 85% and 88% at a regeneration temperature of 205 °C and 185 °C, respectively (Figure 8.3.a), whereas at the initial concentration of 3.0 mass% the *RE* dropped gradually to reach 78% in the last cycle when the adsorbent regenerated at 205 °C. However, it was almost stable at around 89% at the regeneration temperature of 185 °C from the first regeneration cycle through to the last cycle (Figure 8.3.b).

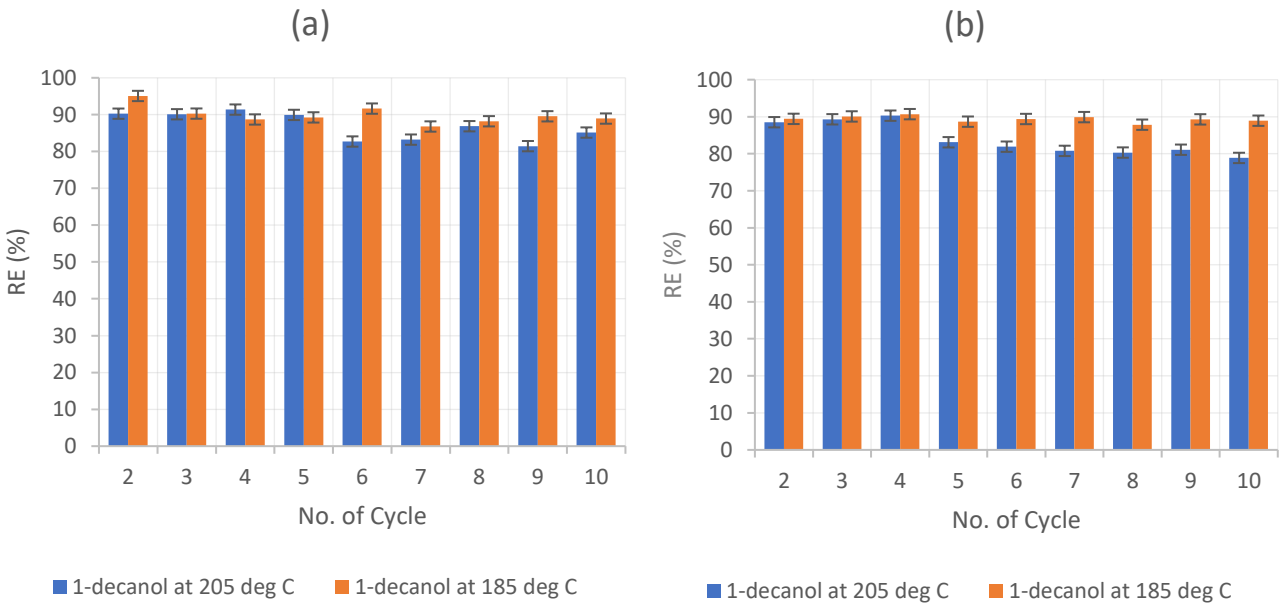

Figure 8.3: Regeneration efficiency for 1-decanol system throughout ten regeneration cycles at different regeneration temperatures and at (a) initial concentration 0.5 mass%, and (b) initial concentration 3.0 mass%

The drop in *RE* is expected, and may be attributed to the loss of adsorbent structure (Momina, Shahadat and Isamil, 2018). This can be observed from Figure 8.4 where the loss of adsorbent mass is depicted for the regenerated adsorbent after the last cycle. The adsorbent's mass dropped drastically after the first regeneration experiment at both regeneration temperatures, whereafter the adsorbent's weight was maintained over the successive nine adsorption/regeneration cycles at the respective conditions investigated. The variation in adsorbent mass between the adsorbents utilized in the 1-hexanol and 1-decanol systems was more remarkable at a regeneration temperature of 205 °C for both initial concentration systems, indicating greater weights for adsorbents than those used in the 1-decanol system, whereas there was no perceptible difference in the adsorbent's mass for those regenerated at 185 °C, at respective conditions. This is expected as at higher regeneration temperatures, the molecules with higher boiling point and heavier molecular weight, in this case the 1-decanol, are more subject to stronger physisorption and chemisorption during both adsorption and thermal regeneration at higher temperatures, which makes it more difficult to desorb the 1-decanol

molecules during the regeneration process (Dutta *et al.*, 2019). Collectively, the fresh adsorbents lost 5% of their mass, on average.

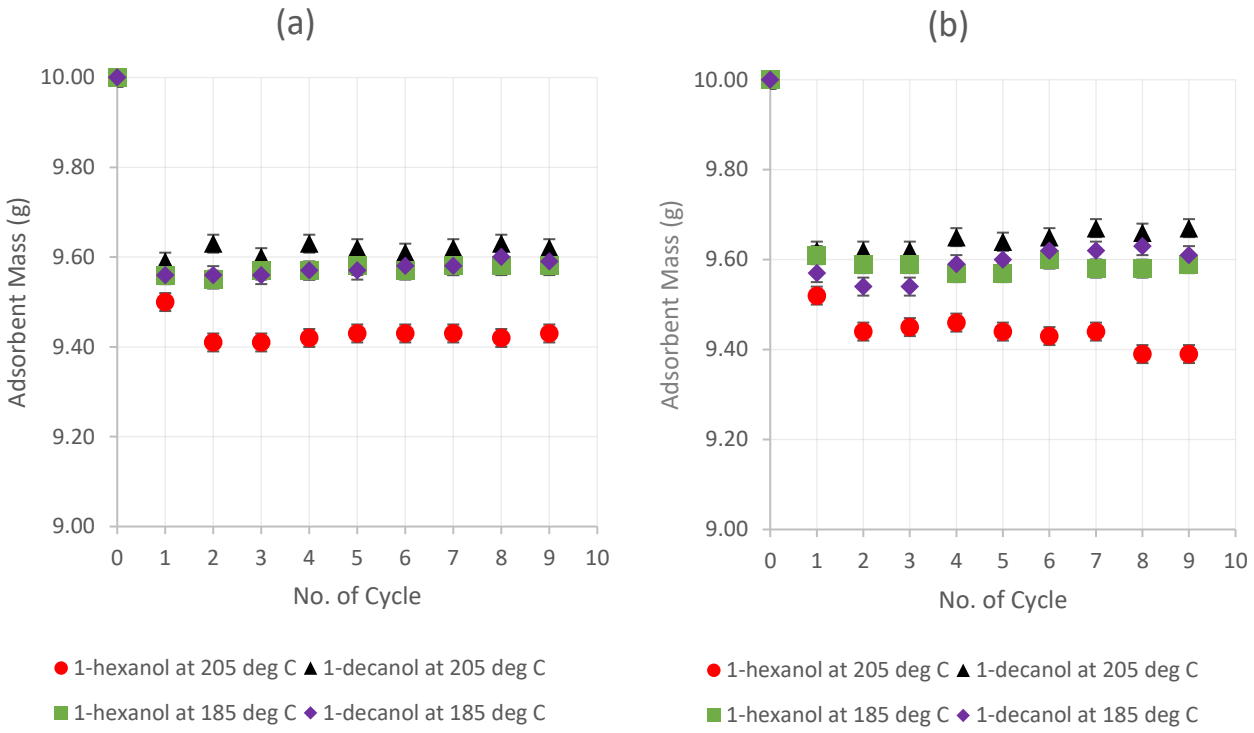

Figure 8.4: Drop in adsorbent's mass over the adsorption/regeneration cycles at different regeneration temperatures and at (a) initial concentration 0.5 mass%, and, (b) initial concentration 3.0 mass%

A scanning electron microscope (SEM) was used to further investigate the regeneration impact on the adsorbent's structure after the last cycle of regeneration experiment. Figures 8.5 through 8.8 show various images taken as visual comparisons between the adsorbents regenerated at the two different regeneration temperatures. It can be observed from the images that the adsorbents regenerated at the higher temperature of 205 °C (Figure 8.5.a, 8.6.a, 8.7.a and 8.8.a), exhibited a significantly more dense structure than those regenerated at 185 °C (Figure 8.5.b, 8.6.b, 8.7.b and 8.8.b). It became more obvious at the higher initial concentration of adsorbates. Presumably, this is due to either the higher impact of the higher regeneration temperature on the adsorbent's morphology, or the chemisorbed molecules onto the active sites on the adsorbent's surface or pores at the higher regeneration temperatures, as discussed earlier in this section. Moreover, the adsorbents used to adsorb a single 1-decanol component seemed to have a denser structure than those utilized to adsorb a single 1-hexanol component. This substantiates the findings in this section, which suggest that the 1-decanol may have exhibited a higher interaction with active sites of the utilized adsorbent during the adsorption and regeneration cycles because of its higher boiling point and molecular weight. As a result, more 1-decanol molecules may be left during the regeneration experiments, and/or new compositions may occur due to higher chemisorption

potentiality during the adsorption and regeneration processes than the 1-hexanol (Dutta *et al.*, 2019). As the initial concentration increased, the adsorbed molecules increased, and consequently, more molecules could be chemisorbed and/or left during the regeneration experiments. This may explain the more dense appearance for the adsorbents used to adsorb the 1-alcohols at greater initial concentration.

(a) (b)

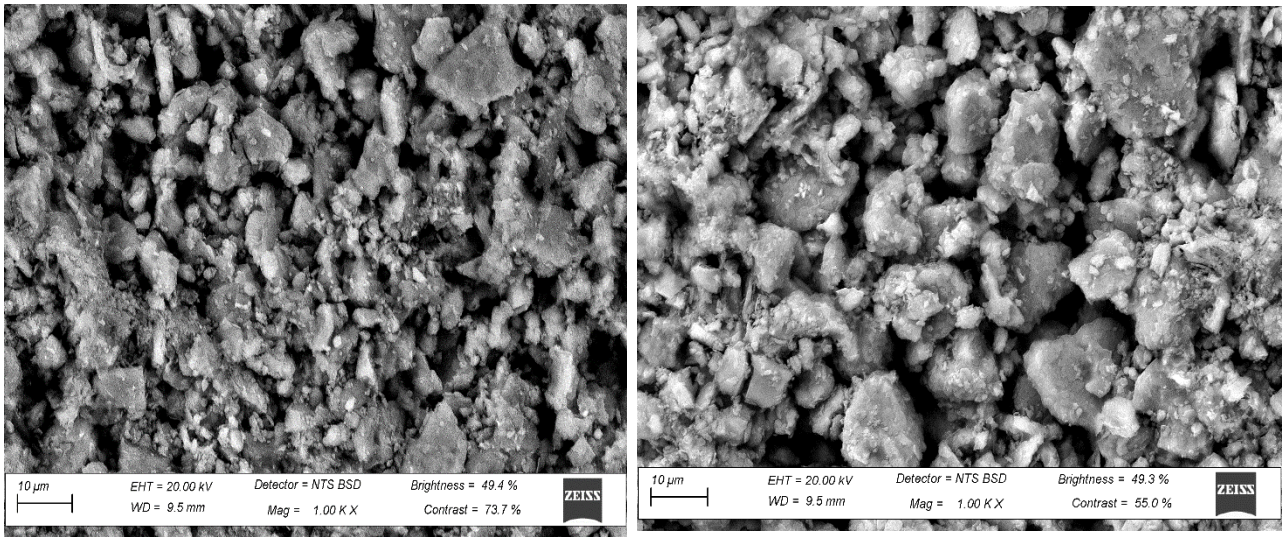

Figure 8.5: Images of activated alumina utilized to adsorb single 1-hexanol component after the last regeneration cycle regeneration temperature (a) 205 °C; and (b) 185 °C (initial concentration 0.5 mass%)

(a) (b)

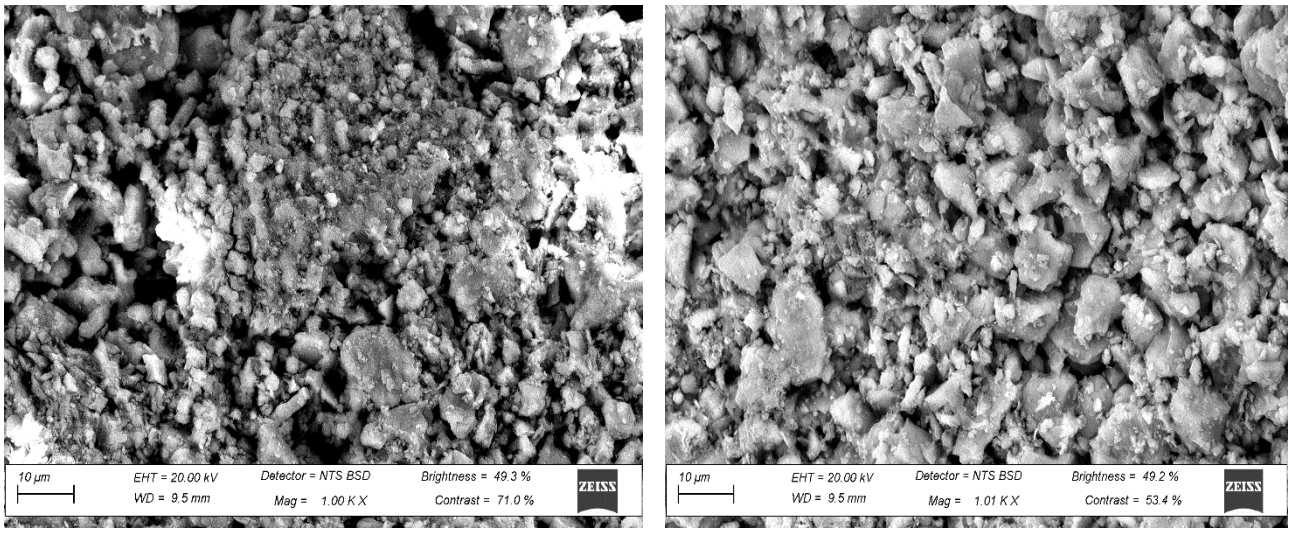

Figure 8.6: Images of activated alumina utilized to adsorb a single 1-hexanol component after the last regeneration cycle regeneration temperature (a) 205 °C; and (b) 185 °C (initial concentration 3.0 mass%)

(a) (b)

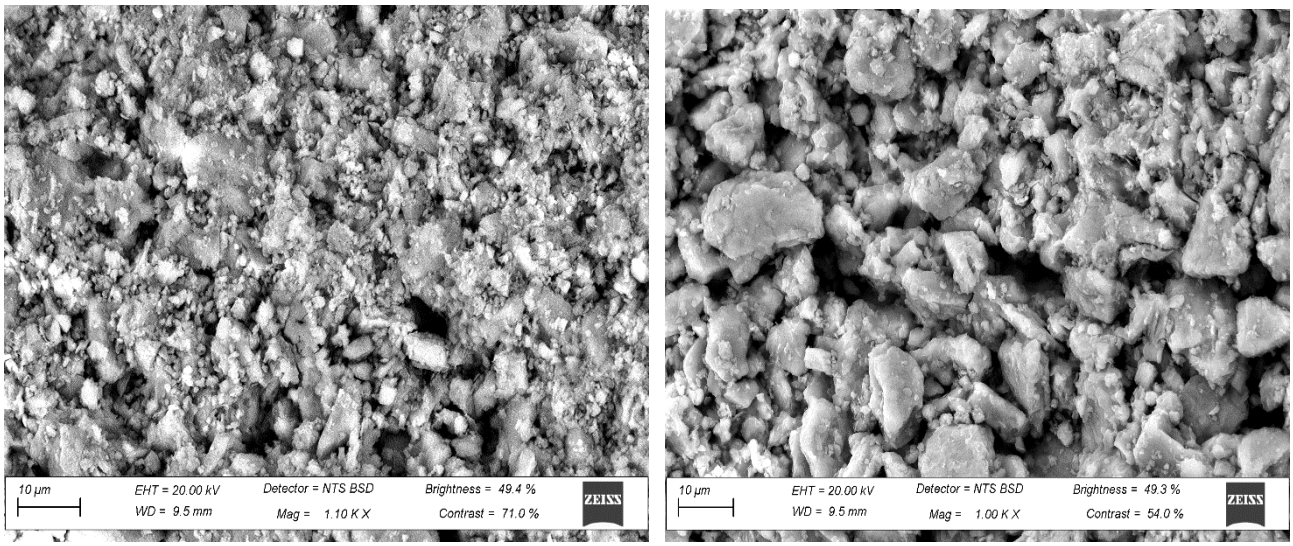

Figure 8.7: Images of activated alumina utilized to adsorb a single 1-decanol component after the last regeneration cycle regeneration temperature (a) 205 °C; and (b) 185 °C (initial concentration 0.5 mass%)

(a) (b)

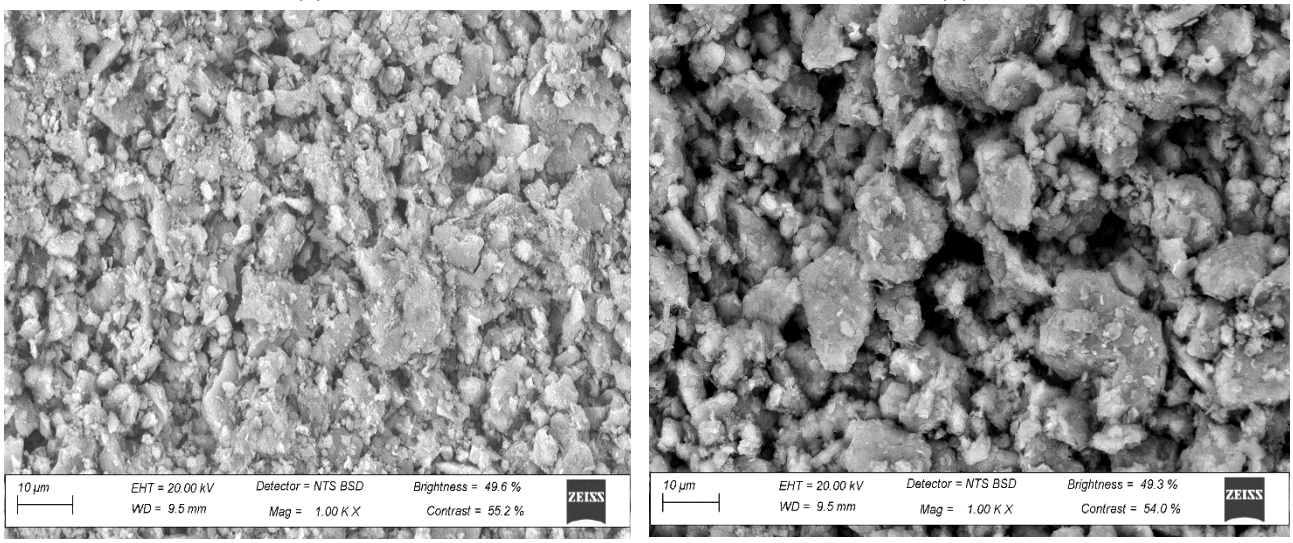

Figure 8.8: Images of activated alumina utilized to adsorb single 1-decanol component after the last regeneration cycle regeneration temperature (a) 205 °C; and (b) 185 °C (initial concentration 3.0 mass%)

8.3.2 Results and Discussion for Binary-component adsorption system

Figure 8.9 illustrates the adsorption capacity of 1-hexanol and 1-decanol in the binary system over ten adsorption/regeneration cycles at different regeneration temperatures. It can be observed that the adsorption capacity for both components declined drastically after the first cycle, and thereafter the adsorption capacity seemed to be stable for all consecutive cycles. This was the case for the

experiments conducted at both regeneration temperatures, 205 °C (Figure 8.9.a) and 185 °C (Figure 8.9.b).

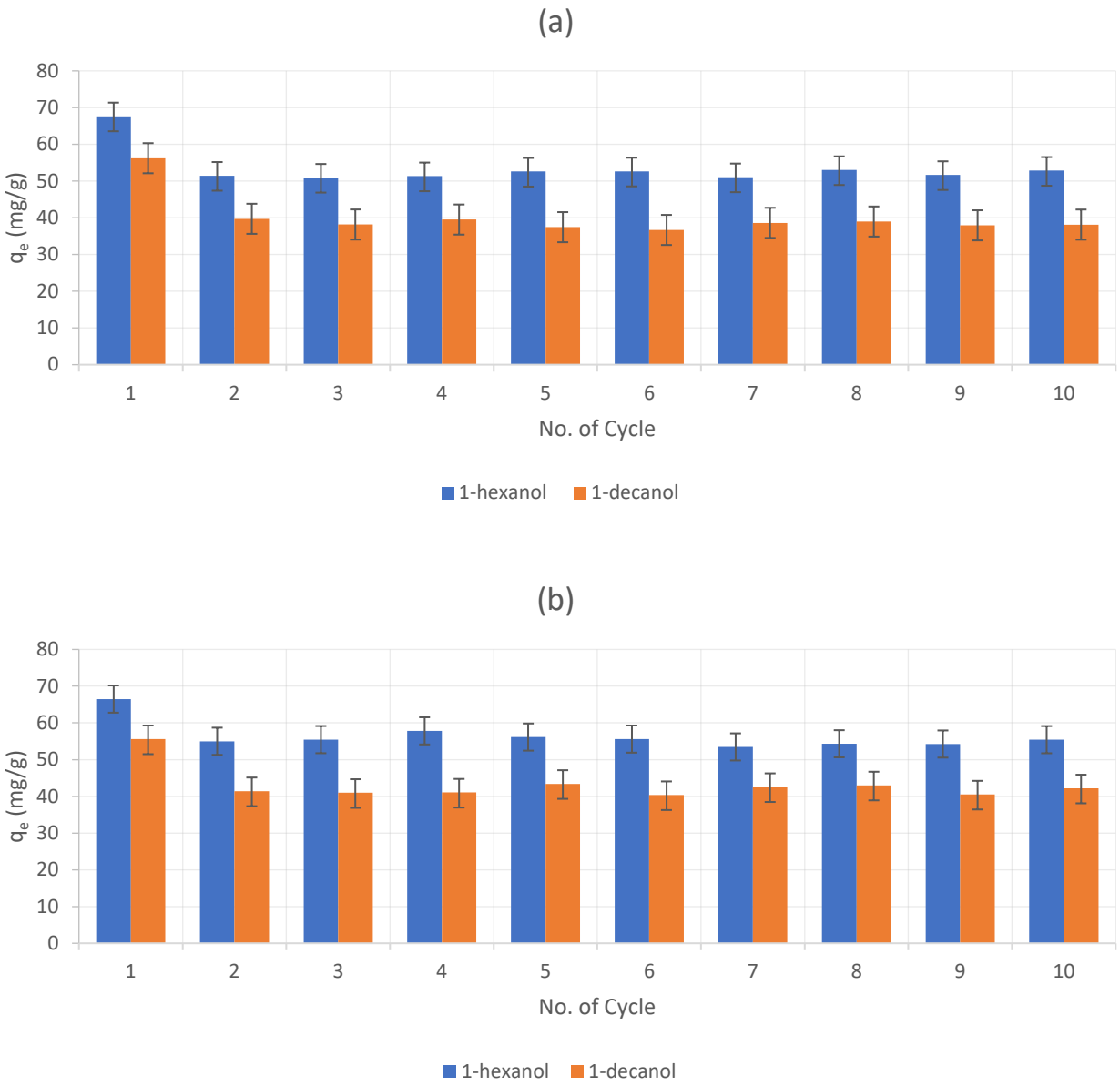

Figure 8.9: Degradation of equilibrium adsorbent loading over 10 successive adsorption/regeneration cycles at regeneration temperature (a) T = 205 °C, and (b) T = 185 °C (initial concentration 0.5 mass%)

The *RE* for the applied activated alumina adsorbent in the binary systems is represented in Figures 8.10 and 8.11 for the adsorption of 1-hexanol and 1-decanol, respectively. From Figure 8.10, it can be observed that the *RE* was almost stable at different initial concentrations of 1-hexanol at both regeneration temperatures. The *RE* for the regenerated adsorbents at 185 °C was generally higher than those regenerated at 205 °C. As for the single-component adsorption systems, the binary

systems at a higher initial concentration, 3.0 mass%, exhibited higher *RE*. The *RE* for 1-hexanol adsorption in the last cycle for initial concentration of 0.5 mass% was 83% at regeneration temperature 185 °C, and 77% at regeneration temperature 205 °C. On the other hand, at the initial concentration of 3.0 mass%, the *RE* at the regeneration temperature of 185 °C was 96%, whereas it was 88% at the regeneration temperature of 205 °C.

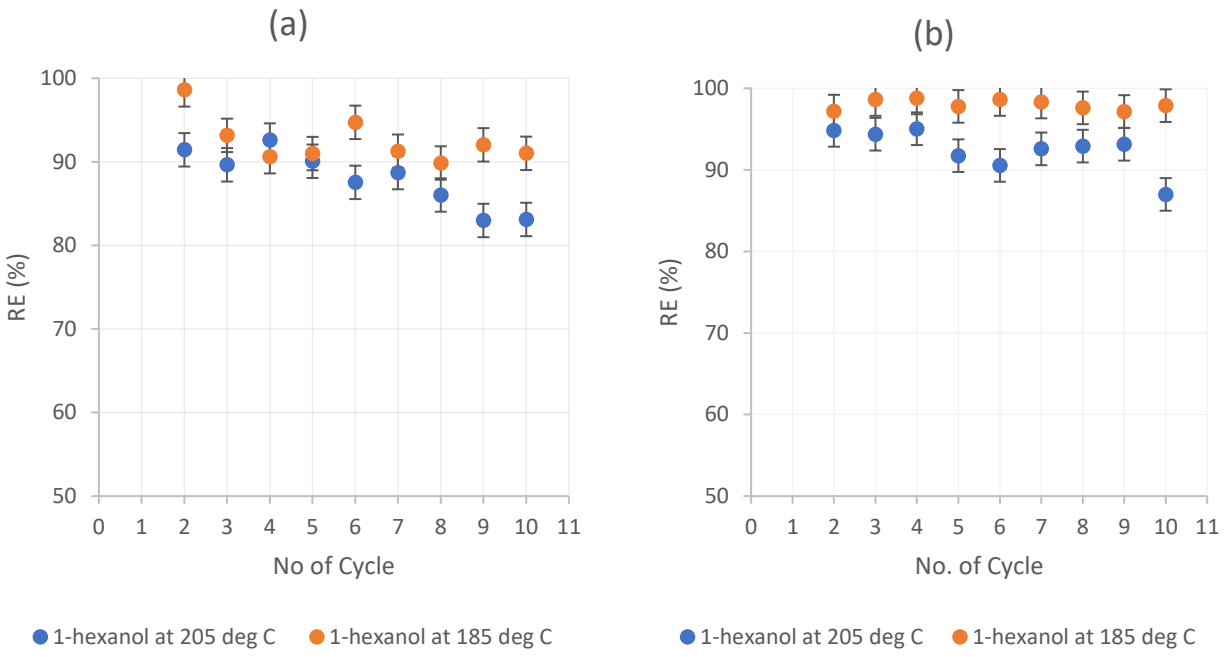

Figure 8.10: Regeneration efficiency for 1-hexanol in binary-component adsorption system throughout ten regeneration cycles at different regeneration temperatures and at (a) initial concentration 0.5 mass%; and (b) initial concentration 3.0 mass%

For 1-decanol, the *RE* was relatively stable throughout the successive cycles at an initial concentration of 0.5 mass% (Figure 8.11.a) for both regeneration temperatures investigated in this study. On the contrary, the *RE* pattern dropped gradually over the succeeding cycles for the systems at the initial concentration of 3.0 mass%. At the regeneration temperature of 205 °C, the *RE* was almost 100% in the second cycle, after which it dropped and became stable for the subsequent three cycles. Eventually it dropped at cycle 7 and seemed to be stable thereafter through to cycle 10. At the regeneration temperature of 185 °C, the *RE* was stable at cycles 2, 3 and 4, before it dropped at cycle 5 and showed a relatively stable trend for the subsequent cycles until the last cycle investigated in this study. The *RE* for 1-decanol exhibited lower values than 1-hexanol.

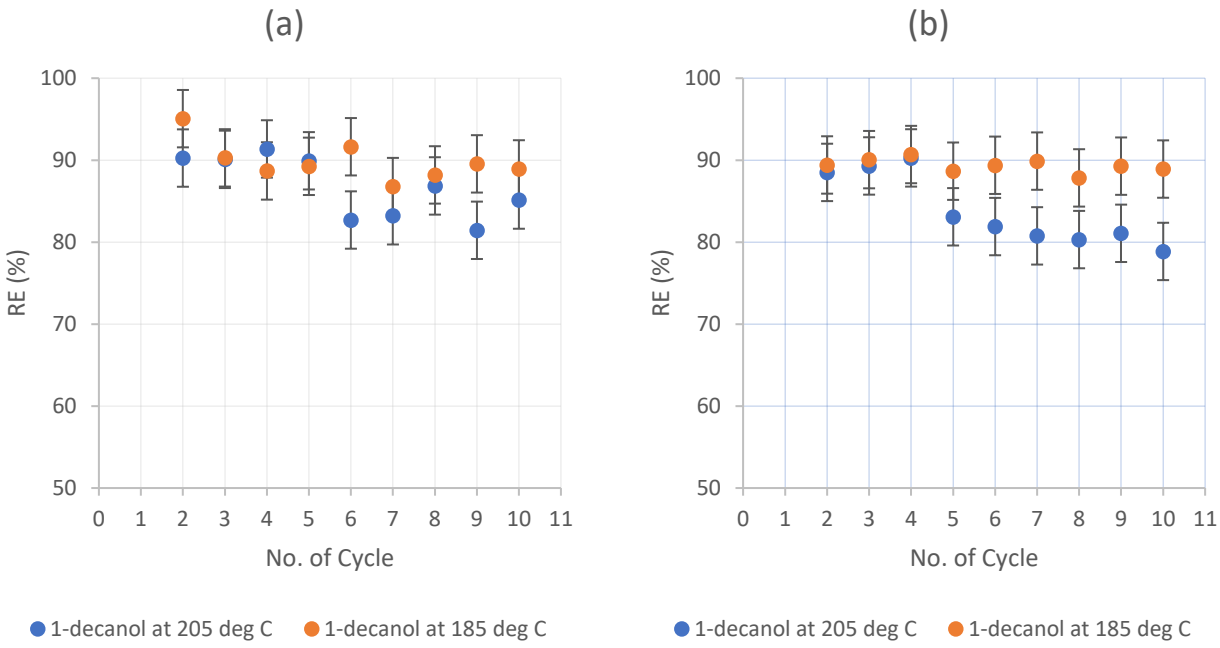

Figure 8.11: Regeneration efficiency for 1-decanol in binary-component adsorption system throughout ten regeneration cycles at different regeneration temperatures and at (a) initial concentration 0.5 mass%; and (b) initial concentration 3.0 mass%

Ultimately, the drop in the *RE* may be ascribed to the change in the adsorbent's morphology, possible chemisorption and stronger physiosorbed molecules left during the regeneration process (Dutta *et al.*, 2019). The drop in the adsorbent's mass was remarkable after the first cycle, where the fresh adsorbent was used. The degradation in the adsorbent's mass is depicted in Figure 8.12.

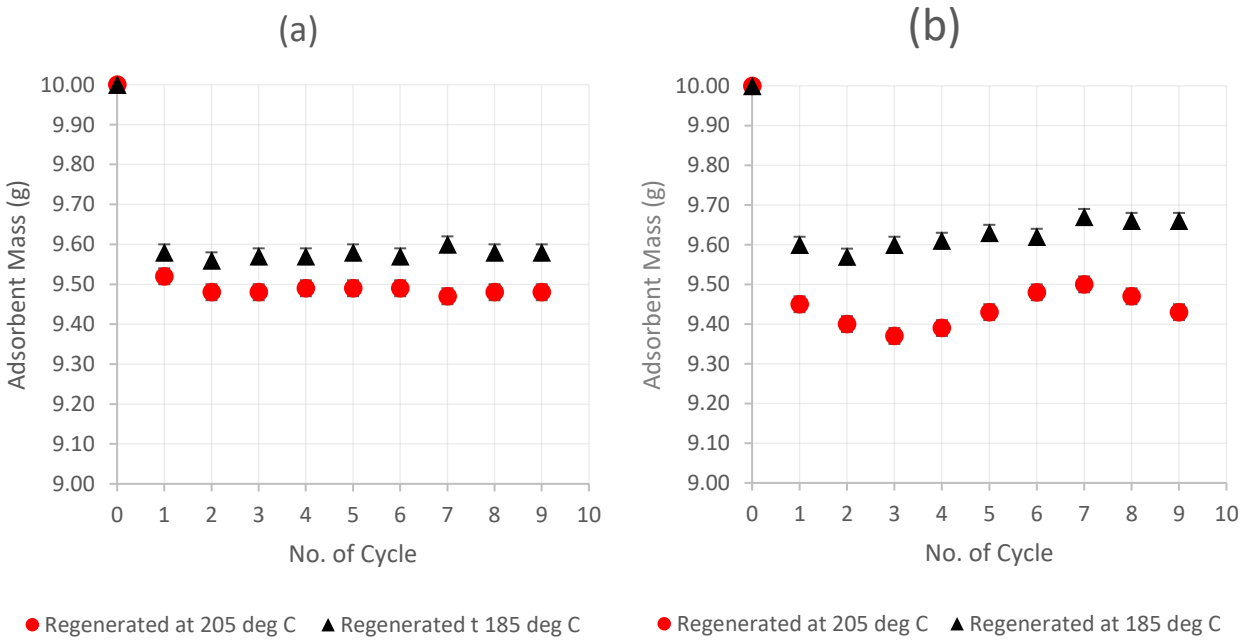

Figure 8.12: Drop in adsorbent's mass used in binary systems over the adsorption/regeneration cycles at different regeneration temperatures and at (a) initial concentration 0.5 mass%; and, (b) initial concentration 3.0 mass%

As shown in Figure 8.12, the degradation was remarkably significant at the higher regeneration temperature. The adsorbent lost around 5% of its initial mass, on average.

Figures 8.13 and 8.14 show the changes in the adsorbents' structure of the regenerated adsorbents used at different adsorbates' initial concentration systems, and at the different regeneration temperatures using the SEM. Similar to a single-component adsorption system, the adsorbents regenerated at a higher temperature, 205 °C (Figure 8.13.a and Figure 8.14.a), seemed to have a more dense structure than the adsorbents regenerated at 185 °C (Figure 8.13.b and Figure 8.14.b). This may again be attributed to the higher regeneration temperature, chemisorbed molecules and/or incomplete desorption process (Dutta *et al.*, 2019).

(a) (b)

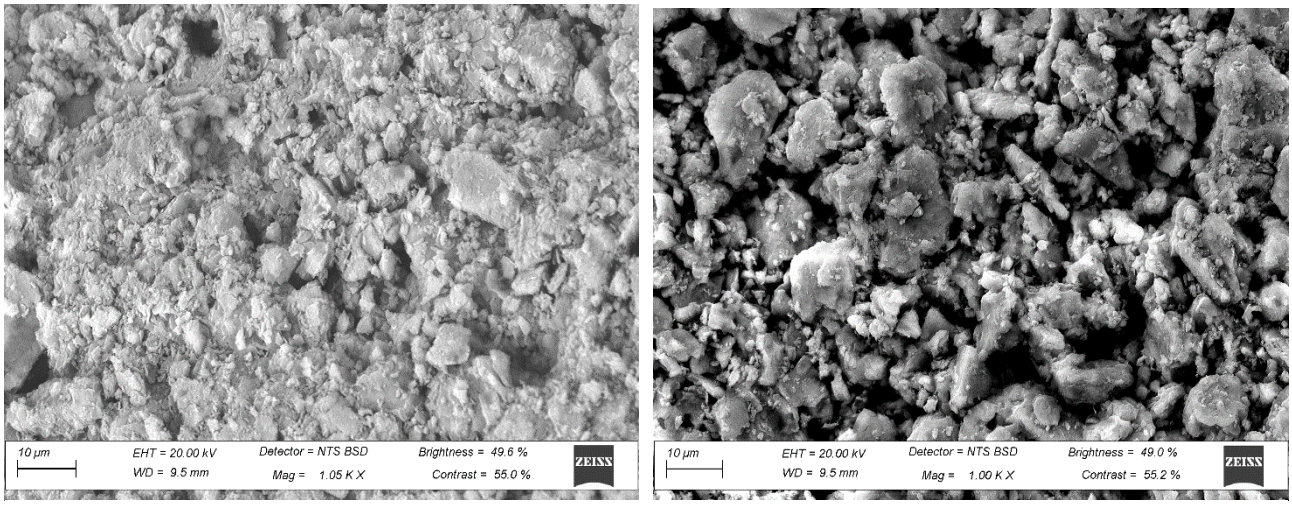

Figure 8.13: Images of activated alumina utilized to adsorb binary 1-alcohols components after the last regeneration cycle at regeneration temperature (a) 205 °C; and (b) 185 °C (initial concentration 0.5 mass%)

(a) (b)

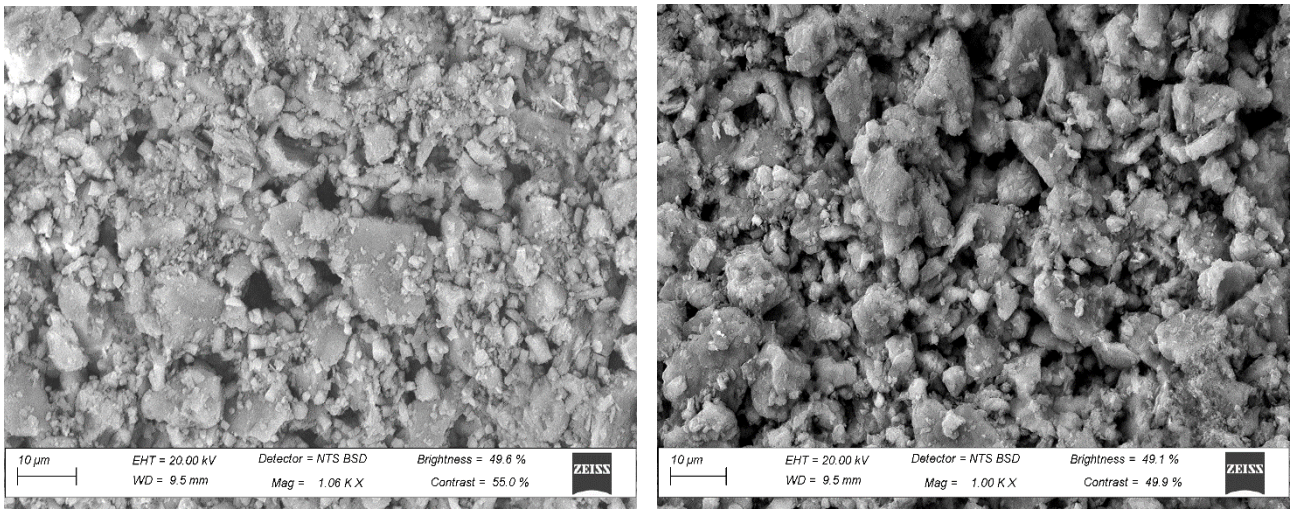

Figure 8.14: Images of activated alumina utilized to adsorb binary 1-alcohols components after the last regeneration cycle at regeneration temperature (a) 205 °C; and, (b) 185 °C (initial concentration 3.0 mass%)

8.3.3 EDX Analysis

In this section, the impact of the regeneration temperatures of 205 °C and 185 °C on the adsorbent's chemical composition is investigated. Surprisingly, the initial concentration of the adsorbates did not prove to show significant changes to the chemical composition, as can been seen in Figures 8.13, 8.14 and 8.15.

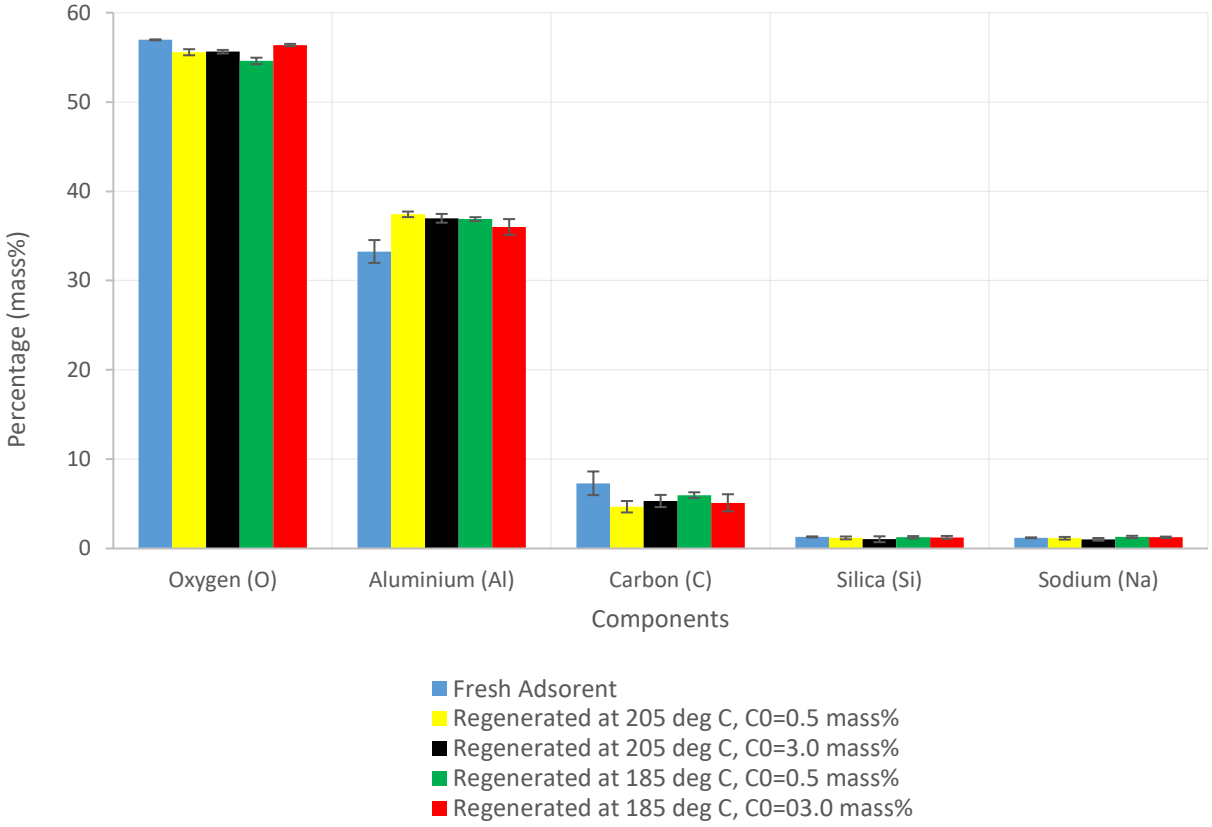

Figure 8.13: The variation in chemical compositions of regenerated activated alumina used to adsorb single 1-hexanol at different initial concentration

Figure 8.13 compares the chemical compositions of the fresh adsorbent and the regenerated beads at 205 °C and 185 °C, which were utilized to adsorb single 1-hexanol from the n-decane solvent. At both regeneration temperatures, the oxygen and carbon percentage declined from their original values when using the fresh adsorbent. However, the respective fractions seemed to be similar regardless of the initial concentration. Since the possibility of strong physical and/or chemical adsorption was not expected due to the boiling point of the 1-hexanol being lower than the regeneration temperature investigated, the increase in the oxygen and carbon compositions, which are also available in the alcohols' composition, was not expected either.

In contrast, the carbon fraction in the adsorbents applied to adsorb 1-decanol witnessed a slight increase after the last regeneration cycle (Figure 8.14). The oxygen composition, on the other hand,

exhibited different behaviour. At regeneration temperature of 205 °C, the oxygen fraction decreased from its original value regardless of the initial concentration of the 1-decanol. However, its fraction was somewhat greater than at the higher initial concentration. After the last regeneration cycle of 185 °C, the oxygen composition increased as the initial concentration increased, and in both cases it was similar and greater than the original values at the lower and higher initial concentrations, respectively. The 1-decanol has a greater boiling point than the regeneration temperatures investigated, and this may explain these findings, in particular at the regeneration temperature of 185 °C.

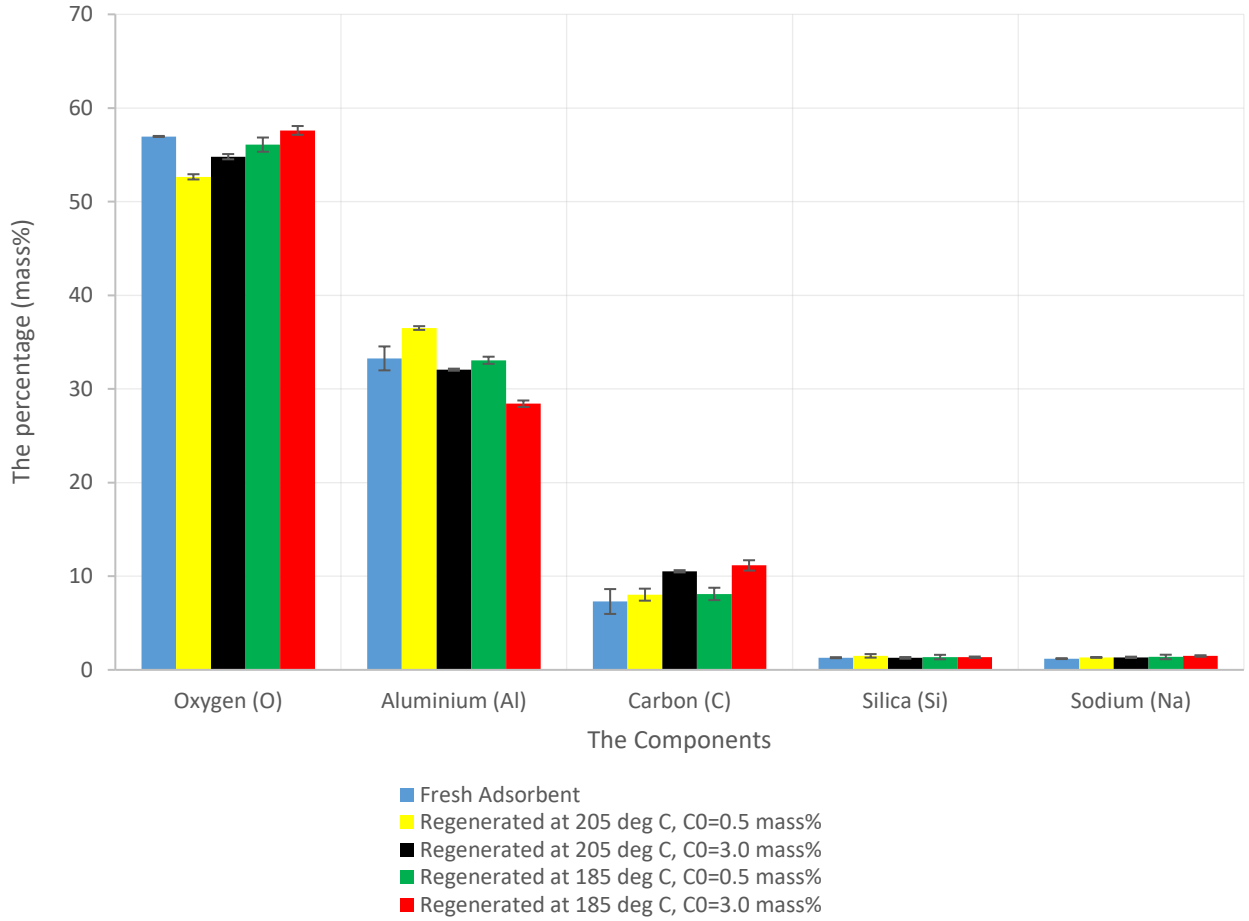

Figure 8.14: The variation in chemical compositions of regenerated activated alumina used to adsorb single 1-decanol at different initial concentrations

Figure 8.15 denotes the variation in the adsorbent's chemical composition with the change in the regeneration temperatures and initial concentration of the binary components. There was no change in the oxygen fraction when the adsorbent regenerated at 205 °C, while its percentage declined at the lower regeneration temperature, 185 °C. This may be attributed to the strongly physiosorbed 1-decanol left during the regeneration cycles. The carbon fraction did not exhibit a discernible change in the initial concentration and regeneration temperatures within the range of uncertainties.

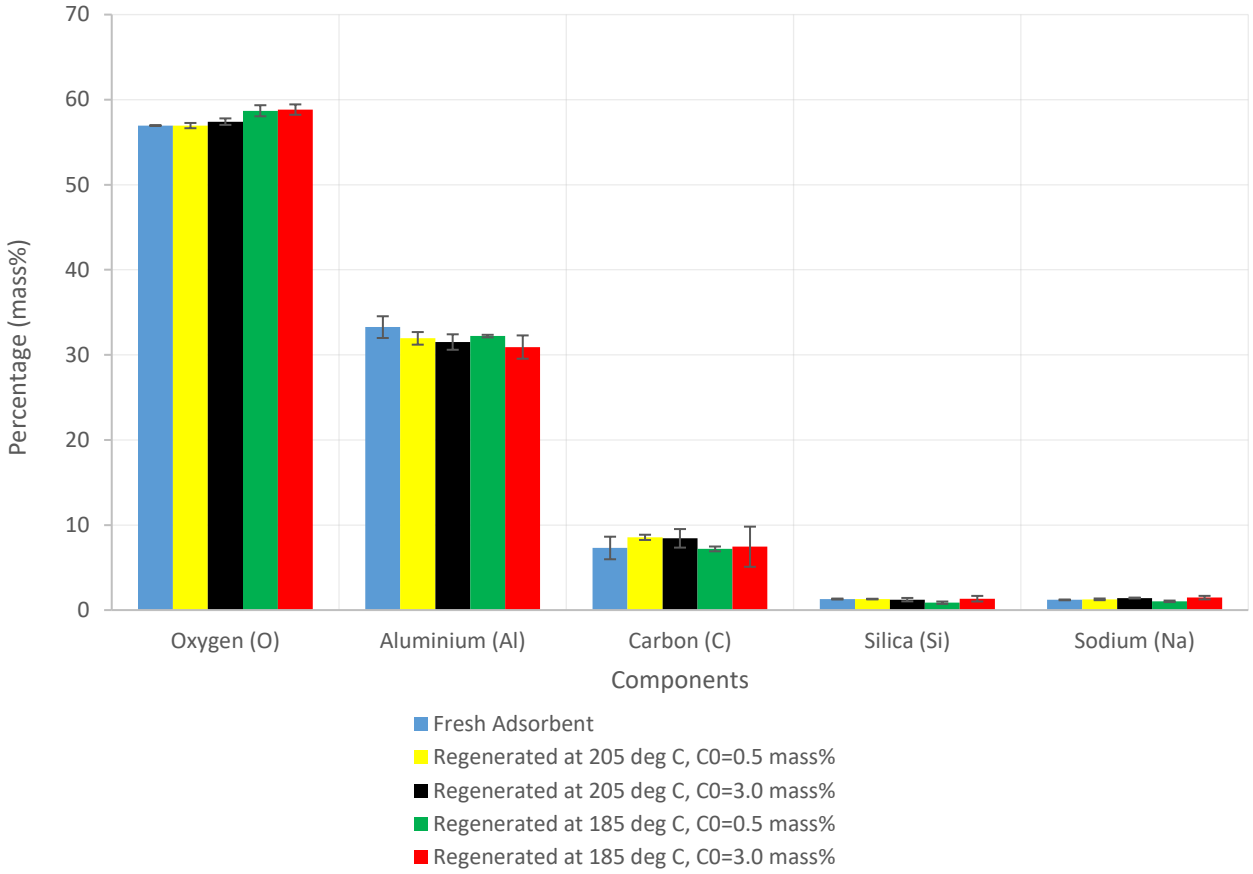

Figure 8.15: The variation in chemical compositions of regenerated activated alumina used to adsorb binary 1-alcohols at different initial concentration

To summarize, the change in the chemical composition of the activated alumina investigated is more favourable in the presence of the 1-decanol. This can be attributed to its lower boiling point than the regeneration temperatures conducted in this study, and as a result, strongly physiosorbed and/or chemisorbed 1-decanol could not be desorbed during the regeneration cycles. Furthermore, this may justify the higher regeneration efficiency for the adsorbents applied to adsorb 1-hexanol, as most of the adsorbed molecules were desorbed, and more active sites become available for the successive adsorption cycle.

8.3.4 Regeneration Temperature Profile

The temperature profile of the regeneration experiments helps to further understand the adsorbent's behaviour during the regeneration cycles. Figure 8.16 shows the variation in temperature profile for the various temperatures used in this study.

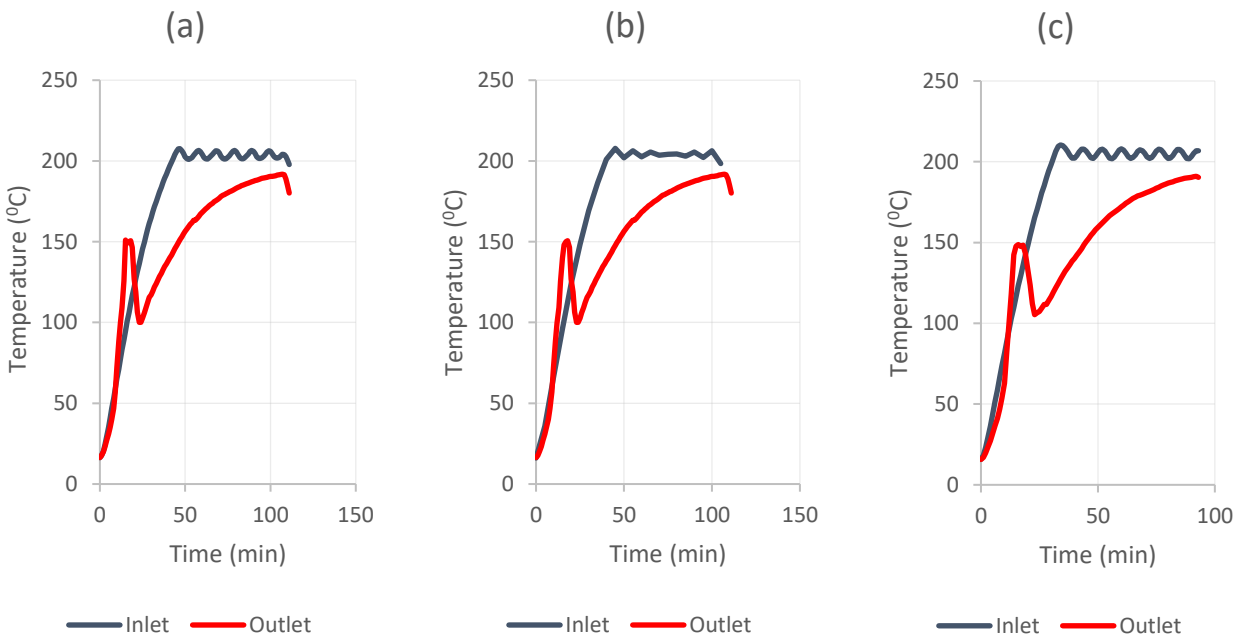

Figure 8.16: Temperature profile at regeneration temperature 205 °C for (a) single 1-hexanol adsorption system; (b) 1-decanol adsorption system; and (c) binary-component adsorption system

Interestingly, the initial concentration and carbon chain length did not show a discernible change on the temperature profile pattern. As can be seen in Figure 8.16, the outlet temperature did not reach the inlet temperature of the three systems within the duration time of the experiment. This may indicate that the desorption process was not complete at 205 °C, and more molecules could be desorbed, as the desorption can be considered complete when the temperature of the regeneration column effluent is equal to the inlet temperature (Kumar and Glenn, 1986).

At the beginning the of regeneration cycle, the outlet temperature is increased gradually during the first 15 minutes to reach 150 °C, whereafter it abruptly decreased to 100 °C before rising again at a lower increase rate compared to the rate of the first 15 minutes. During the first 15 minutes, only weakly adsorbed molecules were desorbed by the increased heat and flow of the nitrogen gas through the column's bed. The desorbed amount of molecules increased with the increase in the heat supplied as time progressed (Salvador *et al.*, 2015). As time passed, more heat was absorbed by the system to reach the required energy to desorb the strongly adsorbed materials. As a result, the majority of adsorbed molecules were desorbed and appeared in the effluent of the regeneration column. The desorbed molecules, however, were colder than the system, which resulted in a decrease in the outlet temperature. This might explain the sudden decrease in the outlet temperature between the first 15 and 20 minutes.

Figure 8.17 illustrates the temperature profile at 185 °C, where desorption can be considered complete after 75 minutes, at which the outlet temperature became the same as the inlet temperature, suggesting that the desorption process was complete.

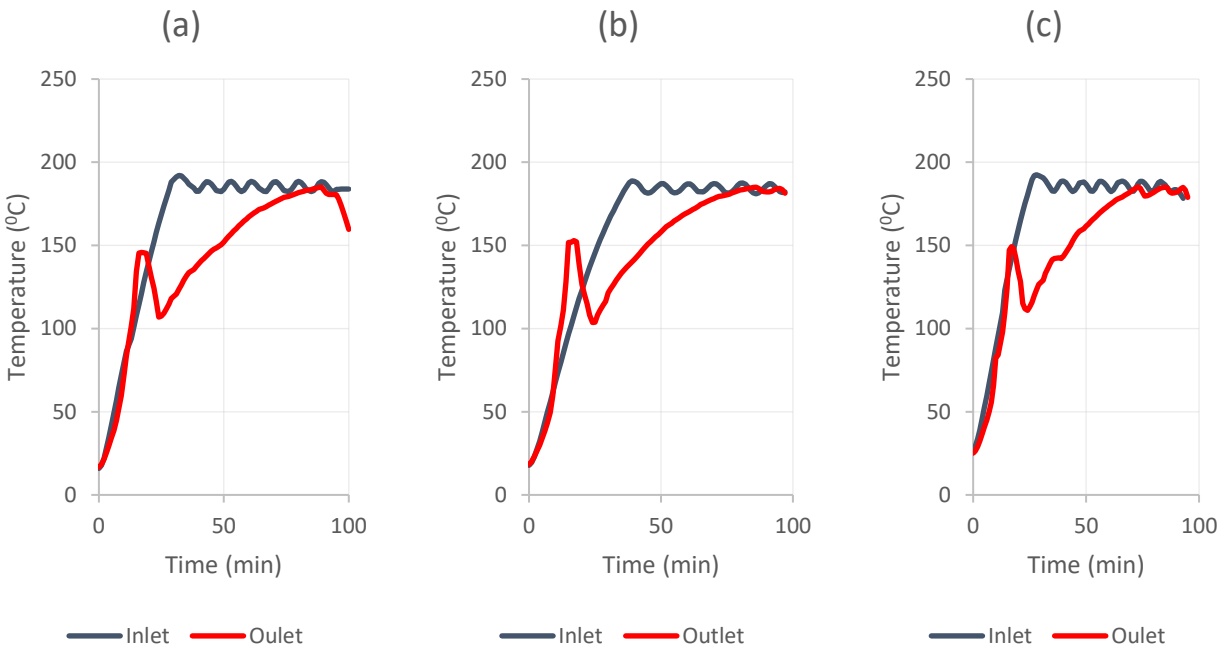

Figure 8.17: Temperature profile at regeneration temperature 185 °C for (a) single 1-hexanol adsorption system; (b) 1-decanol adsorption system; and (c) binary-component adsorption system

8.4 Results of Regeneration Temperature 165 °C

The impact of lower regeneration temperature of 165 °C was investigated on the applied adsorbent used to adsorb single 1-hexanol and binary components in order to ascertain the possibility of lower energy consumption as well as the energy cost on the systems studied.

8.4.1 Results and Discussion for Single-component adsorption systems

Fifteen cycles of adsorption/regeneration experiments were carried out on the single 1-hexanol adsorption system at three different concentrations. Figure 8.18 denotes the degradation in regeneration efficiency (*RE*) over the 15 cycles at two different initial concentrations.

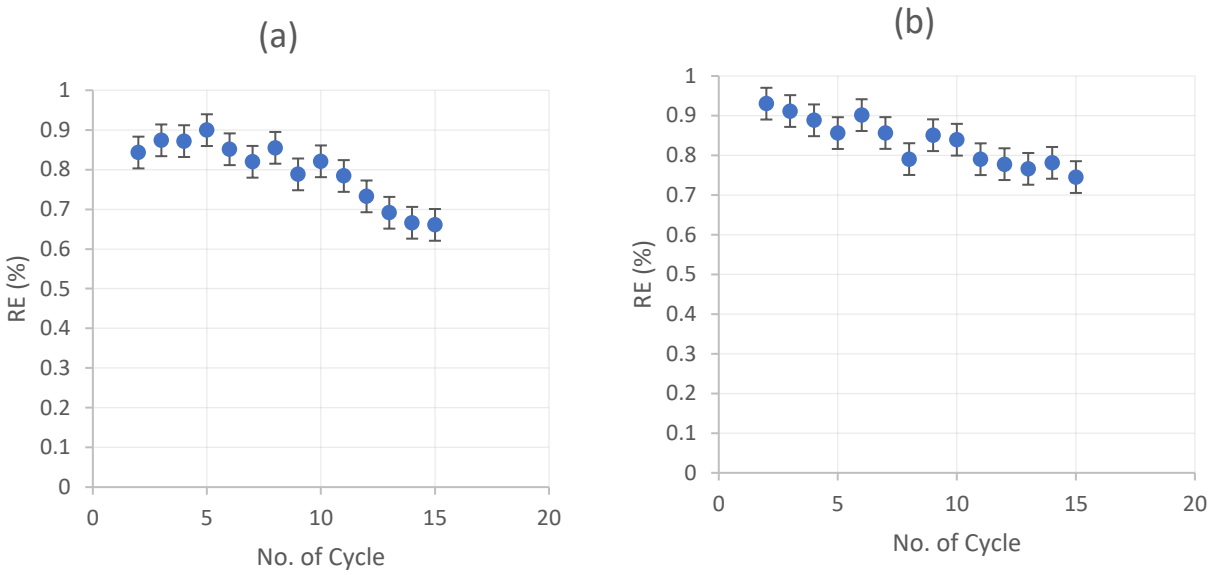

Figure 8.18: Regeneration efficiency for 1-single 1-hexanol adsorption system throughout 15 regeneration cycles at different regeneration temperatures and at (a) initial concentration 0.5 mass%; and (b) initial concentration 3.0 mass%

As can be seen in Figure 8.18, the initial concentration had a slight impact on the regeneration efficiency of the activated alumina adsorbent applied. At the initial concentrations of 0.5 mass% and 3.0 mass%, the adsorbent lost 33% and 25% of its initial performance, respectively. A notable drop in the adsorbent's performance was observed in the 2nd adsorption cycle, and another remarkable decline was also observed in the 11th adsorption cycle, and thereafter at both initial concentration systems. The drop in the *RE* can be ascribed to the loss and/or the change in the adsorbent's morphology, the strong adsorbed molecules that left during the regeneration cycles, as well as to the possible chemisorbed molecules (Dutta *et al.*, 2019).

Compared to the regeneration temperatures of 205 °C and 185 °C, the RE tends to be lower at 165 °C and among the temperatures examined at various initial concentrations (Figure 8.19). This could be attributed to more molecules leftover during the regeneration cycles (Dutta *et al.*, 2019). As the regeneration temperature of 165 °C is closer to the boiling point of 1-hexanol, 157 °C, more strongly physiosorbed alcohols may tend to be retained on the adsorbent's active sites.

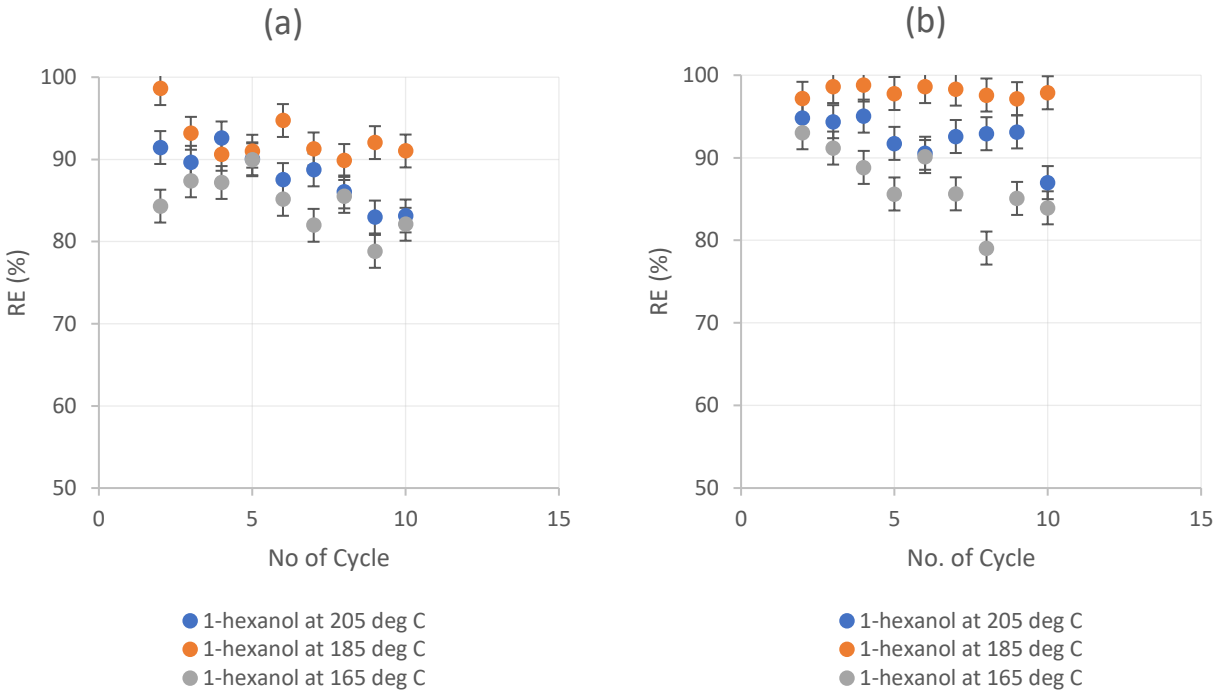

Figure 8.19: Comparison between regeneration efficiency for 1-single 1-hexanol adsorption system throughout 10 regeneration cycles at different regeneration temperatures and at (a) initial concentration 0.5 mass%; and (b) initial concentration 3.0 mass%

The SEM images presented in Figure 8.20 show the adsorbent used to adsorb single 1-hexanol component and regenerated at 165 °C. The adsorbent utilized to adsorb the lower concentration (Figure 8.20.a) tends to have a more open structure than the adsorbent applied to adsorb a higher concentration (Figure 8.20.b). Moreover, both of them have a higher density than those regenerated at 205 °C and 185 °C at the respective initial concentrations (refer to Figures 8.5 and 8.6). This might be ascribed to more cycles that were investigated at 165 °C than those conducted at 205 °C and 185 °C, which could have resulted in more changes in the adsorbent's morphology. In addition, it can be attributed to the molecules retained during the regeneration cycles due to a lower regeneration temperature compared to those regenerated at 205 °C and 185 °C.

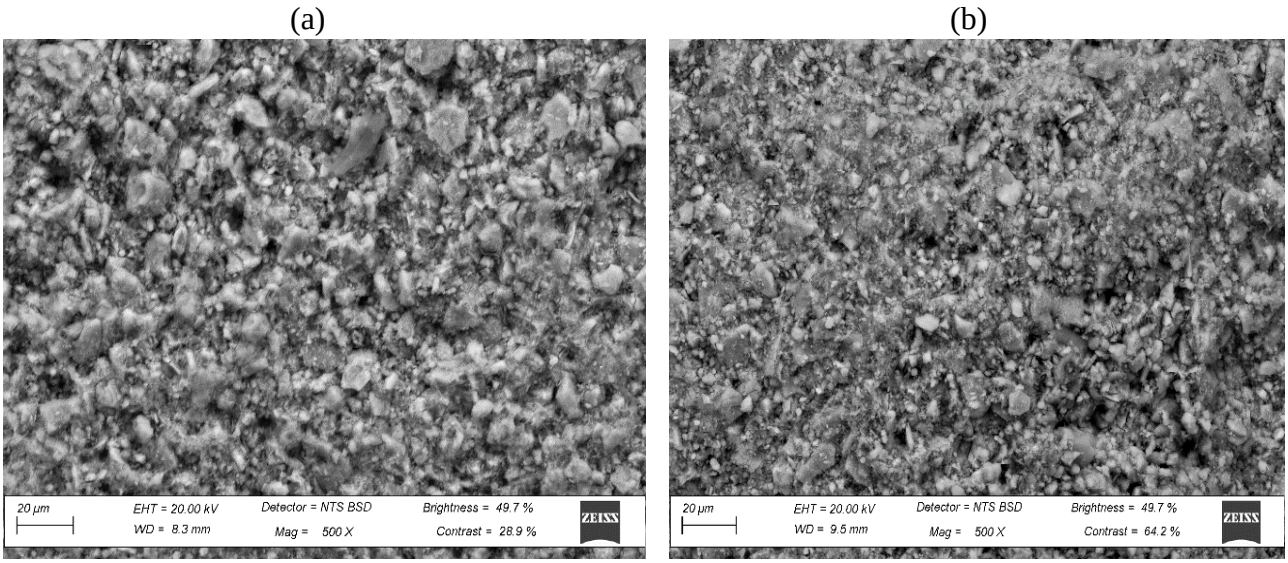

Figure 8.20: Images of activated alumina utilized to adsorb single 1-hexanol component after the 15th regeneration cycle at initial concentrations (a) 0.5 mass%; and (b) 3.0 mass%

The variation in chemical composition was carried out using EDX analysis. Figure 8.21 exhibits an increase in the oxygen and carbon fraction. This might be as a result of the 1-hexanol molecules retained during the regeneration temperature. Moreover, the amount of molecules retained seemed to be higher at a greater initial concentration.

Compared to the regeneration temperatures of 205 °C and 185 °C, the 1-hexanol molecules retained tend to be greater at the regeneration temperature of 165 °C. This is expected as, at lower regeneration temperatures, more molecules could remain on the adsorbent during the regeneration cycle, due to the lack of energy required to desorb the strongly adsorbed molecules (Salvador *et al.*, 2015; Dutta *et al.*, 2019).

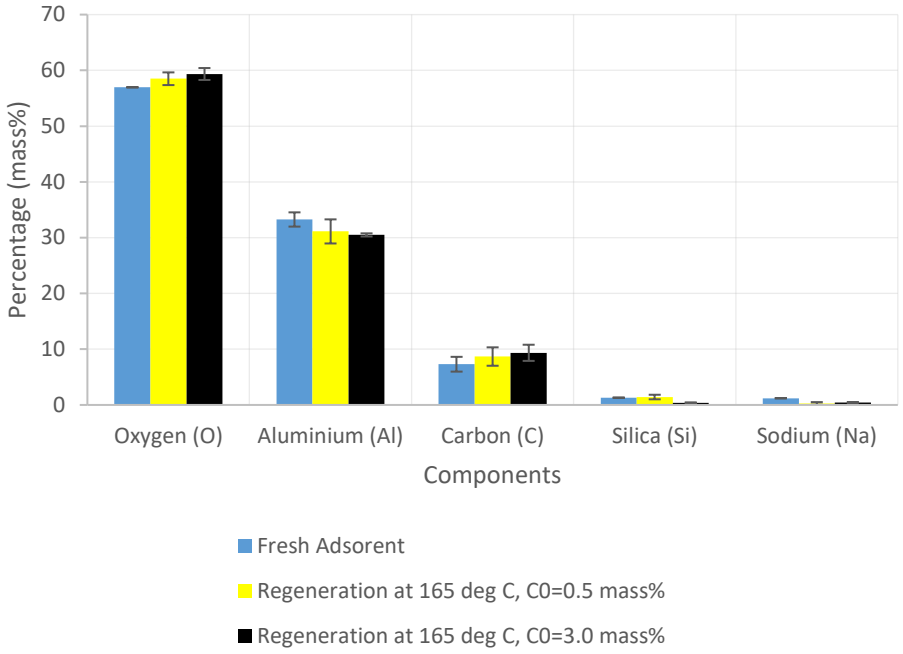

Figure 8.21: The variation in chemical compositions of regenerated activated alumina at 165 °C and used to adsorb single 1-alcohols at different initial concentrations

8.4.2 BET Analysis

The BET analysis was applied to quantify the variation in physical properties between the fresh adsorbent and regenerated adsorbents at 205, 185 and 165 °C that were utilized to adsorb 1-hexanol at an initial concentration of 3.0 mass%. Table 8.1 depicts the different values of the adsorbent's physical properties.

Table 8.1: Physical properties of the fresh adsorbent and regenerated adsorbents at different temperatures

Adsorbent	BET Surface Area (m^2/g)	Total Pore Volume (cm^3/g)	Average Pore Diameter (Å)
Fresh activated alumina	354.36	0.48	52.10
Activated alumina Regenerated at 205 °C	326.73	0.47	56.52
Activated alumina Regenerated at 185 °C	336.97	0.47	54.48
Activated alumina Regenerated at 165 °C	311.5	0.46	58.01

As can be seen in Table 8.1, the surface area of the adsorbents regenerated at 165 °C is notably lower than the fresh adsorbent and those regenerated at 205 and 185 °C. This might be ascribed to

the larger number of molecules retained after the regeneration cycles. The adsorbents regenerated at 165 °C had slightly lower total pore volumes which might also explain the lower adsorption capacity compared to those regenerated at 205 and 185 °C. The variation in the average pore size did not follow a regular trend at the various regeneration temperatures considered in this study.

8.4.3 Results and Discussion for Binary-component Adsorption Systems

Similar to the regeneration temperatures of 205 °C and 185 °C, the presence of 1-decanol affected the *RE* of the utilized activated alumina at the regeneration temperature of 165 °C. Referring to Figure 8.22, the *RE* for both components was greater at the higher initial concentration. Furthermore, the *RE* for 1-hexanol was greater than the *RE* for 1-decanol. This can be attributed to the preference of 1-hexanol adsorption over 1-decanol, as discussed in Section 5.2.2.3. Interestingly, the adsorbent lost more than 50% of its performance using 1-decanol adsorption at the 11th cycle at an initial concentration of 0.5 mass%, while its efficiency increased to ≥65% at the higher initial concentration for both components.

The lower *RE* at lower initial concentration systems can be attributed to stronger adsorption at lower initial concentration, as for lower concentration system the target species can be adsorbed by the highest binding energy sites. In contrast, the weaker binding sites can adsorb more molecules as the initial concentration increases (Kumar *et al.*, 2019). As a result, higher energy might be needed to recover the adsorbent's performance at lower initial concentrations, in particular the energy required to free the molecules trapped in the micropores.

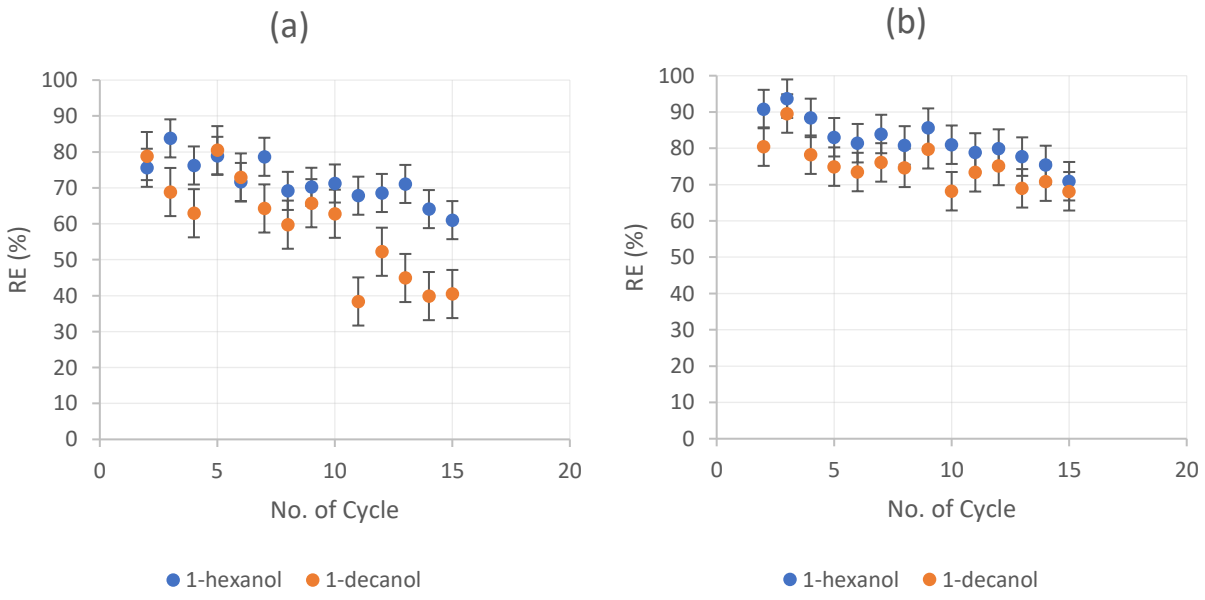

Figure 8.22: Regeneration efficiency for binary-alcohols adsorption system throughout 15 regeneration cycles at regeneration temperature 165 °C and at (a) initial concentration 0.5 mass%; and (b) initial concentration 3.0 mass% (50:50 is the adsorbates' mass ratio)

The surface morphology of the adsorbent did not seem to have major changes with the variation in initial concentration (Figure 8.23). However, it inclined to have a less open structure than those regenerated at 205 °C and 185 °C. This might be attributed to molecules retained after the regeneration cycle.

(a) (b)

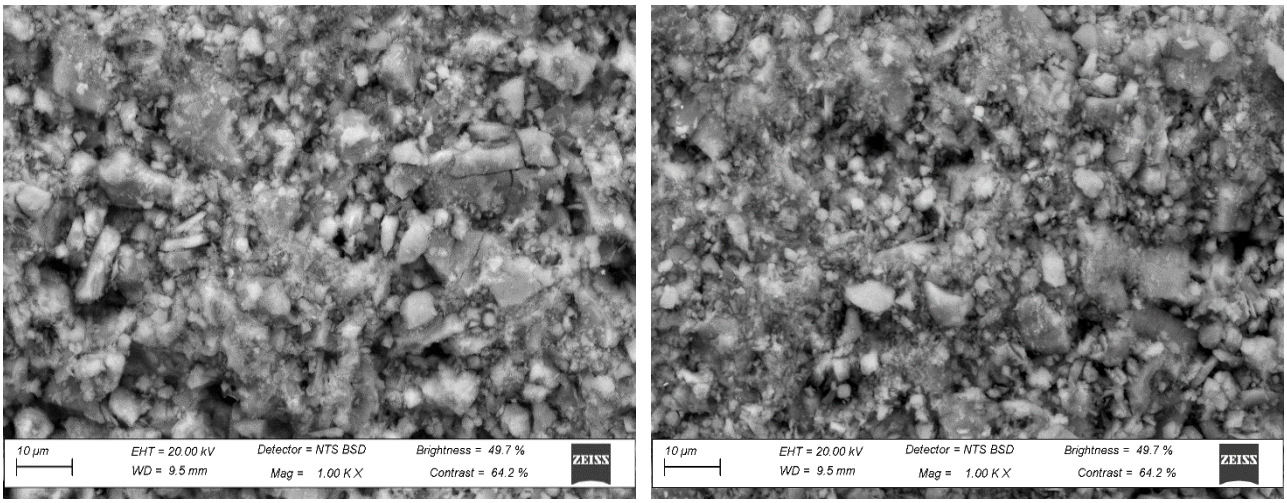

Figure 8.23: Images of activated alumina utilized to adsorb binary components after the 15th regeneration cycle at initial concentrations (a) 0.5 mass%; and (b) 3.0 mass% (regeneration temperature = 165 °C)

A notable increase in the carbon and oxygen compositions of the adsorbent applied was observed (Figure 8.24). This could be ascribed to the presence of the 1-decanol in the binary-component adsorption systems. Moreover, the increase in the carbon and oxygen compositions at the regeneration temperature of 165 °C inclined to be greater than those obtained from the adsorbents regenerated at 205 °C and 185 °C.

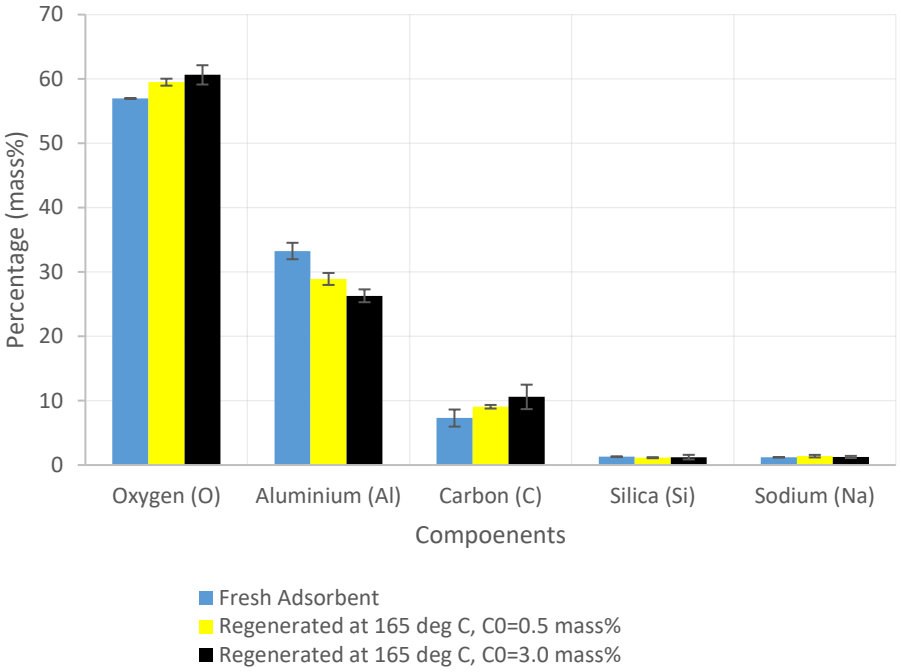

Figure 8.24: The variation in chemical compositions of regenerated activated alumina at 165 °C and used to adsorb single 1-alcohols at different initial concentration

8.3.5 Regeneration Temperature Profile

Regeneration temperature profile at 165 °C for single 1-hexanol and binary-component adsorption systems is illustrated in Figure 8.25. It can be observed that they followed the same pattern of temperature profiles of 205 °C and 185 °C. However, the completion of desorption time at 165 °C is much lower than that obtained at 185 °C. This would suggest that more adsorbed molecules were left during the regeneration cycle due to lower regeneration temperature.

Interestingly, the desorption completion time for the adsorbent utilized to adsorb binary-component adsorption system (Figure 8.25.b) was greater than that obtained to adsorb single 1-hexanol system (Figure 8.25.a). This might be explained by the presence of 1-decanol in the binary system, which had a much higher boiling point than the temperature investigated.

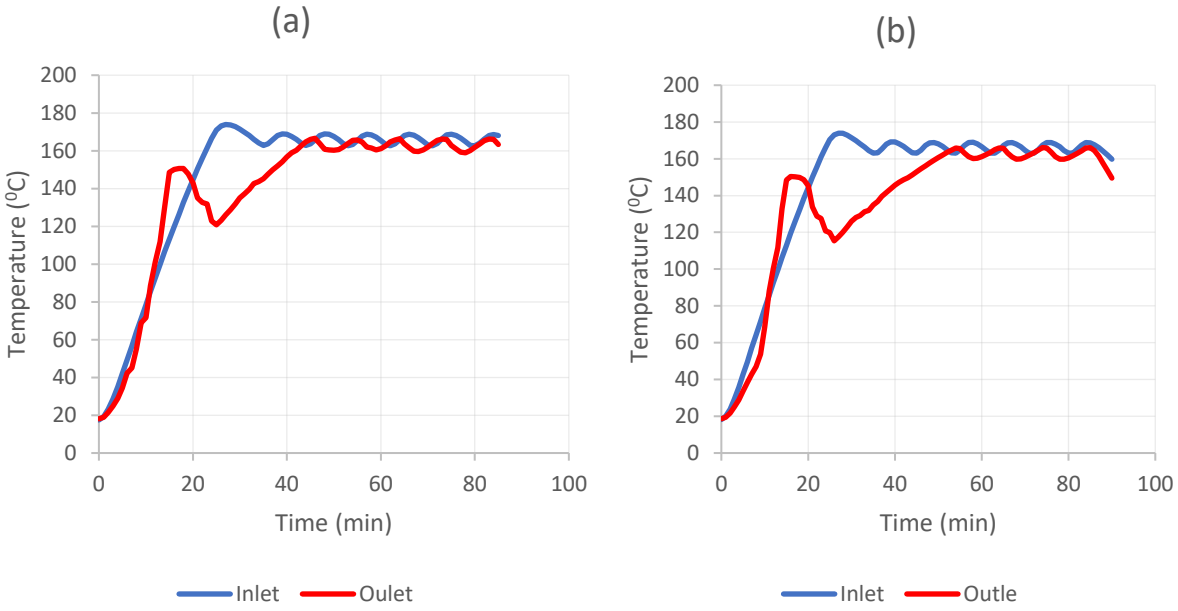

Figure 8.25: Temperature profile at regeneration temperature 165 °C for (a) single 1-hexanol adsorption system; and (b) 1-binary-component adsorption system

8.5 Chapter Summary

The objective of this chapter was to discuss the thermal regeneration impact on the activated alumina adsorbent utilized in this study. This was achieved through the measurement and investigation of the equilibrium adsorbent loading data of four single-component adsorption systems (2 different adsorbates at two different initial concentrations), and two binary-component adsorption systems (the same binary components at two different initial concentrations). Activated alumina adsorbents were used for ten consecutive adsorption/regeneration cycles at two regeneration temperatures of 205 °C and 185 °C, and 1-hexanol and binary-component adsorption systems for 15 cycles at the regeneration temperature of 165 °C.

The drop in adsorption loading was investigated for the single-component and binary-component adsorption systems. For the single-component adsorption of 1-hexanol and 1-decanol, the drop in adsorption capacity was remarkably higher for the 1-decanol than the 1-hexanol system at the second adsorption cycle, although the adsorbent applied proved to have marginally greater loadings for 1-decanol than 1-hexanol in the first adsorption cycle. The adsorption capacity for both systems, however, exhibited a relatively stable trend for the regeneration temperatures studied for 10 cycles, with a slight preference for the systems regenerated at a lower temperature, 185 °C, while a remarkable drop was observed at the 11^{th} cycle at regeneration temperature of 165 °C. The variation in adsorption capacity for binary-component adsorption systems followed the same trend of single-

component adsorption systems. In addition, the regeneration efficiency (*RE*) was determined for single and binary systems. The *RE* for all systems was notably greater for adsorbents regenerated at 185 °C than 205 °C and 165 °C. What is more, the *RE* increased by increasing the adsorbates' initial concentrations, due to the possibility of stronger adsorption at a lower initial concentration. The adsorbent kept its performance to over 90% for the 1-hexanol adsorption system when regenerated at 185 °C (as the best performance amongst the investigated regeneration temperatures was investigated), while its worst performance was below 50% when applied to adsorb 1-decanol from the binary-component adsorption system and regenerated at 165 °C.

A scanning electron microscope (SEM) was used to further investigate the regeneration impact on the adsorbent's structure after the last cycle of regeneration experiments. The images of adsorbents regenerated at 165 °C exhibited higher density than those regenerated at 205 °C and 185 °C. This might be attributed to higher exposure to high temperatures for longer cycles of adsorption/regeneration experiments. However, the adsorbent regenerated at 205 °C tended to be denser than those regenerated at 185 °C. This could be ascribed to extreme heat supplied at the regeneration temperature 205 °C which could have affected the structure of the adsorbent.

EDX analysis revealed that the change in adsorbent's chemical composition is more favourable in the presence of 1-decanol. The regeneration temperatures investigated in this study were much lower than the 1-decanol boiling point, which increased the potentiality of leaving more 1-decanol molecules during the regeneration experiments.

BET analysis suggested that the surface area of the regenerated adsorbents was affected by the regeneration process. The surface area notably dropped at the regeneration temperature of 165 °C, suggesting that more adsorbate molecules were retained during the regeneration process. This explained the severe drop in the adsorbent's performance at 165 °C than those estimated at 205 and 185 °C.

Ultimately, above findings aided in gaining more insight into the recyclability of activated alumina adsorbent used to adsorb 1-alcohols from an n-alkane solvent. The adsorption and regeneration data of various systems were measured and discussed, addressing and fulfilling objective (III) of this study.

Chapter 9 : Conclusion & Recommendation

9.1 Conclusions

The aim of this research was to gain knowledge and insight into the application and reusability of an industrially used activated alumina for the adsorption of single and binary 1-alcohol components from a paraffin solvent. This aim was successfully achieved through research related to three objectives: (I) measurement and investigation of adsorption experimental data; (II) equilibrium and kinetic modelling for data obtained from the first adsorption experiment; and (III) measurement and investigation of equilibrium adsorbent loading of regenerated adsorbents throughout successive adsorption/regeneration cycles.

9.1.1 Adsorption Experimental Results

The first objective was to measure and investigate the adsorption data of two single-component and one binary 1-alcohol systems using one type of activated alumina adsorbent.

9.1.1.1 Experimental Measurements

Equilibrium and kinetic data for single-component adsorption were measured for 1-hexanol and 1-decanol adsorption from an n-decane solvent, using one type of activated alumina as adsorbent. The data were measured at one temperature, 65 °C, at a specific range of the adsorbates' initial concentrations. Moreover, equilibrium and kinetic data were also measured for one binary-component system: 1-hexanol + 1-decanol. The binary-component kinetic data was measured for equal mass fraction of 1-alcohol mixtures. The same adsorbent, adsorption temperature and initial adsorbates' concentrations were used for the single-component adsorption experiments.

9.1.1.2 Variables Influencing Adsorption

For the first cycle of adsorption processes, and among the two variables investigated in this study, it was demonstrated that the initial adsorbate concentration had the most notable effect on the adsorption of 1-alcohols for both single and binary-component systems. The adsorption increased by increasing the initial overall adsorbate concentration to approximately 2.5 mass% and 2.0 mass% at single 1-decanol and binary-component adsorption systems, whereas the adsorption capacity of the single 1-hexanol adsorption system exhibited a marginal increase when the initial concentration was increased from 2.5 mass% to 3.0 mass%. For initial adsorbate concentrations greater than 2.0 to 3.0 mass%, the equilibrium adsorbent loading was found to remain relatively constant for most systems.

The carbon chain length of the respective alcohols used in this research work proved to have the least notable effect on the adsorption of these alcohols, for the ranges investigated. For the single-component adsorption systems, the adsorption rate at the beginning of the adsorption process was greater in the shorter carbon chain alcohols system than the adsorption rate in the longer carbon chain alcohol system, whereafter the equilibrium adsorbent loading was marginally higher for longer chain alcohol at the equilibrium stage. On the contrary, the shorter chain alcohol in a binary system was found to adsorb slightly better than the longer chain alcohol in the same system.

9.1.1.3 Comparison of Single and Binary-component Adsorption

When the initial concentration of one type of alcohol in a single-component adsorption system was similar to its initial concentration in a binary-component adsorption system (the initial concentration of adsorbates in binary systems is 50:50), it was found that the adsorption of this component was remarkably poorer in a binary-component system than it adsorbed in the respective single-component adsorption system.

9.1.1.4 Interaction Effect in Binary-component Systems

A competitive antagonistic behaviour was found to be predominant in the binary-component system investigated in this study at various initial concentrations of adsorbates. Furthermore, the adsorption of the longer chain alcohol was inhibited more significantly in the presence of a shorter chain alcohol than vice versa.

9.1.2 Adsorption Equilibrium and Kinetic Modelling

After investigation of the experimental results, equilibrium isotherm modelling, as well as adsorption kinetic modelling, was done for both the single and binary-component systems.

9.1.2.1 Adsorption Equilibrium Modelling

Three equilibrium isotherm models were investigated for the single and binary systems. The Freundlich (FM) and Sips models (SM) exhibited a good correlation for the single-component data. On the other hand, the Extended Freundlich Model was found to have the best correlation of data for the binary system. However, the isotherm models investigated for the binary system did not provide a good correlation of adsorption data.

As FM and SM are the most compatible isotherm models for the single-component systems, it is suggested that these systems are mostly inclined to multilayer adsorption; these systems presented as more heterogeneous, and the model parameters suggest that physisorption is more favourable

than the chemisorption. None of the multicomponent isotherm models investigated in this study can be assumed to verify the binary-component systems properly.

9.1.2.2 Adsorption Kinetic Modelling

The adsorption reaction kinetic and diffusional kinetic models were investigated for the single and binary-component adsorption systems.

For reaction kinetic models, it was found that all three reaction models investigated provided a good fit to the single and binary-component data. However, the Elovich Model (EM) proved to be superior. The diffusional model, Intra-particle Diffusional Model (IPDM), was also found to fit kinetic measured data well. Hence, it can be assumed that the adsorption process was influenced by the external (film) and internal diffusion, as well as by the surface reaction.

9.1.3 Adsorbent's Performance Throughout Adsorption/Regeneration Cycles

Thermal regeneration was applied to investigate the adsorbent's performance throughout successive adsorption/regeneration cycles. Ten adsorption/regeneration cycles were conducted at three different thermal regeneration temperatures: 205 °C and 185 °C for the all systems, and 15 cycles at 165 °C for single 1-hexanol and binary-component adsorption systems.

For both single and binary-component adsorption systems, the regeneration efficiency (*RE*) declined significantly in the second adsorption cycle, after which the adsorption capacity was relatively well maintained for the successive cycles. This was the case for all regeneration temperatures carried out in this study. However, the adsorbents regenerated at 185 °C exhibited better *RE* than those regenerated at 205 °C and 165 °C. This was observed for the systems investigated at different initial concentrations of the adsorbents.

At similar regeneration temperatures, the initial concentration of adsorbates showed less effect on the regenerated adsorbent's performance than the carbon chain length. The adsorbent's efficiency of those used to adsorbed 1-hexanol exhibited higher performance than those applied to adsorb 1-decanol. This was the case in both single and binary adsorption systems.

9.2 Recommendations

This section discusses the recommendations for future works based on the findings gained in this study.

9.2.1 Experimental Design

It is recommended that dynamic experimental design is used to investigate the adsorption of 1-alcohols from paraffin solvents. In industry, the adsorption process and frequency of regeneration can vary notably between different applications. It is therefore necessary to expand the study of the respective systems using dynamic experiments.

9.2.2 Types of Adsorbents

It is suggested that different types of activated alumina adsorbents be used for similar adsorption systems in future works and their efficiency should be compared throughout consecutive adsorption/regeneration cycles. In addition, it is recommended that different types of adsorbents other than activated alumina, such as zeolite, should be investigated and compared to activated alumina adsorbents.

9.2.3 Adsorption Experiment

The adsorbent's efficiency over successive adsorption/regeneration cycles should be investigated at different adsorption temperatures to investigate the impact of temperature on adsorption and on the regeneration process. Furthermore, using different adsorption temperatures is essential to study adsorption thermodynamics, namely enthalpy, entropy, and Gibbs' free energy. Identifying these thermodynamic parameters is important in distinguishing between the physisorption and chemisorption, and consequently, can indicate the degree of recyclability of the adsorbents (Awad *et al.*, 2020).

In addition, the adsorbates' initial concentration may be increased to more than 3.0 mass% in order to have more insight into the influence of the initial concentration on the efficiency of the adsorbents.

9.2.4 Regeneration Experiment

It is recommended that the regeneration experiments should be carried out at a wider range of temperatures. However, the investigation of regeneration temperatures between 185 °C and 205 °C is highly recommended. What is more, other factors affecting the regeneration process should be investigated as well, such as the duration of the regeneration experiment and flow rate of purging gas. In addition, conducting concentration profile analysis during the regeneration cycle is also highly recommended in order to further understand the thermal regeneration behaviour of the applied systems.

References

Aamir, M., Yin, S., Zhou, S., Xu, C., Liu, K., Liu, W., 2019. Congener-specific C10–C13 and C14–C17 chlorinated paraffins in Chinese agricultural soils: Spatio-vertical distribution, homologue pattern and environmental behavior, *Environmental Pollution*. 245, pp. 789–798.

Abd-Elrahman, W. R., Hamed, A.M., El-Emam, S.H., Awad, M.M., 2011. Experimental investigation on the performance of radial flow desiccant bed using activated alumina, *Applied Thermal Engineering*. 31(14–15), pp. 2709–2715.

Abou-Ziyan, H., Abd El-Raheim, D., Mahmoud, O., Fatouh, M., 2017. Performance characteristics of thin-multilayer activated alumina bed, *Applied Energy*. 190, pp. 29–42.

Al-Ghouti, M. A., Khraisheh, M.A.M., Ahmad, M.N.M., Allen, S., 2009. Adsorption behaviour of methylene blue onto Jordanian diatomite: A kinetic study, *Journal of Hazardous Materials*. 165(1–3), pp. 589–598.

Al-Ghouti, M. A. and Da'ana, D. A., 2020. Guidelines for the use and interpretation of adsorption isotherm models: A review, *Journal of Hazardous Materials*.

Alturki, A., 2017. A Single-component Adsorption of Alcohols in Zeolites.

Androutsopoulos, G.P., and Salmas, C.E. 2000. A new model for capillary condensation-evaporation hysteresis based on a random corrugated pore structure concept: Prediction of intrinsic pore size distributions. 1. Model formulation, *Industrial and Engineering Chemistry Research*. 39(10), pp. 3747–3763.

Anusha, G., 2013. Principles of Adsorption, *Shodhganga*. pp. 41-65.

Armarego, W.L.F., 2017. Common Physical Techniques Used in Purification, *Purification of Laboratory Chemicals*. pp. 1-70.

Ashok, B., Nanthagopal, K., Darla, S., Chyuan, O.H., Ramesh, A., Jacob, A., Sahil, G., Thiyagarajan, S., Geo, V.E., 2019. Comparative assessment of hexanol and decanol as oxygenated additives with calophyllum inophyllum biodiesel, *Energy*. pp. 494–510.

Auta, M., Darbis, *N.D.A.*, Din, A.T.M., Hameed, B.H., 2013. Fixed-bed column adsorption of carbon dioxide by sodium hydroxide modified activated alumina, *Chemical Engineering Journal*. 233, pp. 80–87.

Auta, M. and Hameed, B.H., 2014. Adsorption of carbon dioxide by diethanolamine activated alumina beads in a fixed bed, *Chemical Engineering Journal*. 253, pp. 350–355.

Awad, A.M., Jalab, R., Benamor, A., Nasser, M.S., Ba-Abbad, M., El-Naas, M., Mohammad, A.W., 2020. Adsorption of organic pollutants by nanomaterial-based adsorbents: An overview, *Journal of Molecular Liquids*. 301.

Ayawei, N., Ebelegi, A.N., Wankasi, D., 2017. Modelling and Interpretation of Adsorption Isotherms, *Journal of Chemistry*.

Azarfar, S., Noorbakhsh, F., Salmani, M., Ansari, S., Soleymani, R., Sadighi, S., 2016. Experimental Study and Characterization of Activated Alumina Adsorbent, *Proceedings of Iran International Aluminum Conference (IIAC2016)*. pp. 2–7.

Banerjee, S., and Chattopadhyaya, M.C., 2017. Adsorption characteristics for the removal of a toxic dye, tartrazine from aqueous solutions by a low cost agricultural by-product, *Arabian Journal of Chemistry*. 10, pp. S1629–S1638.

Belekar, R.M. and Dhoble, S.J., 2018. Activated Alumina Granules with nanoscale porosity for water defluoridation, *Nano-Structures and Nano-Objects*. 16, pp. 322–328.

Bish, D.L., 2013. Parallels and distinctions between clay minerals and zeolites, *Developments in Clay Science*. 5A, PP. 783-80.

Bosman, C.E., 2019. Single and binary-component adsorption of 1-alcohols from an alkane using various activated alumina adsorbents.

Butler, J.A.V., and Ockrent, C., 1929. Studies in Electrocapillarity. III, *The Journal of Physical Chemistry*, 34, pp. 2841–2859.

Cai, S., and Sohlberg, K., 2003. Adsorption of alcohols on γ-alumina (1 1 0 C), *Journal of Molecular Catalysis A: Chemical*. 193(1–2), pp. 157–164.

Cannio, M., Novak, S., Besra, L., Boccaccini, A.R., 2012. Electrophoretic Deposition, *Ceramics and Composites Processing Methods*, pp. 2733–2738

Cavalcante, C.L., 2000. Industrial Adesorption Separation Processes : Fundementals , Modeling and Applications, *Latin American Applied Research*. 30, pp. 357–364.

Chang, Q., 2016. Surface of Solids, *Colloid and Interface Chemistry for Water Quality Control*. pp. 175-225.

Chen, C. and Ahn, W.S., 2011. CO_2 capture using mesoporous alumina prepared by a sol-gel process, *Chemical Engineering Journal*. 166(2), pp. 646–651.

Chen, D., Wang, L., Ma, Y., Yang, W., 2016. Super-adsorbent material based on functional polymer particles with a multilevel porous structure, *NPG Asia Materials*. 8, pp. e301–e309.

Cheraghi, E., Ameri, E., and Moheb, A., 2016. Continuous biosorption of Cd(II) ions from aqueous solutions by sesame waste: thermodynamics and fixed-bed column studies, *Desalination and Water Treatment*, 57(15), pp. 6936–6949.

Chiou, C.T., 2003. Fundamentals of the Adsorption Theory, *Partition and Adsorption of Organic Contaminants in Environmental Systems*. pp. 39–52.

Do, D.D., 1998. Fundamentals of Diffusion and Adsorption in Porous Media. *Series on Chemical Engineering*. 2.

Dong, L., Yanyan, L Junxia, Y., Yigang, D., 2017. Removal of copper(II) from aqueous solution with rape stalk modified by citric acid, *Journal of Dispersion Science and Technology*, 38(2), pp. 180–186.

Dutta, T., Kim, T., Vellingiri, K., Tsang, D.C.W., Shon, J.R., Kim, K.H., Kumar, S., 2019 Recycling and regeneration of carbonaceous and porous materials through thermal or solvent treatment, *Chemical Engineering Journal*. 364, pp. 514–529.

Emam, E.A., 2018. Clay Adsorption Perspective on Petroleum Refining Industry, *Industrial Engineering*. 2(1), p. 19-25.

Erkey, C., 2011. Thermodynamics and dynamics of adsorption of metal complexes on surfaces from supercritical solutions, *Supercritical Fluid Science and Technology*. 1, PP. 41-77.

Figueiredo, H. and Quintelas, C., 2014. Tailored zeolites for the removal of metal oxyanions: Overcoming intrinsic limitations of zeolites, *Journal of Hazardous Materials*. 274, pp. 287–299.

Fletcher, A.J., Yüzak, Y., Thomas, K.M., 2006. Adsorption and desorption kinetics for hydrophilic and hydrophobic vapors on activated carbon, *Carbon*, 44(5), pp. 989–1004.

Fouladgar, M., Beheshti, M., Sabzyan, H., 2015. Single and binary adsorption of nickel and copper from aqueous solutions by γ-alumina nanoparticles: Equilibrium and kinetic modeling, *Journal of Molecular Liquids*. 211, pp. 1060–1073.

Freundlich, H.M.F., 1906. Over the adsorption in solution', *J. Phys. Chem*, 57, pp. 385–470.

Frey, S.J., Forte, P., Yonkers, N.Y., 1997. United States Patent. 19.

Fritz, W. and Schlunder, E.U., 1981. COMPETITIVE ADSORPTION OF TWO DISSOLVED ORGANICS ONTO ACTIVATED CARBON-I, *Chemical Engineering Science*. 36, pp. 721–730.

Fu, E., Somasundaran, P., Maltesh, C., 1996. Hydrocarbon and alcohol effects on sulfonate adsorption on alumina, *Colloids and Surfaces A: Physicochemical and Engineering Aspects*. 112(1), pp. 55–62.

Gabelman, A., 2017. Adsorption basics: Part 2, *Chemical Engineering Progress*. 113(8), pp. 1–6.

Girish, C.R., 2017. Various isotherm models for multicomponent adsorption: A review, *International Journal of Civil Engineering and Technology*, 8(10), pp. 80–86.

Grande, C.A. 2012. Advances in Pressure Swing Adsorption for Gas Separation, *ISRN Chemical Engineering*, 2012, pp. 1–13.

Groenewald, J., 2019. Evaluation and Comparison of three industrially relevant adsorbents of their ability to remove alcohol contaminants from an alkane solvent.

Guan, Y.T., Wang, S.H., Wang, M.H., Hou, Z.X., Hu, X.D., Wang, H., Fan, H.L., Zhang, N., 2014. Effect of initial concentration of Cu2+ on the adsorption performance of hydroxyapatite, *Advanced Materials Research*, 989–994, pp. 312–315.

Guo, X., and Wang, J., 2019. A general kinetic model for adsorption: Theoretical analysis and modeling, *Journal of Molecular Liquids*. 288, p. 111100.

Ho, Y., and Mckay, G., 1999. Pseudo-Second-Order model for sorption processes, *Process Biochemistry*, 34(6), pp. 451–465.

Ho, Y.S., 2006. Review of second-order models for adsorption systems, *Journal of Hazardous Materials*, 136(3), pp. 681–689..

Hu, H., Chen, D., Liu, H., Yang, Y., Cai, He., Shen, J., Yao, H., 2017. Adsorption and reaction mechanism of arsenic vapors over Γ-Al2O3 in the simulated flue gas containing acid gases, *Chemosphere*. 180, pp. 186–191.

Hu, X. Fan, M., Towler, B.F., Radosz, M., Bell, D.A., Plumb, O.G., 2011. Hydrogen Adsorption and Storage, *Coal Gasification and Its Applications*. 2011, pp. 157-245

Iftekhar, S., Ramasamy, D.L., Srivastava, V., Asif, M.B., Sillanpää, M., 2018. Understanding the factors affecting the adsorption of Lanthanum using different adsorbents: A critical review, *Chemosphere*, 204, pp. 413–430.

Jafari, M., and Sabori, A., 2011. Phase Distribution of Al_2O_3-ZnO Co-Precipitation as Sulphur Absorber Catalyst, in *International Conference Advances and Trends in Engineering Materials and their Applications*. 41(8), pp. 2–4.

Karimi, S., Tavakkol, Y.M., Karri, R.R., 2019. A comprehensive review of the adsorption mechanisms and factors influencing the adsorption process from the perspective of bioethanol dehydration, *Renewable and Sustainable Energy Reviews*. 107, pp. 535–553.

Karthikeyan, S., Sivakumar, B., Sivakumar, N., 2010. Film and pore diffusion modeling for adsorption of reactive red 2 from aqueous solution on to activated carbon prepared from bio-diesel industrial waste, *E-Journal of Chemistry*. 7, pp. 175–185.

Kaushal, A. and Singh, S.K., 2017. Adsorption Phenomenon and its Application in Removal of Lead from Waste Water: A Review, *International Journal of Hydrology*, 1(2). pp. 1-11.

Khalil, I., Thomas, K., Jabraoui, H., Bazin, P., Maugé, F., 2020. Selective elimination of phenol from hydrocarbons by zeolites and silica-based adsorbents—Impact of the textural and acidic properties, *Journal of Hazardous Materials*. 384, pp. 121397.

Khas, H. and Delhi, N., 2013. Steam Regeneration of Adsorbents: An Experimental and Technical Review, *Chemical Science Transactions*, 2(4), pp. 1078–1088.

Kulprathipanja, S., 2010. Zeolites in Industrial Separation.

Kumar, K.V., Gadipelli, S., Wood, B., Ramisetty, K.A., Stewart, A.A., Howard, C.A., Brett, D.J.L., Rodriguez-Reinoso, F., 2019. Characterization of the adsorption site energies and heterogeneous surfaces of porous materials, *Journal of Materials Chemistry A*. 7, pp. 10104–10137.

Kumar, K.V., Porkodi, K., Rocha, F., 2008. Comparison of various error functions in predicting the optimum isotherm by linear and non-linear regression analysis for the sorption of basic red 9 by activated carbon, *Journal of Hazardous Materials*, 150(1), pp. 158–165.

Kumar, R. and Glenn, D.R., 1986. Nonequillbrium, Nonisothermal Desorption of Single Adsorbate by Purge, *Industrial and Engineering Chemistry Process Design and Development*. 25(2), pp. 456–464.

Kumar, V., Lee, Y.S., Shin, J.W., Kim, K.H., Kukkar, D., Fai Tsang, Y., 2020. Potential applications of graphene-based nanomaterials as adsorbent for removal of volatile organic compounds, *Environment International*. 135, p. 105356.

Kumari, U., Behera, S., Meikap, B.C., 2019. A novel acid modified alumina adsorbent with enhanced defluoridation property: Kinetics, isotherm study and applicability on industrial wastewater, *Journal of Hazardous Materials*. 365, pp. 868–882.

Kurniawan, A. Sutiono, H., Indraswati, N., Ismadji, S., 2012. Removal of basic dyes in binary system by adsorption using rarasaponin-bentonite: Revisited of the Extended Langmuir model, *Chemical Engineering Journal*, 189–190, pp. 264–274.

Langmuir, I., 1918. The Adsorption of Gases on Plane Surfaces of Glass, Mica and Platinum, *Journal of the American Chemical Society*. 40, pp. 1361–1403.

Laskar, I.I., Hashisho, Z., 2020. Insights into modeling adsorption equilibria of single and multicomponent systems of organic and water vapors, *Separation and Purification Technology*. 241, p. 116681.

Le-Minh, N., Sivret, E.C., Shammay, A., Stuetz, R.M., 2018. Factors affecting the adsorption of gaseous environmental odors by activated carbon: A critical review, *Critical Reviews in Environmental Science and Technology*. 48(4), pp. 341–375.

Leckel, D., 2005. Oxygenates in Fischer-Tropsch Waxes : A Threat or Opportunity in Fuels Hydrocracking', in *EuropaCat-VII, Sofia, Bulgaria*.

Leckel, D., 2009. Diesel production from fischer - Tropsch: The past, the present, and new concepts, *Energy and Fuels*. 23(5), pp. 2342–2358.

Lee, K.M., Lim, Y.H., Park, C.J., Jo, Y.M., 2012. Adsorption of low-level CO 2 using modified zeolites and activated carbon, *Industrial and Engineering Chemistry Research*. 51(3), pp. 1355–1363.

Li, X. Zhang, Li., Yang, Z., Wang, P., Yan, Y., Ran, J., 2020. Adsorption materials for volatile organic compounds (VOCs) and the key factors for VOCs adsorption process: A review, *Separation and Purification Technology*. 235, p. 116213.

Li, Y., Li, Q., Wu, C., Luo, X., Yu, X., Chen, M., 2020. The inappropriate application of the regression Langmuir Qm for adsorption capacity comparison, *Science of the Total Environment*, 699, p. 134222.

Li, Y., Li, L., Yu, J., 2017. Applications of Zeolites in Sustainable Chemistry, *Chem*, 3(6), pp. 928–949.

Lin, D.R., Hu, L.J., Xing, B.S., You, H., Loy, D.A., 2015. Mechanisms of competitive adsorption organic pollutants on hexylene-bridged polysilsesquioxane, *Materials*, 8(9), pp. 5806–5817.

Liu, Y., Liu, Y., Qu, R., Ji, C., Sun, C., 2020. Comparison of adsorption properties for anionic dye by metal organic frameworks with different metal ions, *Colloids and Surfaces A: Physicochemical and Engineering Aspects*. 586, p. 124259.

Madero-castro, R.M. and Peng, X., 2022. Adsorption of Linear Alcohols in Amorphous Activated Carbons: Implications for Energy Storage Application, *Sustainable Chemistry & Engineering*. 10, pp. 6509−6520.

Majumder, C., 2018. Arsenic(V) Removal Using Activated Alumina: Kinetics and Modeling by Response Surface, *Journal of Environmental Engineering*, 144(3), p. 04017115.

Mao, H., Huang, R., Hashisho, Z., Wang, S., Chen, H., Wang, H., Zhou, D., 2016. Adsorption of toluene and acetone vapors on microwave-prepared activated carbon from agricultural residues: Isotherms, kinetics, and thermodynamics studies, *Research on Chemical Intermediates*. 42(4), pp. 3359–3371.

Mckay, G. and Al-Duri, B., 1991. The Extended Empirical Freundlich Isotherm for Binary Systems : A Modified Procedure to Obtain the Correlative Constants, *Chem. Eng. Process.* 29, pp. 133–138.

McQuillan, R.V., Stevens, G.W., Mumford, K.A., 2018. The electrochemical regeneration of granular activated carbons: A review, *Journal of Hazardous Materials*. 355, pp. 34–49.

Mekki, A. and Bagane, M., 2012. Thermodynamic study of adsorption alcohols on natural clay by inverse gas chromatography, *Environment and Earth Science*. 2(5), pp. 76–85.

Méndez, C.I. and Ancheyta, J., 2020. Kinetic models for Fischer-Tropsch synthesis for the production of clean fuels, *Catalysis Today*.

Milestone, N.B. and Bibby, D.M., 1983. Adsorption of Alcohols from Aqueous Solution by ZSM-5, *Chem. Tech. Biorechno*. 34A pp. 73–79.

Mokhatab, S., Poe, W.A., Mak, J.Y., 2019. Natural Gas Liquids Rrecovery, *Handbook of Natural Gas Transmission and Processing*. 2019, pp. 361-393.

Momina, M., Shahadat, M., Ismail, S., 2020. Regeneration Potential of Bentonite-Based Paintosorp^{TM} for Removal of Industrial Dye, *Arabian Journal for Science and Engineering*. 45(2), pp. 551–561.

Momina, Shahadat, M., Isamil, S., 2018. Regeneration performance of clay-based adsorbents for the removal of industrial dyes: A review, *RSC Advances*. 8(43), pp. 24571–24587.

Mukherjee, S., Kumar, A., Zaworotko, M.J., 2019. Metal-organic framework based carbon capture and purification technologies for clean environment, *Metal-Organic Frameworks (MOFs) for Environmental Applications*. pp. 5-61.

Mulgundmath, V.P., Tezel, F.H., Hou, F., Golden, T.C., 2012. Binary adsorption behaviour of methane and nitrogen gases, *Journal of Porous Materials*.19(4), pp. 455–464.

Nassar, N. N., Hassan, A., Pereira-Almao, P., 2011. Effect of the particle size on asphaltene adsorption and catalytic oxidation onto alumina particles, *Energy and Fuels*. 25(9), pp. 3961–3965.

Nayakasinghe, M. T., Sivapragasam, N., Burghaus, U., 2017. Adsorption of alcohols on a two-dimensional SiO2 single crystal – Alcohol adsorption on silicatene, *Chemical Physics Letters*. 689, pp. 105–110.

Neubauer, R., Kienzl, N., Bitschnau, B., Schroettner, H., Hochenauer, C., 2017. Thermal in Situ and System-Integrated Regeneration Strategy for Adsorptive On-Board Desulfurization Units, *Energy and Fuels*. 31(11), pp. 12942–12950.

Nunes, K.G.P., Sfreddo, L.W., Rosset, M., Féris, L.A., 2020. Efficiency evaluation of thermal, ultrasound and solvent techniques in activated carbon regeneration, *Environmental Technology*.

Özbay, N., Yargiç, A.Ş., Yarbay-Şahin, R.Z., Önal, E., 2013. Full factorial experimental design analysis of reactive dye removal by carbon adsorption, *Journal of Chemistry*, 2013.

Pal, P., 2017. Physicochemical Treatment Technology, *Industrial Water Treatment Process Technology*, pp. 145–171.

Palou, A., Cruz, J., Blanco, M., Larraz, R., Frontela, J., Bengoechea, C.M., González, J.M., Alcalà, M., 2014. Characterization of the composition of paraffin waxes on industrial applications, *Energy & Fuels*. 28(2), pp. 956–963.

Piccin, J.S., Dotto, G.L., Pinto, L.A.A., 2011. Adsorption isotherms and thermochemical data of FD & C red N° 40 binding by chitosan, *Brazilian Journal of Chemical Engineering*. 28(02), pp. 295–304.

Plazinski, W. and Rudzinski, W., 2009. Kinetics of adsorption at solid/Solution interfaces controlled by intraparticle diffusion: A theoretical analysis, *Journal of Physical Chemistry C*, 113(28), pp. 12495–12501.

Priegnitz, J.W., Kulprathipanja, S., Sohn, S.W., Glover, B.K., Vora, B.V., 2006. PROCESS FOR REMOVAL OF OXYGENATES FROMA PARAFFIN STREAM,(12) Patent Application Publication PuB . No .: US 2006 / 0247481 A1.

Proctor, A. and Toro-Vazquez, J.F., 2009. The Freundlich Isotherm in Studying Adsorption in Oil Processing, Second Edi, *Bleaching and Purifying Fats and Oils: Theory and Practice*. pp. 209-219.

Qian, Q., Gong, C., Zhang, Z., Yuan, G., 2015. Removal of VOCs by activated carbon microspheres derived from polymer: a comparative study, *Adsorption*. 21(4), pp. 333–341.

Qiu, H., Lv, L., Pan, B.C., Zhang, Q.J., Zhang, W.M., Zhang, Q.X., 2009. Critical review in adsorption kinetic models, *Journal of Zhejiang University: Science A*. 10(5), pp. 716–724.

Rabia, A.R., Ibrahim, A.H., Zulkepli, N.N., 2018. Activated alumina preparation and characterization: The review on recent advancement, *E3S Web of Conferences*. 34, pp. 1–8.

Rafique, A., Awan, M.A., Wasti, A., Qazi, I.A., Arhad, M., 2013. Removal of Fluoride from Drinkin Water Using Modified Immobilized Activated Alumina, *Journal of Chemistry*, 2013.

Ramirez, D., Sullivan, P.D., Rood, M.J., Asce, M., Hay, K.J., 2004. Equilibrium Adsorption of Phenol-, Tire-, and Coal-Derived Activated Carbons for Organic Vapors, *Enovironmental Engineering*. 130, pp. 231–241.

Reid, C.R. and Thomas, K.M., 2001. Adsorption kinetics and size exclusion properties of probe molecules for the selective porosity in a carbon molecular sieve used for air separation, *Journal of Physical Chemistry B*. 105(43), pp. 10619–10629.

Remy, T., Cousin Saint Remi, J., Singh, R., Webley, P.A., Baron, G.V., Denayer, J.F.M., 2011. Adsorption and separation of C1-C8 alcohols on SAPO-34, *Journal of Physical Chemistry C*. 115(16), pp. 8117–8125.

Rouquerol, J., Avnir, D., Fairbridge, C.W., Everett, D.H., Haynes, J.H., Pernicone, N., Ramsay, J.D.F., Sing, K.S.W., Unger, K.K., 1994. Recommendations for the characterization of porous solids, *IUPAC*, 66, pp. 1739–1758.

Saadi, R., Saadi, Z., Fazaeli, R., Fard, N.E., 2015. Monolayer and multilayer adsorption isotherm models for sorption from aqueous media, *Korean Journal of Chemical Engineering*. 32(5), pp. 787–799.

Saeed, M.M. and Ahmed, M., 2006. Effect of temperature on kinetics and adsorption profile of endothermic chemisorption process: -Tm(III)-PAN loaded PUF system, *Separation Science and Technology*. 41(4), pp. 705–722.

Safwat, S.M. and Matta, M.E., 2018. Adsorption of urea onto granular activated alumina: A comparative study with granular activated carbon, *Journal of Dispersion Science and Technology*. Taylor & Francis. 39(12), pp. 1699–1709.

Saha, D. and Grappe, H.A., 2017. Adsorption properties of activated carbon fibers, *Activated Carbon Fiber and Textiles*. pp. 143-165.

Salvador, F., Martin-Sanchez, N., Sanchez-Hernandez, R., Sanchez-Montero, M.J., Izquierdo, C., 2015. Regeneration of carbonaceous adsorbents. Part I: Thermal Regeneration, *Microporous and Mesoporous Materials*. 202, pp. 259–276.

Sanciolo, P., Milne, N., Taylor, K., Mullet, M., Gray, S., 2014. Silica scale mitigation for high recovery reverse osmosis of groundwater for a mining process, *Desalination*. 340(1), pp. 49–58.

Saunders, L., 1951. Surface and Colloid Chemistry, *Journal of Pharmacy and Pharmacology*. 3(1), pp. 865–882.

Selley, R.C and Sonnenberg, S.A., 2015. The Physical and Chemical Properties of Petroleum, in *Elements of Petroleum Geology*, pp. 13–39.

Senthil Kumar, P., Ramalingam, S., Abhinaya, R.V., Kirupha, S.D., Murugesan, A., Sivanesan, S., 2012 Adsorption of metal ions onto the chemically modified agricultural waste, *Clean - Soil, Air, Water*. 40(2), pp. 188–197.

Sevim, F., Lacin, O., Ediz, E.F., Demir, F., 2021. Adsorption capacity, isotherm, kinetic, and thermodynamic studies on adsorption behavior of malachite green onto natural red clay, *Environmental Progress and Sustainable Energy*. 40(1), p. e13471.

Shah, I.K., Pre, P., Alappat, B.J., 2014. Effect of thermal regeneration of spent activated carbon on volatile organic compound adsorption performances, *Journal of the Taiwan Institute of Chemical Engineers*. 45(4), pp. 1733–1738.

Shukla, P.R., Chong, S., Pan, G.T., Wang, S., Ang, M., Rudolph, V., 2019. Adsorption of phenolic contaminants from water on activated carbon: An insight into single and multicomponent adsorption isotherms, *Asia-Pacific Journal of Chemical Engineering*. 14(6), pp. 1–14.

Simonin, J.P., 2016. On the comparison of Pseudo-First-Order and Pseudo-Second-Order rate laws in the modeling of adsorption kinetics, *Chemical Engineering Journal*. 300, pp. 254–263.

Sircar, S., 2020. A practical perspective of fluid (gas or liquid) - Solid adsorption equilibrium, *Separation and Purification Technology*. 231, p. 115749.

Sonawanea, G.H. and Shrivastava, V.S., 2011. Removal of hazardous dye from synthetic textile dyeing and printing effluents by archis hypogaea L. shell: A low cost agro waste material, *Desalination and Water Treatment*. 29(1–3), pp. 29–38.

Sl´omkiewicz, P.M., 2006. Determination of the Adsorption Equilibrium of Alcohols and Alkenes on a Sulphonated Styrene–Divinylbenzene Copolymer, *Adsorption Science & Technology*. 24(3), pp. 239–256.

Su, Q., Su, Z., Xie, W., Tian, C., Su, X., Lin, Z., 2020. Preparation of 2D nitrogen-doped magnetic Fe3C/C by in-situ self-assembled double-template method for enhanced removal of Cr(VI), *Environmental Pollution*. 263, p. 114374.

Thomas, J.V., 2019. Selection of adsorbents for different applications and processes: a review, *Analytical Chemistry*. 67(12), pp. 317–319.

Tian, M.J., Liao, F., Ke, Q.F., Guo, Y.J., Guo, Y.P., 2017. Synergetic effect of titanium dioxide ultralong nanofibers and activated carbon fibers on adsorption and photodegradation of toluene, *Chemical Engineering Journal*. 328, pp. 962–976.

Torres-Perez, J., Huang, Y., Bazargan, A., Khoshand, A., McKay, G., 2020. Two-stage optimization of Allura direct red dye removal by treated peanut hull waste, *SN Applied Sciences*. 2(3).

Urlaub, J.., Norwig, J., Schollmayer, C., Holzgrabe, U., 2019. H NMR analytical characterization of mineral oil hydrocarbons (PARAFFINS) for pharmaceutical use, *Journal of Pharmaceutical and Biomedical Analysis*.169, pp. 41–48.

Viswanathan, B., 2017a. Chapter 10 – Hydrogen Storage, *Energy Sources*. pp. 185–212.

Viswanathan, B.., 2017b. Chapter 2 – Petroleum, *Energy Sources*. pp. 29–57.

Wadie, A. and Al-Khawaja, E., 2018. Removal of cadmium Cd(II) and silver Ag(i) from aqueous solutions by nano activated alumina. part i: Batch adsorption experiments, *MATEC Web of Conferences*, 162.

Wang, G., Dou, B Zhang, Z., Wang, J., Liu, H., Hao, Z., 2015. Adsorption of benzene, cyclohexane and hexane on ordered mesoporous carbon, *Journal of Environmental Sciences (China)*. 30, pp. 65–73.

Wang, H., Lashaki, M.J., Fayaz, M., Hashisho, Z., Philips, J.H. Anderson, J.E., Nichols, M., 2012. Adsorption and desorption of mixtures of organic vapors on beaded activated carbon, *Environmental Science and Technology*. 46(15), pp. 8341–8350.

Wang, J. and Guo, X., 2020. Adsorption kinetic models: Physical meanings, applications, and solving methods, *Journal of Hazardous Materials*. 390, p. 122156.

Wang, Y., Li, Q.M., Xing, Y., 2020. Porosity variation of lithium-ion battery separators under uniaxial tension, *International Journal of Mechanical Sciences*.174, p. 105496.

Wang, Y., Huang, S., Teng, X., Wang, H., Wang, J., Zhao, Q., Wang, Y., Ma, X., 2020. Controllable Fe/HCS catalysts in the Fischer-Tropsch synthesis: Effects of crystallization time, *Frontiers of Chemical Science and Engineering*.

Wasti, A. and Awan, A.M., 2016. Adsorption of textile dye onto modified immobilized activated alumina, *Journal of the Association of Arab Universities for Basic and Applied Sciences*.. 20, pp. 26–31.

William Kajjumba, G., Emik, S., Öngen, A., Özcan, H.K., Aydın, S., 2019. Modelling of Adsorption Kinetic Processes—Errors, Theory and Application, *Advanced Sorption Process Application.*

Xia, M., Chen, Z., Li, Y., Li, C., Ahmad, N.M., Cheema, W.A., Zhu, S., 2019. Removal of Hg(ii) in aqueous solutions through physical and chemical adsorption principles, *RSC Advances*. 9(36), pp. 20941–20953.

Xiang, W., Zhang, X., Chen, K., Fang, J., He, F., Hu, X., Tsang, D.C.W., Ok, Y.S., Gao, B., 2020. Enhanced adsorption performance and governing mechanisms of ball-milled biochar for the removal of volatile organic compounds (VOCs), *Chemical Engineering Journal*. 385, p. 123842.

Xu, Z., Cai, J., Pan, B., 2013. Mathematically modeling fixed-bed adsorption in aqueous systems, *Journal of Zhejiang University SCIENCE A*. 14(3), pp. 155–176.

Yadav, K.K., Gupta, N., Kumar, V., Khan, S.A., Kumar, A., 2018. A review of emerging adsorbents and current demand for defluoridation of water: Bright future in water sustainability, *Environment International*. 11, pp. 80–108.

Yang, K., Wu, W., Jing, Q., Jiang, W., Xing, B., 2010. Competitive adsorption of naphthalene with 2,4-dichlorophenol and 4-chloroaniline on multiwalled carbon nanotubes, *Environmental Science and Technology*. 44(8), pp. 3021–3027.

Yu, X. and Khosla, C., 2012. Engineering Escherichia coli for Biotransformation of Biomass into Fatty Acid Derived Fuels, *Current Chemical Biology*. 6(1), pp. 7–13.

Yuh-Shan, H., 2004. Citation Review of Lagergren Kinetic Rate Equation on Adsorption Reactions, *Scientometrics*. 59(1), pp. 171–177.

Zhang, G., Liu, Y., Zheng, S., Hashisho, Z., 2019. Adsorption of volatile organic compounds onto natural porous minerals, *Journal of Hazardous Materials*. 364, pp. 317–324.

Zhang, J., Wang, Y., Wang, F., 2019. Microreactor-assisted synthesis of a nickel-based infinite coordination polymer and its application in the selective adsorption of alcohols, *Inorganic Chemistry Communications*. 109, p. 107566.

Zhang, X., Gao, B., Creamer, A.E., Cao, C., Li, Y., 2017. Adsorption of VOCs onto engineered carbon materials: A review, *Journal of Hazardous Materials*. 338, pp. 102–123.

Zhang, X. and Cresswell, M., 2016. Materials Fundamentals of Drug Controlled Release, *Inorganic Controlled Release Technology*.

Zhao, M., Huang, Z., Wang, S., Zhang, L., Wang, C., 2020. Experimental and DFT study on the selective adsorption mechanism of Au(III) using amidinothiourea-functionalized UiO-66-NH2, *Microporous and Mesoporous Materials*. 294, p. 109905.

Zou, C., Zhao, P., Wang, M., Liu, D., Wang, H., Wen, Z., 2013. Failure analysis and faults diagnosis of molecular sieve in natural gas dehydration, *Engineering Failure Analysis*. 34(8), pp. 115–120.

Zou, W., Gao, B., Ok, Y.S., Dong, Li 2019. Integrated adsorption and photocatalytic degradation of volatile organic compounds (VOCs) using carbon-based nanocomposites: A critical review, *Chemosphere*. 218, pp. 845–859.

Appendix A: Materials and Methods

Appendix Contents

A.1 Experimental Design

A.1.1 Preliminary Experiments to Determine the Time of Equilibrium

Experimental runs were carried out to identify the time required to reach the equilibrium phase. 10 g of the adsorbent was added to 200 ml solution of a known adsorbates' initial concentration. Samples were taken from the mixture over 7 hours to establish when the adsorbates plateau in the concentrated solution. As shown in Figure A.1, the equilibrium phase for single 1-hexanol adsorption and binary-component adsorption was reached after 3 hours, whereas the single 1-decanol adsorption system reached the equilibrium phase after 5 hours.

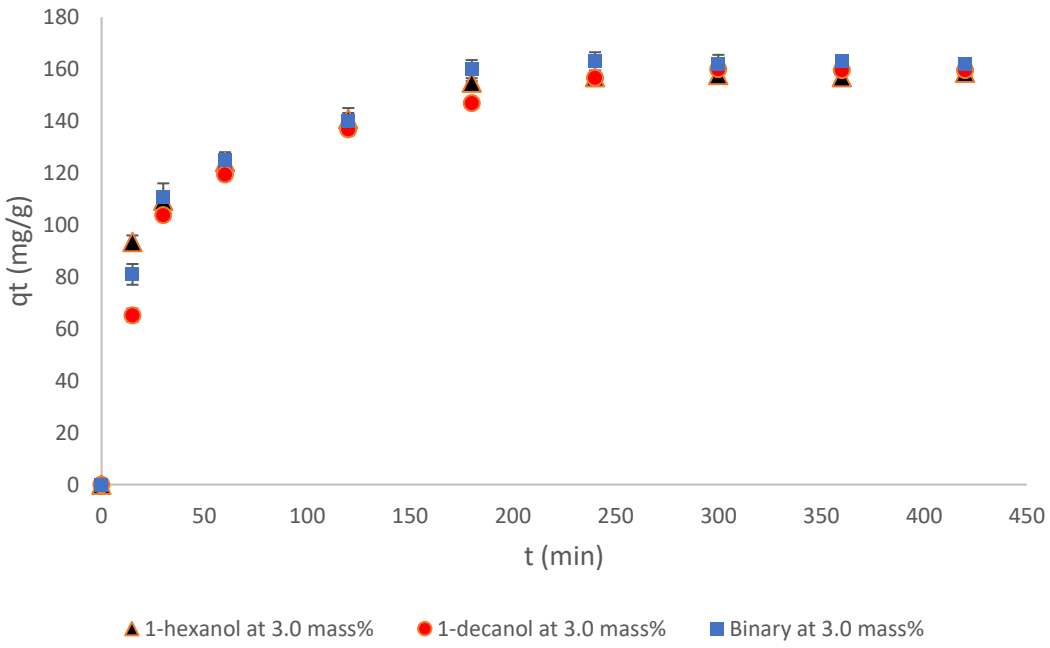

Figure 0.1: Preliminary equilibrium experiments (T = 65 °C)

A.1.2 Solutions Preparation for Adsorption Experiment

The methodology applied in preparing the 200mL solution for the adsorption experiments is briefly explained in this section. The system combines binary adsorbates prepared for the binary-component adsorption experiment of which the initial concentration of each adsorbate is 3.0 mass%, which will be used as an example.

As discussed in Section 3.4.1, the density of each component was considered in calculating the weights required to prepare a solution of 200mL. Equation A.1 was applied to estimate the total weight of the solution required to prepare a solution of 200mL:

$$m_{solution} = \rho_{solution} * V_{solution} \quad (A.1)$$

where $m_{solution}$, $p_{solution}$, *and* $V_{solution}$ are the total mass, total density, and total volume of the solution, respectively. The total volume is 200mL, while the total density was calculated using Equation A.2:

$$\rho_{solution} = (X_{n-decane} * \rho_{n-decane}) + (X_{1-hexanol} * \rho_{1-hexanol}) + (X_{1-decanol} * \rho_{1-decanol}) \quad (A.2)$$

where $X_{n\text{-decane}}$, $X_{1\text{-hexanol}}$, and $X_{1\text{-decanol}}$ are the fractions desired for n-decane, 1-hexanol, and 1-decanol, respectively. $p_{n\text{-decane}}$, $p_{1\text{-hexanol}}$ and $p_{1\text{-decanol}}$ are the density of n-decane, 1-hexanol, and 1-decanol, respectively.

In this example, the values of $X_{n\text{-decane}}$, $X_{1\text{-hexanol}}$, and $X_{1\text{-decanol}}$ are 0.94, 0.03, and 0.03, respectively, while the values of $p_{n\text{-decane}}$, $p_{1\text{-hexanol}}$ and $p_{1\text{-decanol}}$ are 730 kg/m^3, 814 kg/m^3, and 830 kg/m^3. Hence, the total density of the solution is:

$$\rho_{solution} = (0.94 * 730) + (0.03 * 814) + (0.03 * 830) = 735.52\ kg/m^3 = 0.73552 g/mL$$

The total mass of the solution will therefore be:

$$m_{solution} = 0.73552 * 200 = 147.104\ m^3$$

The weight required for each component in the solution can be calculated using Equation A.3:

$$m_{component} = X_{Component} * m_{solution} \quad (A.3)$$

where $m_{component}$ and $X_{component}$ are the mass and fraction of each component in the solution. The mass of n-decane, 1-hexanol, and 1-decanol are:

$$m_{n-decane} = 147.104 * 0.94 = 138.28\ g$$

$$m_{1-hexanol} = 147.104 * 0.03 = 4.41\ g$$

$$m_{1-decanol} = 147.104 * 0.03 = 4.41\ g$$

The steps followed in this section were applied to determine the mass of each component required to prepare the individual solutions of 200mL at different initial mass concentrations for all the systems investigated in this study (single-component as well as binary-component adsorption systems).

A.1.3 Adsorption Experimental Procedure

1. Put the stirrer bar underneath the water bath.

2. Fill the water bath with water, put the water heater in the water bath, set the water heater temperature at the desired temperature and switch on the water heater.

1. Add the magnetic stirrer to the 250ml Schott bottle.
2. Weigh the Schott bottle containing the magnetic stirrer and tare the scale.
3. Add the required amount of the n-alkane, record the weight, and tare the scale.
4. Add the required amount of the 1-alcohols and record the weight.
5. Tighten the Schott bottles into the lid of the water bath and immerse the bottles containing the alcohol-alkane mixture in the water bath once the water reaches the desired temperature.
6. Switch on the magnetic stirring plate and start stirring to the chosen speed (410 rpm).
7. Allow alcohol-alkane mixtures to heat up to the desired temperature.
8. Take the first sample from the solutions.
9. Add a measured amount of the adsorbent (10g) to the adsorbent mesh baskets.
10. Lower the adsorbent mesh baskets into the mixtures once the solutions reach the desired temperature.
11. Let the Schott bottles containing the solutions remain in the water bath, and meanwhile use a pipette to take samples at 15, 30, 60, 120, 180, 195 and 210 minutes for single-component of 1-hexanol and binary-component adsorption systems, and at 15, 30, 60, 120, 300, 315 and 330 minutes for single-component of 1-decanol adsorption system. Sampling is size is 400µL.
12. Transfer the samples into dedicated 4mL vials and mark each of them.
13. Once the last sample is taken, switch off the water heater and magnetic stirring plate.
14. Remove the lid of the water bath to which the Schott bottles were tightened.
15. Remove the adsorbent mesh baskets from the Schott bottles.
16. Transfer the adsorbents into tubes and make sure to close them well.
17. Remove the Schott bottles and dry the outside of the bottles.
18. Transfer the remaining solutions from the Schott bottles to other empty Schott bottles and mark each bottle accordingly.

A.1.4 Regeneration Experimental Procedure

1. Make sure the extraction fan is on.
2. Make sure that the gas cylinder is tightly closed.
3. Ensure that the inlet valves of the three columns are closed.
4. Ensure that the outlet valve of the activated carbon trap is opened.

5. Loosen the bolts of the three regeneration columns and remove them.
6. Remove the support rod that is located at the bottom of the flowmeters and allow the regeneration columns to rest on the supporting bars.
7. Weigh the adsorbent used in the previous adsorption experiment, record the weight, and transfer it into the column's insert.
8. Place the column insert into the regeneration column.
9. Repeat steps 6 and 7 for the other columns.
10. Put the regeneration columns back into their respective top flanges.
11. Put the support rod back in its place.
12. Fasten the bolts of the columns and make sure all the bolts are tightly fastened.
13. Open the outlet valve of the nitrogen gas cylinder, open the inlet valves of each column, and ensure there is a gas flow through the setup.
14. Adjust the inlet valves of each column to the desired flow rate, and allow the nitrogen to flow through the system for 15 minutes to eliminate the all oxygen from the system.
15. Meanwhile, switch on the cooling water recycling pump, open the inlet water valve, ensure the water is recycling through the condensation, and switch on the chiller bath.
16. Switch on the control box and set the regeneration temperature to the desired heat on the six controller programmes.
17. After 15 minutes, insert the USB into the portal that is located at the back of the HMI screen and switch on the electric trace heating.
18. Watch the gas inlet temperature throughout the experimental run.
19. Watch the condenser outlet temperature throughout the experimental run.
20. On completion of the experiment, switch off the electric trace heating.
21. Let the nitrogen gas flow through the setup until the temperature of the nitrogen gas in the outlet columns reaches 40^0C.
22. Close the outlet valve of the nitrogen gas cylinder, as well as the inlet valve of each column.
23. Eject the USB drive to remove it.
24. Close the cooling water inlet valve and switch off the water pump and chiller bath.
25. Close the activated carbon trap outlet valve.

26. Switch off the control box.
27. Loosen the bolts of the three regeneration columns.
28. Remove the support rod that is located in the bottom of the flowmeters.
29. Let the regeneration columns rest on the support bars.
30. Remove the column inserts that are filled with the adsorbents.
31. Weigh the adsorbent and record the mass.
32. Transfer the adsorbents into the tube and make sure to close it well.
33. Weigh the adsorbent in the mesh basket and record the mass.
34. Repeat steps 30 through 33 for the other two columns.

A.1.5 Samples Preparation for GC Analysis

1. Weigh an empty 2mL vial and tare the scale.
2. Using a pipette, add 100µL of the sample to the 2mL vial, record the sample weight, and tare the scale.
3. With a pipette, add 30µL of internal standard (1-pentanol) to the sample, record the standard weight, and reset the scale.
4. Using a pipette, fill the 2mL vial that contains the mixture of the sample and internal standard with the methanol (approximately 1000 µL).
5. Shake the 2mL vial containing the mixture very well.
6. Using a pipette, transfer 200µL of the solution to a second 2mL vial, and fill it with the methanol.
7. Shake the mixture very well.
8. Repeat the steps 1 through 7 for the following samples.

A.1.6 Experimental Setup

(a)

(b)

(c)

(d)

Figure A.2: Modifications done to the Schott bottle caps (a) and (b) the sampling point; (c) the hook where the mesh basket is hung; and, (d) the mesh basket hung into the Schott bottle's cap

(a)

(b)

Figure A.3: (a) Schott bottle tightened to the water bath lid; and (b) adsorption setup

(a)

(b)

*Figure A.4: (a) Regeneration columns and control box; and (b) the condenser **A** and activated carbon trap **B***

Appendix B: Experimental Adsorption Data

Appendix Contents

B.1 Adsorption Equilibrium Data

1. The equilibrium data provided in this section is for that used in the equilibrium modelling.

B.1.1 Single-component adsorption systems

Table B.1: Equilibrium data for single 1-hexanol adsorption system

1-hexanol											
Initial Concentration 0.5 mass%		**Initial Concentration 1.0 mass%**		**Initial Concentration 1.5 mass%**		**Initial Concentration 2.0 mass%**		**Initial Concentration 2.5 mass%**		**Initial Concentration 3.0mass%**	
C_e (mass%)	**q_e (mg/g)**	**C_e (mass%)**	**q_e (mg/g)**	**C_e (mass%)**	**q_e (mg/g)**	**C_e (mass%)**	**q_e (mg/g)**	**C_e (mass%)**	**q_e (mg/g)**	**C_e (mass%)**	**q_e (mg/g)**
0	0	0	0	0	0	0	0	0	0	0	0
0.0002	78.6309	0.0025	104.1656	0.0060	123.7326	0.0115	134.6887	0.0158	150.6998	0.7311	157.7938
0.0002	78.0363	0.0025	104.1875	0.0059	124.2681	0.0115	134.5845	0.0158	150.3408	0.7304	156.9417
0.0002	77.9339	0.0025	104.3125	0.0061	122.2536	0.0115	134.7902	0.0157	151.6402	0.7336	158.6229

Table B.2: Equilibrium data for single 1-decanol adsorption system

1-decanol											
Initial Concentration 0.5 mass%		**Initial Concentration 1.0 mass%**		**Initial Concentration 1.5 mass%**		**Initial Concentration 2.0 mass%**		**Initial Concentration 2.5 mass%**		**Initial Concentration 3.0mass%**	
C_e (mass%)	**q_e (mg/g)**	**C_e (mass%)**	**q_e (mg/g)**	**C_e (mass%)**	**q_e (mg/g)**	**C_e (mass%)**	**q_e (mg/g)**	**C_e (mass%)**	**q_e (mg/g)**	**C_e (mass%)**	**q_e (mg/g)**
0	0	0	0	0	0	0	0	0	0	0	0
0.0003	78.6850	0.0028	115.4054	0.0057	132.2772	0.0120	146.7464	0.0159	157.2955	0.0213	159.9546
0.0003	78.05399	0.0027	117.6362	0.0056	132.4926	0.0120	146.4279	0.0156	161.6625	0.0214	159.6558
0.0003	77.90463	0.0027	117.4253	0.0057	131.9237	0.0120	146.2652	0.0157	159.9086	0.0214	159.6185

B.1.2 Binary-component adsorption systems

Table B.3: Equilibrium data for 1-hexanol in the binary-component adsorption system

1-hexanol											
Initial Concentration 0.5 mass%		**Initial Concentration 1.0 mass%**		**Initial Concentration 1.5 mass%**		**Initial Concentration 2.0 mass%**		**Initial Concentration 2.5 mass%**		**Initial Concentration 3.0mass%**	
C_e (mass%)	**q_e (mg/g)**	**C_e (mass%)**	**q_e (mg/g)**	**C_e (mass%)**	**q_e (mg/g)**	**C_e (mass%)**	**q_e (mg/g)**	**C_e (mass%)**	**q_e (mg/g)**	**C_e (mass%)**	**q_e (mg/g)**
0	0	0	0	0	0	0	0	0	0	0	0
0.0012	68.1249	0.0054	74.9309	0.0106	94.0127	0.0145	95.5142	0.0211	96.3094	0.0253	96.2855
0.0012	67.46467	0.0054	74.9375	0.0106	93.8600	0.0145	96.0078	0.0211	96.4094	0.0252	97.6184
0.0012	67.38902	0.0054	74.8985	0.0106	94.0424	0.0144	96.8059	0.0209	98.2375	0.0254	95.8044

Table B.4: Equilibrium data for 1-decanol in the binary-component adsorption system

1-decanol											
Initial Concentration 0.5 mass%		**Initial Concentration 1.0 mass%**		**Initial Concentration 1.5 mass%**		**Initial Concentration 2.0 mass%**		**Initial Concentration 2.5 mass%**		**Initial Concentration 3.0mass%**	
C_e (mass%)	**q_e (mg/g)**	**C_e (mass%)**	**q_e (mg/g)**	**C_e (mass%)**	**q_e (mg/g)**	**C_e (mass%)**	**q_e (mg/g)**	**C_e (mass%)**	**q_e (mg/g)**	**C_e (mass%)**	**q_e (mg/g)**
0	0	0	0	0	0	0	0	0	0	0	0
0.0020	57.4646	0.0070	52.6040	0.0129	59.6787	0.0173	53.9086	0.0239	55.8522	0.0279	56.6174
0.0022	54.40553	0.0069	52.9393	0.0129	60.0175	0.0173	54.1292	0.0238	56.9209	0.0279	56.2953
0.0020	56.80488	0.0070	52.1835	0.0129	59.3419	0.0173	53.1780	0.0240	55.0220	0.0279	56.5386

B.2 Adsorption Kinetic Data

The data provided in this section is used for adsorption kinetic modelling.

B.2.1 Single-component adsorption system

Table B.5: Adsorption kinetic data for (a) single 1-hexanol adsorption system; and (b) single 1-decanol adsorption system

(a)				(b)			
1-hexanol				*1-decanol*			
Time (minutes)	**Initial Concentration 0.5 mass%** q_t **(mg/g)**	**Initial Concentration 1.5 mass%** q_t **(mg/g)**	**Initial Concentration 3.0 mass%** q_t **(mg/g)**	**Time (minutes)**	**Initial Concentration 0.5 mass%** q_t **(mg/g)**	**Initial Concentration 1.5 mass%** q_t **(mg/g)**	**Initial Concentration 3.0 mass%** q_t **(mg/g)**
0	0	0	0	0	0	0	0
15	40.7719	58.1149	60.3876	15	36.8504	47.2138	53.9843
30	57.1493	69.5587	80.3538	30	47.9304	61.1874	70.3643
60	65.0475	88.8127	114.2069	60	60.8754	85.5013	93.8215
120	73.8078	107.1161	138.8207	120	65.8497	118.0008	123.2952
180	78.6309	123.7326	157.7938	300	78.6850	132.2772	159.9546
195	78.0363	124.2681	156.9417	315	78.0540	132.4926	159.6558
210	77.9339	122.2536	158.6229	330	77.9046	131.9237	159.6185

B.2.2 Binary-component Adsorption systems

Table B.6: Adsorption kinetic data for 1-hexanol and 1-decanol in binary-component adsorption systems

	1-hexanol			***1-decanol***		
Time (minutes)	**Initial Concentration 0.5 mass%**	**Initial Concentration 1.5 mass%**	**Initial Concentration 3.0 mass%**	**Initial Concentration 0.5 mass%**	**Initial Concentration 1.5 mass%**	**Initial Concentration 3.0 mass%**
	q_t (mg/g)	**q_t (mg/g)**	**q_t (mg/g)**	**q_t (mg/g)**	**q_t (mg/g)**	**q_t (mg/g)**
0	0	0	0	0	0	0
15	38.9195	48.2442	39.2757	28.9374	21.6946	18.6956
30	45.8244	57.6440	49.2511	32.4677	33.4579	23.4501
60	54.5596	70.6214	67.9464	42.8160	42.7065	31.2669
120	63.1818	88.3570	84.2747	50.7741	53.0705	47.3478
180	68.1249	94.0127	96.2855	57.4646	59.6787	56.6174
195	67.4647	93.8600	97.6184	54.4055	60.0175	56.2953
210	67.3890	94.0424	95.8044	56.8049	59.3419	56.5386

Appendix C: Processing of Experimental Adsorption Data

Appendix Contents

C.1 Adsorption Data

C.1.1 Normalised Adsorbate Concentration

This section outlines the methodology used to determine the normalised liquid concentration, C_t/C_0, in the bulk solution. The 1-decanol system will be used as an example.

The mass of the mixture's components in the samples was identified by the GC, as can be seen in Table C.1.

Table 0.1: GC raw data of the single 1-decanol adsorption system

Time (minutes)	Mass (mg)	
	1-decanol	n-decane
0	0.378977	66.67311
330	0.0232459	72.44066

Equation C.1 was used to calculate the mass fraction of each adsorbate in the system at any time *t*.

$$C_{i,t} = \frac{m_{i,t}}{m_{total}} \qquad (C.1)$$

Using the data in the Table C.1 and Equation C.1, the mass fraction of the 1-decanol at time 0 and 330 minutes were as follows:

$$C_{1-decanol,0} = \frac{0.378977}{0.378977 + 66.67311} = 0.00565$$

$$C_{1-decanol,330} = \frac{0.0232459}{0.0232459 + 72.44066} = 0.00032$$

Hence, C_t/C_0 of 1-decanol at time 330 minutes was:

$$\frac{C_{1-decanol,330}}{C_{1-decanol,0}} = \frac{0.00032}{0.00565} = 0.05663$$

C.1.2 Adsorbent Loading

Similar data provided in Section C.1.2 will be used to calculate the adsorbent loading. The adsorbent mass and solution weight were 10g and 146130mg, respectively.

Using all data in section C.1.2 and Equation 2.1 in Section 2.1, the adsorbent loading, q_t, at time 0 and 330minutes were calculated as the follows:

$$q_{1-decanol,330} = \frac{\left(C_{1-decanol,0} - C_{1-decanol,330}\right) * V}{m} = \frac{(0.00565 - 0.00032) * 146130}{10}$$

$$q_{1-decanol,330} = 77.45 mg/g$$

For the binary-component adsorption systems, a similar methodology was applied for each component in the mixture, and the total *qt* was determined by the sum of $q_{1\text{-}hexanol,t}$ and $q_{1\text{-}decanol,t}$.

Appendix D: Uncertainty Analysis

Appendix Contents

D.1 Uncertainties Analysis

D.1.1 Measurement of Uncertainties

A standard error and two-tailed student's t-test with the significant level of 0.05 was used to determine the uncertainties for the mass concentration measured in this study using Equation D.1:

$$\Delta_y = \pm \mathrm{t}(\alpha, \mathrm{n}-1) S_n \qquad (D.1)$$

where Δ_y is the uncertainty parameter, $t(\alpha,n-1)$ is the student's t-test, α is the significant level that equals 0.05, n is the number of repeats, and S_n is the standard error.

The standard error was determined using Equation D.1:

$$S_n = \frac{s}{\sqrt{n}} \qquad (D.2)$$

where s is the standard deviation.

The uncertainties, however, are comprised of various components: the uncertainty from measuring repeat experiments, uncertainty from the GC analysis, uncertainty from the different pipettes, and uncertainty from the various scales used to prepare the solutions as well as the scales used to weigh the adsorbents. The total uncertainties were hence estimated using Equation D.3:

$$\Delta_y^2 = \sum \Delta_{y,components\ cosidered}^2 \qquad (D.3)$$

D.1.2 Calculation Sample

The single 1-decanol component adsorption will be used as an example to explain the uncertainties calculation method. The experiment was repeated five times, and the average of the adsorbed 1-hexanol at t = 60 minutes was calculated:

$$x_{average} = \frac{0.0256 + 0.0223 + 0.0233 + 0.0225 + 0.0265}{5} = 0.0241\ mass\%$$

The standard deviation was calculated and found to be 0.19, and the standard error was estimated using Equation D.2:

$$S_n = \frac{0.19}{\sqrt{5}} = 0.085\ mass\%$$

Equation D.1 was applied to calculate the uncertainty using Microsoft Excel®:

Δ_y = 0.23633 mass%

Similar steps were followed to calculate the other uncertainty components and the total uncertainty was found to be 0.23949 mass%.